The Branched-Chain Amino Acid Transporter CD98 Heavy Chain

Facilitates the Development of Colonic Macrophages

Associated with Apoptosis in Macrophage Progenitors

Inauguraldissertation

zur

Erlangung der Würde eines Doktors der Philosophie

vorgelegt der

Philosophisch-Naturwissenschaftlichen Fakultät

der Universität Basel

Von

Philipp Richard Wasilios Wuggenig

aus Schaan, Fürstentum Liechtenstein

Basel, 2019

Genehmigt von der Philosophisch-Naturwissenschaftlichen Fakultät

auf Antrag von

Prof. Dr. med. Gennaro De Libero

Prof. Dr. med. Jan Hendrik Niess

Prof. Dr. med. Udo Markert

Basel, den 25.06.2019

<div align="center">

Prof. Dr. Martin Spiess
Dekan der Philosophisch-Naturwissenschaftlichen Fakultät

</div>

To my brother and my parents

Από ένα μεγάλο αγώνα κατάφερα να εκπληρώσω το όνειρό μου

Table of Content

A. dest.	Aqua destillata
Actb	beta-actin (Actin-β)
AF700	Alexa Fluor 700
APC	allophycocyanin
Bcl2l11	Bcl-2-like protein 11 (apoptosis-related gene)
BM	bone marrow
BMDM	bone marrow-derived macrophage
bp l	base pair
BV	brilliant violet
Casp3	caspase 3 (apoptosis-related gene)
CCL	CC-chemokine ligand
CD	Crohn's disease
CD (with number)	cluster of differentiation
CD98hc	CD98 heavy chain
CD98lc	CD98 light chain
cDC	classical dendritic cell
cDNA	complementary deoxyribonucleic acid
cKO	conditional knock-out
cLP	colon lamina propria
Ct	cycle threshold
CX3CL1	CX3C-chemokine ligand 1 / fractalkine ligand
CX3CR1	CX3C-chemokine receptor 1 / fractalkine receptor
DAI	disease activity index
DC	dendritic cell
DNA	deoxyribonucleic acid
DNase	deoxyribonuclease

DPBS	Dulbecco's phosphate-buffered saline
DSS	dextran sodium sulfate
EDTA	ethylenediaminetetraacetic acid
ELISA	enzyme-linked immunosorbent assay
EYFP	enhanced yellow fluorescence protein
FACS	fluorescence-activated cell sorting
Fas	tumor necrosis factor (apoptosis-related gene)
FC	fold change
Fc	fragment crystallizable
FCS	fetal calf serum
FITC	fluorescein isothiocyanate
FlowSOM	algorithm that utilizes self-organizing maps of a data set
FMO	fluorescence minus one
Fos	proto-oncogene (apoptosis-related gene)
FRP	fusion regulatory protein
GALT	gut-associated lymphoid tissue
GAPDH	glyceraldehyde 3-phosphate dehydrogenase
GFP	green fluorescent protein
H&E	hematoxylin and eosin
i.p.	intraperitoneal
IBD	inflammatory bowel disease
IEC	intestinal epithelial cell
IFN	interferon
Ig	immunoglobulin
IHC	Immunohistochemistry
IL	interleukin
LPS	lipopolysaccharide
mAbs	monoclonal antibodies

M-CSF	macrophage colony-stimulating factor
MFI	median fluorescence intensity
MHC II	major histocompatibility complex II
MLN	mesenteric lymph node
MNP	mononuclear phagocyte
mRNA	messenger ribonucleic acid
Mφ	macrophage
NFκB	nuclear factor dB
NK cell	natural killer cell
NLR	NOD-like receptor
NOD	nucleotide-binding oligomerization domain-containing protein
nt	nucleotide
Osm	oncostatin M (apoptosis-related gene)
PBS	phosphate-buffered saline
PCA	principal component analysis
PCR	polymerase chain reaction
PE	phycoerythrin
PerCP	peridinin chlorophyll
RCF	relative centrifugal force (= x g)
RNA	ribonucleic acid
RPMI	Roswell Park Memorial Institute
RT	room temperature
RT-qPCR	real-time quantitative PCR
SD	standard deviation
SPF	specific-pathogen-free
STRING	Search Tool for the Retrieval of Interacting Genes/Proteins
TGF	tumor growth factor
TLR	Toll-like receptor

TMX or TAM	tamoxifen
TNF	tumor necrosis factor
Treg	regulatory T cell
Tris-Buffer	Tris(hydroxymethyl)-aminomethane
UC	Ulcerative colitis
WT	wild type

*S*UMMARY

CX3CR1[+] mononuclear phagocytes extend processes into the intestinal lumen to monitor the intestinal microbiota as well as the chymus. Whether the constituents of the chymus are required for macrophages is not known. Moreover, the molecular mechanisms that control the intestinal ability to distinguish between "innocuous" and "dangerous" antigens remain poorly understood although macrophages play a key role in this process. A comprehensive macrophage development is critical for gut macrophages performing crucial tasks in the intestinal immune system. However, the underlying mechanisms of this development remain elusive. The amino acid transporter CD98, which was first identified as a lymphocyte activation marker, is a multifunctional protein and is associated with a variety of activities, such as those of amino acid transporters, integrin regulators, and fusion regulators. CD98hc interacts with certain integrin β-subunits to mediate signaling events and consequently controls cell migration, survival, and proliferation. To assess the role of branched-chain amino acids on the development of gut macrophages, we generated an inducible knock-out mouse model for the branched-chain amino acid transporter CD98hc specifically in CX3CR1[+] intestinal macrophages. We showed that CD98 deficient macrophages attenuate the severity of dextran sodium sulfate-induced colitis clinically, endoscopically, and histologically. Single-cell RNA sequencing of colonic lamina propria macrophages obtained from unmanipulated and healthy mice revealed that silencing CD98 blocks the 'monocyte waterfall'-development to mature macrophages. Further, we observed that the arrest in macrophage development is associated with increased expression of apoptotic genes. Moreover, patients with Crohn's disease and ulcerative colitis are characterized by high CD98 expression. Our results demonstrate that CD98 plays a pivotal role in intestinal homeostasis by influencing the development of gut macrophages.

1   I<small>NTRODUCTION</small>

1.1.   Mucosal immune system

The intestinal tract covers an area of approximately 100 m^2 and is, therefore, the largest surface of the human body. Also, the intestine harbors around 10^{14} commensal bacteria, comprising ~1.000 different species. Besides that, it is continuously exposed to dietary and environmental antigens. Intestinal epithelial cells (IECs) and mesenchymal cells are the first line of defense of the mucosal immune system and the host response to infection and tissue damage. The single layer of epithelial cells is covered by the mucus biofilm consisting of trefoil factors and mucins, which is secreted from goblet cells and is the first contact point with the environment (Baumgart and Sandborn, 2012; Varol et al., 2010). Further, Paneth cells located within the epithelial crypts produce antimicrobial peptides, which creates the protective mucus layer (**Figure 1.1**). IECs are not only a stout barrier, but they also function as an initiator of the innate immune response to microbiota and tissue damage. Additionally, IECs have numerous protective mechanisms such as pattern recognition receptors (Toll-like receptors), nucleotide-binding oligomerization-domain protein-like receptors (NLRs), as well as cytokine and chemokine receptors (Baumgart and Sandborn, 2012; Uhlig and Powrie, 2018).

The connective tissue underlying the epithelium is constituted by extracellular matrix components together with the mesenchymal cells, which are abundant in the intestine. Additionally, mesenchymal cells constitute the intestinal stem cell niche (Aoki et al., 2016). Further, as these cell types integrate IEC and immune response, they contribute to the host defense, inflammation, and tissue repair in the intestine. Three major subsets of mesenchymal cells are known: fibroblasts, myofibroblasts, and pericytes. Intestinal inflammation leads to an activation of myofibroblasts in response to inflammatory cytokines and initiates the production of collagen to restore tissue damage. Furthermore, fibroblasts react as sentinels and pericytes, which are also called mural cells and vascular smooth muscle cells, control the endothelial cell differentiation, endothelial signaling, angiogenesis, and excessive extracellular matrix deposition (Lawrance et al., 2017; Mifflin et al., 2011; Uhlig and Powrie, 2018). Besides, activation of nucleotide-binding oligomerization domain containing 2 (NOD2) initiates secretion of the monocyte chemoattractant CCL2 by mesenchymal cells which leads to the protection

of enteric pathogens. In IBD, the pathogenic inflammatory response by mesenchymal cells showed that they are the primary target of pathogenic TNF. Further, the activated phenotype of intestinal fibroblasts has enhanced responsiveness to cytokines and chemokines which are involved in recruitment and retention of leukocytes (Uhlig and Powrie, 2018).
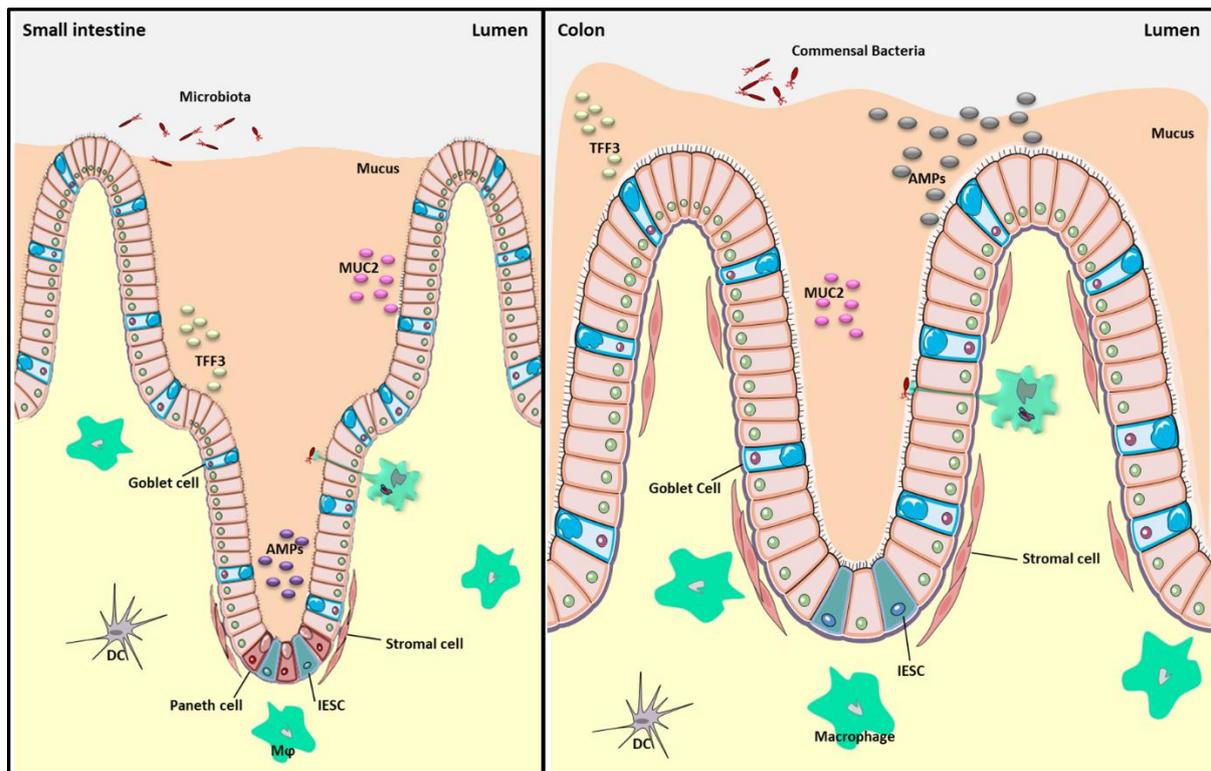
Figure 1.1: Schematic illustration of the mucosal architecture. IECs build the biochemical and physical barrier and is covered by mucus biofilm consistent of trefoil factors (TFF3, trefoil factor 3) and mucins (Muc2). The intestinal epithelial stem cell (IESC) niche controls the continuous renewal of the IEC layer by crypt-resident stem cells. Apart from Paneth cells, the differentiated IESC migrate up the crypt-villus axis. Antimicrobial peptides (AMPs) are secreted by Paneth cells and mucus by goblet cells to promote the exclusion of microbiota from the epithelial surface. Specialized IECs (also known as M cells (microfold cells)) and goblet cells mediate the transport of luminal antigens and live microbiota across the epithelial barrier to DCs, and gut-resident macrophages (Mφ) sample the lumen through their transepithelial dendrites (adapted from: (Peterson and Artis, 2014)).

The intestinal lamina propria harbors diverse mononuclear phagocytes, including conventional dendritic cells (cDC), granulocytes such as neutrophils, monocytes, and monocyte-derived macrophages (Mφ) that play a crucial role in mucosal homeostasis. The mononuclear phagocytes accumulate during

intestinal infection and inflammation. These cells are in the gut-associated lymphoid tissue (GALT) as well as in the subepithelial lamina propria. Typical histological signs of intestinal inflammation are granulomas in CD and neutrophil enriched crypt abscesses in UC. Further, the cell-intrinsic defense mechanism autophagy is involved in xenophagy, which is an innate component of immune responses (Alexander, 2008), and defects are particularly associated with CD. Thus, NOD2 signaling links autophagy-related protein 16 like 1 (ATG16L1) signaling with defective in autophagy in DCs, neutrophils, and monocyte-derived macrophages (Baumgart and Sandborn, 2012; Joeris et al., 2017; Uhlig and Powrie, 2018; Varol et al., 2010).

Focusing on mononuclear phagocytes in the gut, CX3CR1$^+$ mononuclear phagocytes and CD11b$^+$ CD103$^+$ DCs are the significant cell populations in the intestinal lamina propria. Extravasated Ly6C^{high} blood monocytes, which are recruited continuously by a CCR2 dependent manner, give rise to intestinal CX3CR1$^+$ macrophages under steady state and inflammatory conditions. (Gren and Grip, 2016; Italiani and Boraschi, 2014; Joeris et al., 2017; Zigmond et al., 2012). The development from monocytes to macrophages in the lamina propria is a process known as 'monocyte waterfall.' Hence, monocytes develop through intermediates to tissue-resident macrophages which are characterized as CCR2$^+$ CX3CR1^{int} Ly6C^{high} MHC II$^-$ monocytes, CCR2$^+$ CX3CR1^{int} Ly6C$^{high/int}$ MHC II$^+$ monocytes, and CCR2$^+$ CX3CR1^{high} Ly6C^{low} MHC II$^+$ monocytes. From the last stage of the 'monocyte waterfall,' the resident macrophage matures over the immature CD64$^+$ CX3CR1^{high} Ly6C$^-$ MHC II$^-$ macrophage to the mature CD64$^+$ CX3CR1^{high} Ly6C$^-$ MHC II^{high} tissue-resident macrophage (Joeris et al., 2017; Schridde et al., 2017; Tamoutounour et al., 2013). This transition takes approximately 96 hours and requires the CSF-1R (Bain et al., 2013; Joeris et al., 2017). Since tissue-resident macrophages like microglia in the brain, Kupffer cells in the liver, Langerhans cells in the skin, and alveolar macrophages may originate from embryonic or perinatal precursors, gut resident macrophages are mainly replenished by high turnover of extravasated Ly6C^{high} blood monocytes. Resident macrophages are relatively short-lived with a half-life of 3-5 weeks. However, some of these macrophages were not replenished from circulating precursors and are maintained locally by self-renewal. This subset of intestinal macrophages is long-lived, which populate the submucosa and myenteric plexus (De Schepper et al., 2018; Shaw et

al., 2018; Zigmond and Jung, 2013). Importantly, for the establishment and the total number of all resident macrophage subsets in the colonic lamina propria, the live commensal microbiome is required independent of the ontogeny of macrophages. Therefore, microbiota, as well as CCR2-dependent recruitment of Ly6C^{high} monocytes, is required for the homeostasis of tissue-resident intestinal macrophages (Bain et al., 2014; Shaw et al., 2018).

As macrophages are one of the significant cell populations in the colonic lamina propria, they survey the intestinal content by clearing apoptotic cell bodies and ingest and kill microbes that have passed the epithelial barrier (Mowat et al., 2017). Moreover, CX3CR1^{+} macrophages initiate the innate and the adaptive immune response to commensal and pathogenic bacteria (Leonardi et al., 2018; Varol et al., 2010). However, the stimulation of intestinal macrophages with Toll-like receptor (TLRs) ligands does not induce an inflammatory response in the intestine compared to most other tissues (Rogler et al., 1997; Smythies et al., 2005), by preventing uncontrolled inflammation. Therefore, leftovers during microbial clearance from ingested microbes are expelled into the intestinal lumen (Arques et al., 2009). In contrast, gut macrophages might be involved in the pathogenesis of IBD as they are a component of the cellular inflammatory infiltrates in experimental colitis as well as in patients with IBD (Hausmann et al., 2002; Kamada et al., 2008). As Ly6C^{high} monocytes are associated with inflammation, the transition into gut-resident macrophages is impaired during colitis. Thus, gut-resident macrophages are outcompeted by inflammatory CX3CR1^{int} mononuclear phagocytes which are most like Ly6C^{high} monocytes. Consequently, intestinal inflammation leads to disruption of full differentiation of inflammatory Ly6C^{high} monocytes into CX3CR1^{high} gut-macrophages (Bain and Schridde, 2018; Bain et al., 2013; Zigmond et al., 2012).

During intestinal inflammation, macrophages are crucial for tissue repair and restoration of intestinal homeostasis. Nevertheless, pro-inflammatory mediators such as IL-1, IL-6, TNF, IL-23, NO, and reactive oxygen intermediates are found in the inflamed intestine, which is mainly produced by monocytes and macrophages. Also, pro-inflammatory monocytes and macrophages produce chemokines such as CCL2, CCL3, CCL4, CCL5, CCL8, and CCL11. These mediators/chemokines can

4

recruit and activate additional immune effector cells like monocytes, eosinophils, and neutrophils (Arnold et al., 2016; Asano et al., 2015; Joeris et al., 2017; Seo et al., 2015). However, inflammatory monocytes also inhibit the pathological effects of neutrophils during intestinal inflammation, which might reflect the balance between local pathogenic and regulatory mechanisms of the monocyte-macrophage lineage (Joeris et al., 2017).

1.2. Inflammatory bowel disease

Bacteria, viruses, fungi, and parasites colonize or infect the intestine. For a lifelong response to dietary antigens and microbiota, a sufficient epithelial barrier function, as well as innate and adaptive immune regulation, is required. Changes in lifestyle and environment, the occurrence of genetic defects with high functional impact, or accumulation of common genetic susceptibility variants could lead to failure of those evolutionarily adapted mechanisms. Consequently, not only the genetic defects lead to inflammatory bowel disease (IBD), the additional exposures are also involved (Schirmer et al., 2018; Uhlig and Powrie, 2018). IBD is chronic intestinal inflammation with two primary forms: (1) Crohn's disease (CD), and (2) ulcerative colitis (UC). Additionally, there is a subgroup which is placed between colonic CD and UC in terms of variant burden called IBD unclassified. IBDs have a substantial health care problem, and a multifactorial etiology and its onset are in persons 15 to 30 years of age. IBD shows increased incidence and prevalence worldwide. Typical for IBD is a chronic relapsing disease activity of acute flares and intervals of remission. Thus, tissue damage over time including fistulizing and stricturing in CD as well as life-threatening episodes of acute severe UC are caused by these chronic intestinal inflammations with limited treatment options (Abraham and Cho, 2009; Baumgart and Sandborn, 2012; Imhann et al., 2018; Ordas et al., 2012; Uhlig and Powrie, 2018). Although the terminal ileum is mostly affected in CD, lesions can occur anywhere on the entire digestive tract, from the alimentary canal of the mouth to the anus. However, in UC only the mucosal layer of the colon is affected. Compared to CD, in which the inflammation is transmural and patchy, UC begins in the rectum where the disease spreads up through the large intestine (Varol et al., 2010).
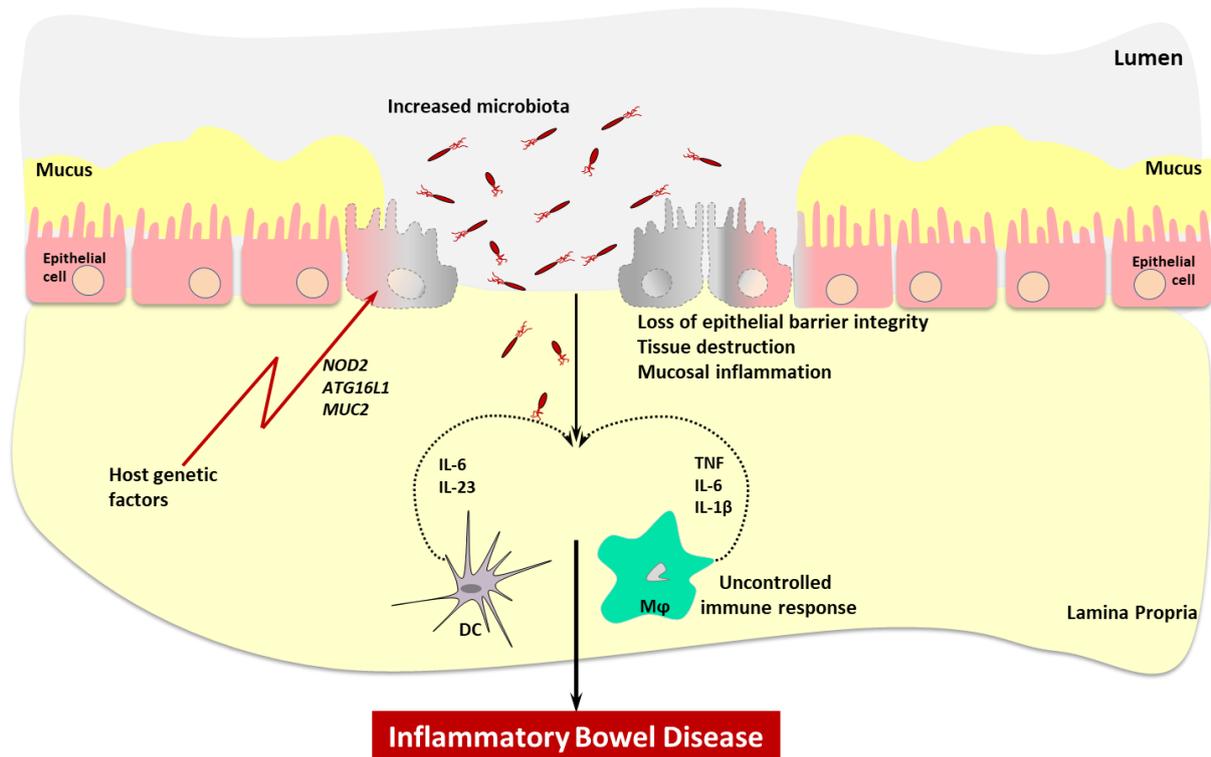
Figure 1.2: Schematic illustration of the onset of inflammatory bowel disease (IBD). Defects of the mucus barrier and epithelial barrier due to genetic aberrations, and the uncontrolled immune response (e.g., by tissue macrophages (Mφ)) leads to an increased gut microbiota which results in tissue destruction and mucosal inflammation (adapted from: (Coskun, 2014)).

In general, the basis of IBD pathogenesis occurs due to defects in the mucus barrier and epithelial barrier which leads to the initiation and augmentation of the intestinal inflammation (**Figure 1.2**). As IBD is a group of polygenic disorders in which over 200 alleles/loci contribute to the overall risk of the disease, genome-wide association studies showed that the innate immunity plays a central role of the IBD pathogenesis (Loddo and Romano, 2015; Torres et al., 2017; Ungaro et al., 2017). Moreover, intestinal macrophages maintain the intestinal homeostasis by clearing of apoptotic or senescent cells and can remodel the tissue at steady state (Torres et al., 2017). Although some loci (such as *NOD2*, *ATG16L1*, and *MUC2*) are specifically associated with CD and others only with UC, the majority of loci are shared between CD and UC with similar directions of effects (Ananthakrishnan, 2015). NOD2, which was the first described susceptibility gene for IBD, recognizes bacterial muramyl dipeptide and transduces signals which activate NF-κB. Thereby, NOD2 regulates the gut microbiota in steady state and stimulates not only the innate but also the adaptive immune system (Burada et al., 2018; Loddo and

Romano, 2015). Furthermore, many of the putative genes which influence the immune system can be divided into influencing innate immune response, adaptive immune response, autophagy, restitution and injury repair, microbial defense and antimicrobial activity, response to oxidative stress, and maintenance of the integrity of the epithelial barrier. Besides, cellular phenotypes such as Paneth cell function might be influenced by the synergy of genetic polymorphisms (Ananthakrishnan, 2015).

Different therapeutic strategies have been explored to treat IBD. As the migration of leukocytes from the circulation into the inflamed intestinal mucosa is well characterized, anti-leukocyte trafficking therapy is a new target for the treatment of IBD. Vedolizumab was the first approved gut-specific anti-integrin antibody for the therapy of CD and UC. It targets the α4β7 integrin on T cells which prevents their migration into the gut mucosa (Rogler, 2015; Sands, 2014). Additionally, other biological therapies have been promising. TNF inhibition by infliximab, adalimumab, certolizumab pegol, and golimumab provide effective treatment by improving long-term outcomes (Sands, 2014). Further, small molecule kinase inhibitors are also promising therapeutic strategies such as Tofacitinib in UC, which is a JAK3 inhibitor. Several additional strategies for the treatment of IBD such as stem cell transplantation for patients who failed with established medications or fecal microbiota transplantation might be an option to attenuate the severity of IBD especially for UC patients (Rogler, 2015). A recommended effective first-line therapy to induce remission in pediatric patients with CD is the exclusive enteral nutrition (EEN) as the sole source of nutrition. The idea in EEN is to reduce the exposure to antigens found in food, alteration in the gut microbiota, improvement of intestinal permeability, and immunomodulatory properties. In general, individual anti-inflammatory supplements such as curcumin, omega-3 fatty acids, vitamin D or the positive effects of prebiotics and probiotics on the intestinal microbiome are used for the treatment of IBD (Limketkai et al., 2018).

Alternative therapies with anti-inflammatory plant-derived natural compounds like phenols and anthocyanidins might attenuate the severity of IBD. For instance, curcumin or curcuma inhibits NF-κB and improved disease symptoms of IBD patients (Camacho-Barquero et al., 2007; Jobin et al., 1999).

Furthermore, as macrophages are identified as the critical target for interventional strategies, no selectively therapy in IBD against monocytes or macrophages is available. However, established and applied therapies also affect these cells. Thus, the PPAR-γ agonist aminosalicylate downregulates NF-κB activation, corticosteroids have an anti-inflammatory effect on cytokine and chemokine release, anti-TNF therapies induce apoptosis by intestinal macrophages, and the recruitment of myeloid cells to the intestine is inhibited by an anti-α4β7 antibody (Atreya et al., 2011; Gren and Grip, 2016; Lim et al., 2007; Linard et al., 2008; Villablanca et al., 2014). However, the anti-inflammatory effects of these beneficial treatments cause a variety of undesired side effects (Gren and Grip, 2016).

Although in recent years the advanced clinical approaches such as nutritional interventions and analysis of pathophysiological processes underlying IBD, the medical treatments have remained unsatisfactory with low response and remission rate (Torres et al., 2017; Ungaro et al., 2017). Thus, a better understanding of immune cells involved in the pathogenesis of IBD to mainly target monocytes and macrophages is required for the development of new treatment options for patients with IBD.

1.3.   Animal models of intestinal inflammation

Animal models are essential to understand the systemic and mucosal immune response and its mechanism. In animal models, dissection of cellular compartments, genetic manipulation, and therapeutic concepts can be tested and investigated (Uhlig and Powrie, 2018). Therefore, mice as a model organism to investigate human biology are predicted on the biological, genetical, and physiological similarities between the species as mice get many of the same diseases, for the same genetic reasons (Perlman, 2016). Thus, mice are used as a convenient animal model in IBD. Further, the translation into clinical practice depends on the efficacy of the mouse model as well as on the associated human IBD disease type. Several kinds of IBD-models (**Table 1**), which are classified into chemically induced models (e.g., Dextran Sodium Sulfate), infection models (e.g., *Citrobacter rodentium*), immune activation-induced (T cell transfer) models, and genetically engineered, have been studied. Besides, genetically engineered mouse models in which a target gene is inducible overexpressed or deleted in a

specific cell type or all cells brought novel concepts on IBD pathogenesis. This type of animal model supports the concept of colitogenic gene-environment interactions and provides functional roles after infection or chemical challenge. Importantly, in many cases, animals with genetic defects do not develop spontaneous colitis. However, genetically modified animals reveal a functional role after infection or chemical challenge, supporting the concept of colitogenic gene-environment interactions. In general, there is no standard mouse model which is accepted by the US Food and Drug Administration (FDA) or the European Medicines Agency (EMA) (Koelink et al., 2018; Mizoguchi, 2012; Uhlig and Powrie, 2018) or the Swissmedic.

Table 1: Description of IBD-models

Models	Induction	Mechanism	Advantage/Disadvantage
Chemical (Wirtz et al., 2017)	2,4,6-tri-nitro-ben-zene sul-fonic acid (TNBS)	The hapten reagents of TNBS and oxazolone induces a T cell-mediated immunity against haptenized microbiota-derived proteins and luminal antigens.	Chemical-induced models are widely used as they are comfortable and rapid to develop and can be used with WT mice.
	Oxazolone DSS	DSS leads to IEC death, compromising barrier function, and subsequent intestinal inflammation.	Luminal microbiota may play a role in the development of the chemical induced intestinal inflammation
Infectious (Eckmann, 2006)	*Citrobacter rodentium*	*C. rodentium* attaches to the colonic and cecal epithelium and forms subcellular attaching and effacing (A/E) lesions. A/E-lesion forming pathogens do not spread systemically or invade more profound layers of the mucosa. *C. rodentium* is a predominantly mucosal pathogen.	Determination of the interactions between the host immune system and microbial pathogens in the intestinal tract, physiological consequences of neutralizing, and antimicrobial signaling pathways of the host defense.
	Salmonella typhimurium	In antibiotics pretreated mice, disseminated *S. typhimurium* infection resembles many aspects of human infection such as mucosal inflammation by rapid crypt loss, epithelial erosion, goblet cell loss, mucosal and submucosal infiltration with acute inflammatory cells, and edema.	Colonization of bacteria is limited to the intestinal mucosa. Loss of effective host defense due to stronger stimulus results in exacerbate mucosal inflammation. A few bacteria can reach the systemic side or the bloodstream. In the case of *S. typhimurium* pretreatment with antibiotics is needed.

| Immune activation (Eri et al., 2012) | T cell transfer | Two important concepts of the adoptive CD4^{+} T cell-based pathogenesis: (1) naïve CD4^{+} CD45RB^{high} T cells from the spleen and/or lymph nodes trafficking to the intestine where they cause severe intestinal inflammation, and (2) regulatory T cells are able to overcome the effect of the CD4^{+} effector T cells. Adoptive transfer of naïve T cells (CD4^{+} CD45RB^{high}) into immune deficient Rag KO mice react on gut antigens and become colitogenic T cells secreting cytokines that results in severe gut inflammation involving small as well as large intestines. | Studying multiple drug targets interfering the T cell-mediated cytokine production. Closer synchronization of the onset and severity of intestinal inflammation.

Introduction of homeostatic proliferation as an additional variable predisposing mouse to autoimmunity. |
| --- | --- | --- | --- |
| Genetically engineered (Mizoguchi et al., 2016) | Gene deletion

Gene insertion and/or alteration | In most gene deletion models (KO mice), genes encoding immune factors are deleted. This results in perturbations to the gut immune system and physiology. There are two ways of gene deletion: (1) conventional gene knock-out, (2) conditional knock-out. In conditional knock-out, a gene is deleted from a specific cell type.

Gene insertion affects the protein product due to a frameshift mutation. Gene expression can be altered by changing the structure and function of chromatin. Acetylation or deacetylation of histones may later transcriptional activity. Thus, gene insertion and/or alteration for example in the *NOD2* genes leads to increased susceptibility to CD but not to UC. | Genetically engineered mouse models carry the susceptibility genes which are identified in human IBD. Cutting-edge technologies such as cell-specific and conditional knock-out systems enhanced the ability to provide relevantly, and unexpected rationales for developing new therapeutic strategies for IBD.

Developmental abnormalities due to genetic defects or interindividual variability in the penetrance and activity of colitis. |

In general, murine models have been widely used in biomedical research due to the advanced knowledge of their genetics and the availability of many genetically modified mouse models facilitate the functional research (Nguyen et al., 2015; Perlman, 2016). Collectively, the mammalian digestive tract is strongly conserved. However, major differences between species being likely driven by diet, although humans and mice share strong similarities (Nguyen et al., 2015). Thus, the anatomy of the gastrointestinal tract

differs between these two species. Humans have evolved towards a smaller cecum and colon and a relatively longer small intestine as compared to the mouse digestive tract. In mice, the fermentation of indigestible food components is compartmentalized in the cecum. By contrast, in humans, the fermentation is taken over by the colon, and the cecum is vestigial. Additionally, the human colon is divided by haustra, small pouches caused by sacculation (sac formation), which give the colon its segmented appearance, whereas the mouse colon is rather smooth (Nguyen et al., 2015; Perlman, 2016). Further, the two species provide different environments that support the development of different gastrointestinal microbiota (Perlman, 2016). Nevertheless, the genetic and epigenetic similarities and differences between mice and humans as well as external factors such as living conditions and diet might influence the ability of murine models to represent disease-related changes that occur in humans (Nguyen et al., 2015; Perlman, 2016).

1.4. The amino acid transporter 4F2/CD98 heavy chain

The glycoprotein CD98, which was originally termed 4F2 and identified as an activation antigen of lymphocytes in 1981 (Haynes et al., 1981), is an integral membrane protein that contains a single-pass heavy chain which is covalently linked to a multi-pass light chain via a disulfide bond. CD98 is ubiquitously expressed in many cell types and almost all cell lines. Biochemical analysis revealed that the glycosylated protein CD98 is a type II transmembrane protein of around 80 kDa (CD98 heavy chain (CD98hc)) which is encoded by the gene *SLC3A2* for human and *Slc3a2* for mouse, and a protein of around 37 kDa (CD98 light chain (CD98lc)) encoded by the genes *SLC7A5/Slc7a5* (Cantor and Ginsberg, 2012; Deves and Boyd, 2000; Nakamura et al., 1999). Initially, CD98hc was also designated as fusion regulatory protein (FRP-1) to reflect its function in events of cell fusion, which leads to multinucleated giant cells such as osteoclasts (Cantor and Ginsberg, 2012; Mori et al., 2001; Mori et al., 2004; Tsurudome and Ito, 2000). The glycoprotein CD98 has two known biochemical function (Fenczik et al., 2001) in which the CD98hc binds to β1A and β3 integrins, and the CD98lc binds via disulfide bonds to the CD98hc (**Figure 1.3**). The CD98hc-integrin-interaction mediates adhesive signals which lead to the control of cell spreading, cell survival, as well as cell growth (Bajaj et al., 2016; Feral et al.,

2005; Prager et al., 2007). The CD98lc can be one of six several permease-type amino acid transporters. The two-best known CD98lc are the large amino acid transporters LAT-1, encoded by *SLC7A5/Slc7a5*, and the LAT-2, encoded by *SLC7A8/Slc7a8*. LAT-1 and LAT-2 import branched-chain amino acids (valine, leucine, isoleucine) and aromatic amino acids (phenylalanine, tryptophan, tyrosine) at the plasma membrane (Maeda et al., 2018). Thus, through the exchange of several essential amino acids, CD98 contributes to the survival and growth of many different cell types. Furthermore, CD98 is also involved in antigen presentation (Tsumura et al., 2012). Importantly, as CD98hc is expressed independently, the surface expression of the CD98lc is dependent on the presence of the CD98hc (Boulter et al., 2018; Cantor and Ginsberg, 2012; Reynolds et al., 2007; Verrey, 2003).
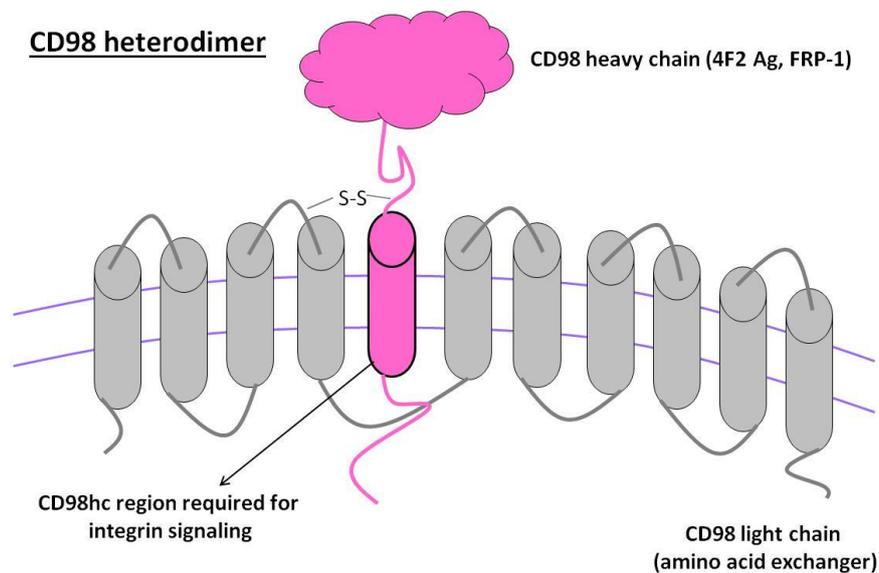
Figure 1.3: Schematic illustration of CD98. Type II transmembrane protein CD98 with a large, heavily glycosylated extracellular domain, and a short transmembrane domain and a cytoplasmic tail. Heterodimer of CD98 is formed by disulfide bonds between the membrane-proximal section of CD98hc (extracellular domain) and one of at least six possible CD98lc (LAT-1 or LAT-2). Integrin signaling of CD98hc is dependent on the transmembrane and cytoplasmic domains. The unusual protein CD98 combines functions of adhesive signaling as well as amino acid transport (adapted from: (Cantor and Ginsberg, 2012)).

Further, as CD98 was first identified in lymphocytes, it has been shown that anti-CD98 antibody or CD98 crosslinking have an effect in B and T cell activation and proliferation or has an effector function (Komada et al., 2006), by acting as a co-stimulatory receptor. Moreover, CD98 can prevent T-cell-

12

mediated autoimmunities, such as type 1 diabetes or multiple sclerosis. Additionally, the glycoprotein CD98 is crucial for the clonal expansion of B cells, which raises the opportunity that CD98 might serve a therapeutic target to block inappropriate adaptive immune responses (Cantor et al., 2009; Cantor et al., 2011; Cantor and Ginsberg, 2012).

The glycoprotein CD98 plays a crucial role in gut homeostasis and the intestinal innate immune responses (Yadav et al., 2016). IBD has been strongly correlated with increased expression of CD98 in humans but also mouse models. Additionally, pro-inflammatory cytokines induce upregulated expression of CD98 in intestinal epithelial cells, and CD98 is highly expressed in intestinal immune cells such as monocytes and macrophages. Overexpression of CD98hc by intestinal epithelial cells induces dysregulated gut homeostasis which leads to exacerbated colitis and colitis-associated cancer (Laroui et al., 2014; Nguyen et al., 2011). It has also been shown that the oral administration of nanoparticles loaded with CD98hc small interfering RNA attenuates the severity of colitis by decreasing CD98 expression in intestinal macrophages and epithelial cells (Xiao et al., 2014). Further, CD98hc-deficient Treg cells showed impaired proliferation ability (Ikeda et al., 2017). Thus, maintaining low levels of CD98 in intestinal epithelial cells and monocytes and macrophages could represent a potential therapeutic target for the treatment of IBD by improving the mucosal barrier which further leads to a decreased intestinal tissue damage (Yadav et al., 2016).

1.5. Aims of the study

The glycoprotein CD98, which was initially termed 4F2, was first identified in 1981. This type II transmembrane protein was originally described as a lymphocyte activation antigen. The glycoprotein CD98 contains a heavy chain which covalently links to the light chain via disulfide bonds. CD98hc can also bind to integrin β1A and β3 tails which leads to the regulation of integrin activation. As increased CD98 expression levels correlate with IBD, this study aims to elucidate the impact of CD98 on intestinal mononuclear phagocytes in a colitis-associated mouse model. Therefore, CD98hc$^{flox/flox}$ mice were crossed with Cx3cr1^{CreER} mice to obtain CD98hc$^{\Delta CX3CR1}$ animals. In the CD98hc$^{\Delta CX3CR1}$ mice, the

tamoxifen-induced Cre-mediated recombination leads to the knock-out of CD98hc (*Slc3a2*) in CX3CR1$^+$ mononuclear phagocytes. Further, this study shows that the conditional deletion of CD98 in CX3CR1$^+$ mononuclear phagocytes in the gut results in the impairment of Ly6C^{high} monocytes differentiation into macrophages, leading to attenuated colitis.

Aim I – Identification of amino acid transporter CD98hc in colonic mononuclear phagocytes.

CD98hc and CD98lc expression levels were elucidated in progenitor cells of mononuclear phagocytes homing in the mouse bone marrow, in mononuclear phagocytes of the mouse intestine *in vivo*, and CD98hc in BMDMs *in vitro*. Additionally, immunohistological staining of CD98hc in human colonic biopsies was implemented.

Aim II – Development of a mouse model to silence the expression of CD98hc in colonic CX3CR1$^+$ mononuclear phagocytes.

A newly generated mouse line, CD98hc$^{\Delta CX3CR1}$ mouse, was used in which the tamoxifen-inducible Cre/*lox*P-system leads to the deletion of CD98hc in CX3CR1$^+$ mononuclear phagocytes. Further, the kinetics revealed the optimal time frame of the CD98hc deletion in mononuclear phagocytes as well as their turnover/replenishment in the gut.

Aim III – Analysis of CD98hc deficient colonic mononuclear phagocytes and the impact on the colonic monocyte-macrophage development.

Investigation of CD98hc deletion in steady state as well as under inflammatory conditions highlighted the impact of the amino acid transporter on intestinal mononuclear phagocytes. Furthermore, the transcriptomic analysis revealed the effect of CD98hc on monocyte differentiation into intestinal macrophages.

2   METHODS

2.1.   Animals

C57Bl/6, CD98hc$^{flox/flox}$, Cx3cr1-GFP (B6.129P2-Cx3cr1$^{tm1Litt/J}$) and Cx3cr1^{CreER} (B6.129P2(Cg)-*Cx3cr1$^{tm2.1(cre/ERT2)Litt}$*/WganJ) were bred and maintained under specific pathogen free (SPF) conditions in the animal facility of the Department of Biomedicine, University of Basel, Basel, Switzerland. Dr. Hideki Tsumura, Division of Laboratory Animal Resources, Nation Research Institute for Child Health and Development, Tokyo, Japan, provided cryopreserved CD98hc$^{flox/flox}$ embryos (Tsumura et al., 2012). Embryo transfers were conducted in the Center for transgenic animals, University of Basel, Switzerland, and a colony of CD98hc$^{flox/flox}$ mice was established. CD98hc$^{flox/flox}$ mice were then crossed with Cx3cr1^{CreER} mice and called after that CD98hc$^{\Delta CX3CR1}$ mice, in which the tamoxifen-inducible, Cre-mediated recombination will lead to the excision of CD98hc (*Slc3a2)* in CX3CR1$^+$ cells. Female and male mice (6–12 weeks of age) were used for the experiments. The local animal welfare committee (animal protocol #2854_27600 (Canton Basel Stadt)) approved the experiments. All experiments were conducted by following the Swiss Federal and Cantonal regulations.

2.2.   CD98hc cKO mouse construct

Dr. Hideki Tsumura and Dr. Morihiro Ito provided cryopreserved CD98hc$^{flox/flox}$ embryos which were generated by flanking exon 3 with *loxP* sites (**Figure 2.1**). A neomycin selection cassette flanked by an Flp site was inserted into intron 3. The CD98hc neo mice were bred onto Flp deleter strain to excise the neomycin selection cassette. The CD98hc conditional knock-out mice (CD98hc$^{flox/+}$) were congenically rebred to C57BL/6N for eight generations (Tsumura et al., 2012).
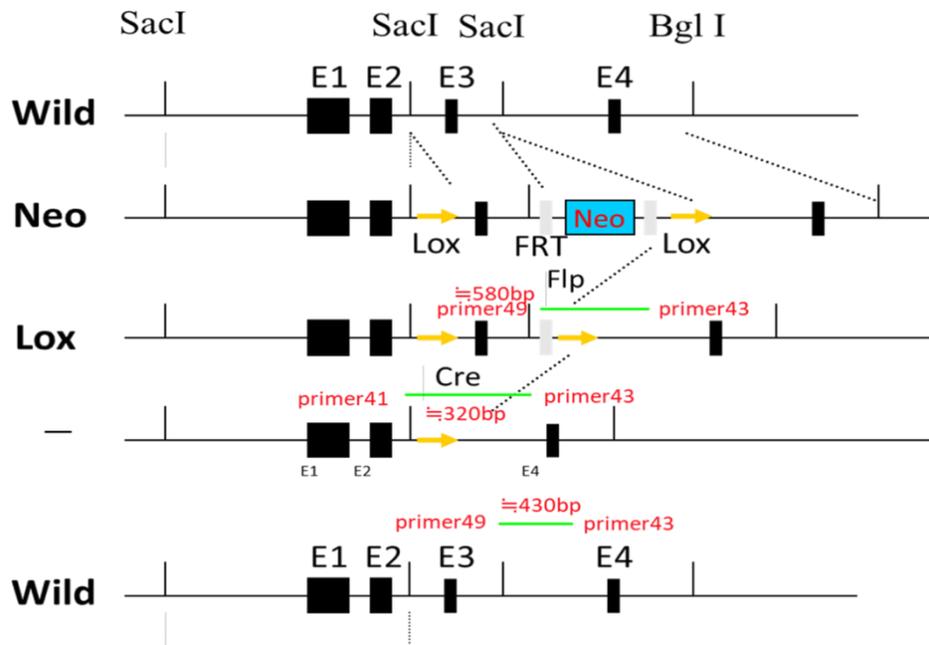
Figure 2.1: CD98hc cKO mouse construct (Tsumura et al., 2012)

2.3.   Patients and study population

Biopsies from 31 patients with Crohn`s disease (CD) and 31 patients with ulcerative colitis (UC) in RNAlater® stabilization solution were received from the Swiss Inflammatory Bowel Disease Cohort Study (SwissIBD cohort project 2016-12) and stored at -80ºC. This Swiss national cohort of patients with inflammatory bowel disease (IBD) was started in 2006 (Pittet et al., 2009). Gastroenterologists recruited patients with a diagnosis of CD or UC confirmed by endoscopy, radiology or surgery at least four months before inclusion in private practice, regional hospitals, and tertiary centers participating in the SwissIBD cohort study. Exclusion criteria were other forms of colitis or ileitis, no permanent residency in Switzerland or when informed consent was not admitted. Patients with active IBD ileocolonoscopic was performed to assess the activity of the disease and to rule out complications of the course of the disease. Patients with quiescent IBD surveillance ileocolonoscopic were carried out. Biopsies were taken from segments that appeared macroscopically inflamed. **Table S1** gives detailed patient`s characteristics. The biopsies used for immunofluorescence were obtained from the inflamed

and non- inflamed regions of patients from the Basel IBD cohort. Patient characteristics are given in **Table S2** (ethic protocol EKBB 139/13 (PB 2016.02242) (Ethics Committee for Northwest and Central Switzerland (EKNZ))).

2.4.   CD98 silencing

Tamoxifen (Free Base, MP Biomedicals) was dissolved in corn oil at a concentration of 20 mg/ml overnight at 37°C (shaking) and protected from light. The dissolved tamoxifen was stored at 4°C (protected from light stable up to one month). 75 mg tamoxifen/kg body weight were i.p. injected for five consecutive days into CD98hc$^{flox/flox}$ x Cx3cr1^{CreER} mice to activate the Cre-recombinase which leads to the silencing of CD98hc. Control CD98hc$^{flox/flox}$ x Cx3cr1^{CreER} mice received the carrier corn oil without tamoxifen.

2.5.   Nutrition of CD98hc$^{flox/flox}$ and CD98hc^{ΔCX3CR1} mice

Mice were fed by the mouse and rat chow #3436 (extrudate), produced by Granovit AG, Switzerland, which is the standard chow of the Department of Biomedicine (DBM), University Basel, Basel, Switzerland. For the experiments described in **3.3**, 5%/kg more L-leucine and 5%/kg more L-isoleucine was supplemented to the standard chow. Mice were fed with the amino acid enriched diet 4 weeks in advance before starting the experiments and during the experiments.

2.6.   Isoflurane anesthesia

Mice were anesthetized with the inhalation narcotic isoflurane for the collection of the liver. For induction of narcosis, mice were placed in a narcosis chamber that was flooded with 2-3% isoflurane in oxygen at 1-2 l/min. Anesthesia was confirmed by assuring a decrease in the respiration rate and by

testing for the absence of the pedal withdrawal reflex. For hepatectomy, anesthetized mice were placed under a mask with isoflurane flow as described above.

2.7. Euthanasia

Individual animals were euthanized by isoflurane overdose (5% isoflurane in oxygen, at 1-2 l/min), followed by exsanguination. Larger groups of animals were euthanized with CO_2 by flooding a euthanasia chamber with CO_2 at 2 l/min. Death of animals was confirmed by controlling for a color change of the eyes and the absence of respiratory movements, palatable heartbeat, and response to a toe pinch.

2.8. Dextran Sodium Sulfate induced colitis

Dextran Sodium Sulfate (DSS; 1.5 to 2.5%; MW: 36,000–50,000) was added to the drinking water of co-housed, weight-matched female (6–12 weeks of age) for five days. DSS containing water was sterile filtered before it was given to the animals. On day 5, DSS in drinking water was exchanged by regular drinking water to induce recovery from colitis. Mice were daily monitored for clinical signs of colitis as described in section **2.9**. The variation of DSS concentrations resulted due to the different Lot-Numbers of the product.

2.9. Clinical colitis score

Clinical signs of colitis were observed by using the following scores (Steinert et al., 2017): rectal bleeding: 0 - absent, 1 - bleeding; rectal prolapses: 0 - nil, clear prolapse - mice euthanized; stool consistency: 0 - normal, 1 - loose stools, 2 - diarrhea; position: 0 - normal movement, 1 - reluctance to move, 2 - hunched position; appearance of the fur: 0 - normal appearance, 1 - ruffled fur, 2 - spiky fur; weight loss: 0 – no loss, 1 - body weight loss 0-5%, 2 - body weight loss >5 - 10%, 3 - body weight loss

> 10 - 15%, 4 - body weight loss > 15%. Once per day the blinded investigator observed the animals. If the total score was ≥ 4, the animals were monitored twice per day. The respective animal was euthanized, when the total score was ≥ 6, when an individual animal lost > 15 % body weight, when gross bleeding occurred, or when rectal prolapse was noted.

2.10. Isolation of bone marrow cells

After the preparation of femurs and tibias, connective tissues and muscles were removed from femurs and tibias, and the bones were opened at the epiphysis. A syringe with a 25-gauge needle was placed into the ends of the opened femurs and tibias. Bone marrow cells were flushed out with RPMI 1640 medium. The collected cells were passed through a 70 μm cell strainer to remove cell clumps and bone fragments. Cells were pelleted by centrifugation. The cells were counted and processed for *in vitro* cultures (bone marrow-derived macrophages - BMDMs) or for flow cytometry analysis.

2.11. Colonic lamina propria cell isolation

The isolated colon was opened longitudinally and washed with PBS to remove debris and mucus. The intestinal epithelium was removed by incubation in 5 mM EDTA in Ca^{2+}/Mg^{2+}-free PBS at 37°C under gentle shaking for 10 min for a total of three incubations. After every incubation cycle, the tubes were vortexed for 30 s, and the tissue pieces were transferred into fresh EDTA/PBS. The colon was washed in PBS to remove residual EDTA. The tissue was cut as small as possible and digested with 0.5 mg/ml Collagenase type VIII and 10 U/ml DNase in RPMI 1640 for 20-25 min at 37°C in a water bath with continuous shaking (200 rpm). Every 5 min, the tubes were manually vortexed for 30 s. Supernatants were collected and passed through a 70 mm cell strainer, and cLP cells were pelleted by centrifugation. The cells were counted and processed for flow cytometry analysis.

2.12. Yolk sac cell isolation

The yolk sac (YS) was harvested from embryos at E8.5. Embryos were exsanguinated through decapitation in PBS containing 3% FCS. To obtain a single-cell suspension, the YS was incubated in RPMI 1640 medium containing 1 mg/ml collagenase type VIII, 100 U/ml DNase I and 3% FCS at 37°C for 30 min. The digested YS was poured through a 70 µm cell strainer, and erythrocytes were lysed (3–5 min at RT with Tris-Lysing buffer). Cells were counted and processed for flow cytometry analysis.

2.13. Liver perfusion and liver cell isolation

The portal vein of an anesthetized (Isoflurane) animal was punctured with a 25-gauge needle. The liver was perfused with 10 ml liver perfusion medium followed by 5 ml liver digest medium after cutting the lower vena cava. After removing the gallbladder, the liver was placed into a petri dish and cut into small pieces. The tissue pieces were transferred into a 50 ml tube containing 5 ml liver digest medium and digested for 30 min at 37°C. Afterward, the digested tissue was poured and mashed through a metal cell strainer to remove connective tissue and centrifuged for 5 min and 500 rpm at RT. The supernatant (solution A) and pellet (solution B) were separated into two tubes. The solution A was centrifuged for 5 min and 1,400 rpm at RT. To solution B 40 ml PBS was added and centrifuged for 5 min and 500 rpm at RT. The supernatant from solution A was discarded and the supernatant form solution B was added to the pellet of solution A. After centrifugation for 5 min and 1,400 rpm at RT, the supernatant was discarded, and the pellet frothed up with 3 ml of PBS/2% FBS supplemented with 0.1% w/v sodium azide and 10 mM EDTA and 3.5 ml 70% Percoll to obtain the 'Cell-Percoll-Suspension'. A Percoll gradient was prepared and centrifuged for 20 min and 2,000 rpm without break. The fat layer on the top has been removed, and the interphase which contains the lymphocytes and erythrocytes as well as the whole upper liquid phase to increase the cell yield were collected. After the erythrocytes were lysed (3–5 min at RT with Tris-Lysing buffer), the cells were counted and processed for flow cytometry analysis.

2.14.   Langerhans cell isolation

After cutting off the mouse ears, the ears are divided into dorsal and the ventral halves, from which the cartilage is removed with forceps. The ears were then placed dermal side down onto PBS containing 2.5 mg/ml dispase II and were incubated for 2 hours at 37°C. The dissociated epidermal sheets are placed in stop medium (2% FCS in PBS) and further transferred into a 50 ml tube with 20 ml RPMI 1640 medium containing 10% FCS and supplemented with 0.05mM 2-mercaptoethanol (2-ME), 100 U/ml penicillin, and 100 mg/ml streptomycin. To release the Langerhans cells, the tube was gently shaking for 30 min at 37°C in a water bath. The remaining epidermal pieces and cell suspension were filtered through a 70 µm cell strainer and cells pelleted by centrifugation. The cells were counted and processed for flow cytometry analysis.

2.15.   Bone marrow-derived macrophages

Murine bone marrow cells were cultured in 6-well plates in RPMI 1640 medium containing 10% FCS and supplemented with 0.05 mM 2-ME, 100 U/ml penicillin and 100 µg/ml streptomycin. Macrophages were generated by adding 20 ng/ml M-CSF. After seven days, macrophages were either stimulated with 100 ng/ml Lipopolysaccharide (LPS) from *Escherichia coli* O111:B4 (Sigma) and 10 ng/ml recombinant mouse IFN-γ or with 10 ng/ml recombinant mouse IL-4 and 10 ng/ml recombinant mouse IL-13 for 6 hours before cells were analyzed. RT-qPCR was used for the characterization of LPS + IFN-γ or IL-4 + IL-13 stimulated BMDMs by specific primer sequences for the amplification of *Actb* (Actin-β), *Tnf, iNos, Il-6, Mcp-1, Il-6, Il-1β, Kc, Chil3, Retnla1, Mrc1, Mgl1,* and *Il-10,* which are listed in **Table S3**. For *in vitro* CD98 silencing tamoxifen dissolved in DMSO (Roth) was added into the culture during the macrophage generating and during LPS + IFNγ or IL-4 + IL-13 stimulation or D-phenylalanine was added 1 hour prior and during LPS + IFNγ or IL-4 + IL-13 stimulation.

2.16. Surface staining for flow cytometry

Following cell isolation, cells were counted and distributed at 0.5-2.0 x 10^6 cells per well to 96-well V-bottom plates. The cells were pelleted (600 RCF for 2 min), the supernatant flicked off, and the cells were washed with PBS. Subsequently, to exclude dead cells from the analysis, the cells were incubated with 100 µl of a fixable viability dye diluted in PBS. Simultaneously, a mAb (Clone 93) directed against the FcγRIII/II CD16/CD32 (0.5 µg mAb/10^6 cells) was added to prevent the unspecific binding of mAbs, which were used for cell labeling in consecutive steps, to Fc receptors, and incubated for 20 min at 4°C. Cells were washed in PBS/2% FBS supplemented with 0.1% w/v sodium azide and 10 mM EDTA, incubated with the relevant mAb for 20 min at 4°C and washed again twice. When primary antibodies were biotin-coupled antibodies, cells were incubated with fluorescently labeled streptavidin for 20 min at 4°C. Data were acquired with the BD LSRFortessa™ X-20 flow cytometer and analyzed using FlowJo software version 10.5.3. Cell sorting was carried out with the BD FACSAria™ III equipment. In all experiments, forward scatter (FSC)-H versus FSC-A was used to gate on singlets, with dead cells excluded, and CD3, CD19, NK1.1, Ly6G, and Ter119 expressing cells were removed from further analysis. **Table S4** lists the utilized antibodies. In cases when the acquisition was not conducted on the same day, cells were fixed with 4% formalin solution for 15 min in the dark at RT, washed twice, and stored in FACS buffer for acquisition within the following three days.

2.17. Intracellular staining of cytokines

In order to detect cytokine production in DSS-induced colitis of tamoxifen- or corn-oil-treated animals, up to 2.0 x 10^6 freshly isolated cells were seeded into 96-well V-bottom plates and washed once with FACS buffer. Following viability and surface staining, cells were fixed and permeabilized for 20 min at 4°C with 100 µl per well BD Cytofix/Cytoperm solution. Afterward, cells were washed twice with BD Perm/Wash buffer and then incubated with dilutions of the relevant antibodies shown in **Table S5** in 50 µl Perm/Wash buffer. After 20 min of incubation at 4°C, cells were washed twice and either resuspended in FACS buffer for acquisition on the same day or fixed with Cytofix/Cytoperm solution for a second time to allow for acquisition within the following three days.

2.18. Endoscopy

After anesthetizing the mice by intraperitoneal injection of 200 µl anesthetic solution containing 1 mg/ml xylazine (Xylazin Streuli ad us. vet., injection solution) and 100 mg/ml ketasol (Ketasol®-100 ad us. vet., injection solution) in sterile PBS, the distal 3 cm of the colon and the rectum were examined with a tele pack vet X LED RP100 endoscope (Karl Storz).

2.19. Tissue embedding in paraffin

Tissue sections of approximately 0.5 cm length were taken from the colon of healthy or diseased mice and directly placed in 1 ml 4% formalin in a 1.5 ml reaction tube. The tissue samples were fixed for a minimum of 48 hours at RT, washed once with PBS, and stored in 70% ethanol at 4°C until further usage. For dehydration and embedding, the fixed tissue was transferred into histology cassettes. Dehydration was performed by submerging the samples in increasing concentrations of ethanol: 70% ethanol for 2 x 30 min, 96% ethanol for 2 x 30 min, and 100% ethanol for 2 x 30 min. The ethanol was then cleared by incubation in xylene for 2 x 1 hour. Afterward, the tissues were infiltrated with melted paraffin for 1 hour at 60 °C. After a second infiltration step in melted paraffin overnight, the tissue samples were embedded in paraffin blocks.

2.20. H&E staining and histological colitis score

Colonic tissue was fixed in 4 % formalin and embedded in paraffin blocks. Six-micrometer sections were prepared using an electronic rotary microtome (Thermo Fisher Scientific). Before Hematoxylin and Eosin (H&E) staining, the glass slides containing the sections were incubated for 10 - 20 min at 60°C to bond the tissue to the glass and to melt the paraffin. All of the following steps were conducted by submerging the glass slides in the appropriate chemicals filled into cuvettes. First, the tissue sections were deparaffinized in xylene I (2 min), and xylene II (5 min). Second, the sections were rehydrated in a decreasing ethanol row: 100% ethanol I (2 min), 100% ethanol II (5 min), 96% ethanol I (2 min), 96%

ethanol II (5 min), 70% ethanol (2 min), 50% ethanol (2 min), and finally A. dest. (3 min). Third, sections were stained with Mayer's hematoxylin solution (5 – 10 s) and differentiated under flowing tap water (2 min) before staining with 1% eosin (45 – 60 s). Afterward, the sections were washed with A. dest. I, and II (2 min each) and dehydrated with 90% ethanol I (2 min), 90% ethanol II (2 min), 100% ethanol I (2 min), and 100% ethanol II (5 min). In the last steps, the sections were cleared in xylene I (2 min), and xylene II (2 min) before mounting with mounting medium. Images of H&E stained sections were acquired with an Olympus BX63F (Olympus) microscope and processed with cellSens Dimension software (Olympus).

2.21. Histological assessment

Histological features of colonic inflammation was scored with a previously published scoring system (Souza et al., 2017): extent of destruction of normal mucosal architecture (0: normal; 1: mild; 2: moderate; 3: extensive damage), presence and degree of cellular infiltration (0: normal; 1: mild; 2: moderate; 3: transmural infiltration), extent of muscle thickening (0: normal; 1: mild; 2: moderate; 3: extensive thickening), presence or absence of crypt abscesses (0: absent; 1: present), and the presence or absence of goblet cell depletion (0: absent; 1: present). Each feature score was summed up to a maximum possible score of 11. Histological scores were assessed by two independent investigators in a blinded fashion and for each animal, the mean histological score was determined.

2.22. Immunohistochemistry and immunofluorescence

Cryopreserved biopsies of patients with CD or with UC embedded in Tissue-Tek O.C.T. compound were acquired from the Basel IBD cohort. Immunohistochemistry (IHC) was performed on six-μm sections using a polyclonal rabbit anti-human CD98hc. Primary antibody binding was detected with an Alexa Flour 647 goat anti-rabbit IgG secondary antibody. The six-μm sections from cryopreserved mouse tissues were fixed in 4% formalin for 15 min at RT. Afterward, sections were blocked with goat serum in DPBS/0.4% Triton-X-100 for 30 min and stained with the primary monoclonal rabbit anti-

24

mouse CD98 mAb overnight in a humidified container at 4°C. Primary antibody binding was detected with an Alexa Flour 647 goat anti-rabbit IgG secondary antibody. Sections were counterstained with NucBlue™ Live Cell Stain Ready Probes™ reagent and imaged with a Nikon A1R Nala confocal microscope.

2.23. Genotyping of CD98hc^{flox/flox} and CD98hc^{ΔCX3CR1} mice

The determination of mouse genotypes has been done by taking toe clippings from mice of less than three weeks of age. The biopsies were digested with 0.4 mg/µl Proteinase K (Roche) in 100 µl DirectPCR (Tail) (Viagen Biotech) overnight at 56°C in a PCR cycler. Afterward, the enzyme was heat inactivated at 85°C for 45 min. Two separate PCR reactions amplified the CD98hc^{flox/flox} and the CD98hc^{ΔCX3CR1} gene locus in order to genotype the transgenic mice. The DreamTaq PCR Master Mix (2x) (Thermo Fisher Scientific) was used in 25 µl reactions, and in accordance with manufacturer's instructions with 1 µl of the digested tissue, and the appropriate forward and reverse primers shown in **Table S6** in a final concentration of 0.6 µM for CD98hc^{flox/flox} or 1.2 µM for CD98hc^{ΔCX3CR1} per primer sequence. The following conditions were used for the DNA amplification in a PCR thermocycler (Biometra):

CD98hc^{flox/flox}

Initial Denaturation	95°C	5 min
Denaturation	95°C	60 s
Annealing	55°C	30 s
Elongation	72°C	45 s
Final elongation	72°C	10 min

Denaturation, Annealing, Elongation: 40 cycles

CD98hc$^{\Delta CX3CR1}$

Initial Denaturation	95°C	3 min
Denaturation	95°C	30 s
Annealing	60°C	30 s
Elongation	72°C	2 min
Final elongation	72°C	10 min

35 cycles (Denaturation, Annealing, Elongation)

The samples were cooled at 4 °C for short term storage. The amplified DNA fragments were separated by gel electrophoresis in a 2% agarose gel, and prepared and run in TRIS-acetate-EDTA (TAE)-buffer for 60 min at 80 V. For the visualization of the DNA fragments under UV light nuclear dye RedSafe™ was added during the preparation of agarose gels. A typical result of CD98hc$^{flox/flox}$ and CD98hc$^{\Delta CX3CR1}$ mice is given in **Figure 2.3**
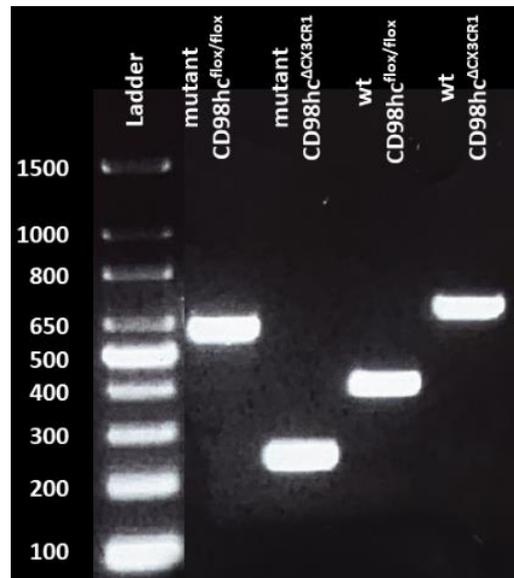
Figure 2.3: Genotyping of CD98hc$^{flox/flox}$ and CD98hc$^{\Delta CX3CR1}$. Product size CD98hc$^{flox/flox}$: Flox: ∼ 600bp; Wild: ∼ 400bp. Product size CD98hc$^{\Delta CX3CR}$: Wild: ∼ 695bp; Mutant: ∼ 300bp.

2.24. RNA isolation from cells and tissues

RNA was extracted from indicated tissues or cells by guanidinium thiocyanate-phenol-chloroform extraction. The samples were lysed in TRI-Reagent (ZymoResearch). Cells were lysed by repetitive pipetting, and tissues were homogenized using 2.0 ml Lysing Matrix D tubes (1.4 mm ceramic beads) with a FastPrep-24 5G Instrument (MP Biomedicals) at speed 6 for 30 – 60 s. Then, 200 µl chloroform per milliliter of TRI-reagent was added to the lysed sample, mixed vigorously, and incubated for 2-3 min at RT to isolate the RNA. After centrifugation for 15 min at 12,000 RCF and 4°C, the RNA-containing aqueous phase was transferred into 500 µl cold isopropanol and incubated for 10 min to allow precipitation of the RNA. The precipitated RNA was pelleted at 12,000 RCF and 4°C for 10 min, the supernatant was discarded, and the RNA pellet was washed with 1 ml ice-cold 75% ethanol. Subsequently, the washed RNA pellet was centrifugation at 7,500 RCF and 4°C for 5 min. The ethanol supernatant was carefully removed, and the pellet air-dried for ∼ 5 min. The RNA was dissolved in 20 µl nuclease-free water and incubated in a heat block at 55°C for 10 min. The NanoDrop 2000 (Thermo Fisher Scientific) was used for the spectrophotometric measurement at 260/280 nm to determine the RNA concentration. Contaminating DNA was removed with the TURBO DNA-free™ Kit (Invitrogen) according to the manufacturer's instructions.

2.25. RNA isolation from DSS-treated animals

Samples from the intestine of DSS-treated mice were purified by spin-columns to ensure complete removal of DSS residues from the RNA preparations. Therefore, the RNA was extracted with the DirectZol Miniprep Kit including the provided on-column DNase treatment (Zymo Research) after the guanidinium thiocyanate-phenol-chloroform extraction described in **2.24**. The procedure has been done according to the manufacturer recommended user manual.

2.26. Reverse transcription

To reverse-transcribe, the DNase-treated RNA into cDNA, the MultiScribe™ Reverse Transcriptase Kit (Applied Biosystems) was used. The procedure has been done according to the manufacturer recommended user manual.

2.27. Gene expression analysis

The determination of the gene expression has been performed by qPCR with gene-specific primers. The used mouse/human primer sequences for the amplification of *Gapdh/GAPDH* (glyceraldehyde 3-phosphate dehydrogenase), *Actb* (Actin-β), *Il1β, Il6, Il10, Tnf, Slc7a5, Slc7a6, Slc7a7, Slc7a8, Slc7a10, Slc7a11, Il19, IFNγ, Chil3, Mgl1, Mcp-1, Mrc1, Retnla, iNos, Kc, SLC3A2*, and *SLC7A5* are listed in **Table S3**. qPCR was carried out using the SsoFast™ EvaGreen® Supermix (Bio-Rad Laboratories) according to the manufacturer recommended user manual. The PCR-reactions were run as a 10 μl reactions in 384-well plates on a ViiA 7 Real-Time PCR System (Applied Biosystems). 15 ng – 25 ng of cDNA was used per reaction. To determine the relative gene expression, the cycle threshold (Ct) values computed by the ViiA7 Software v1.2 (Applied Biosystems) was used. Normalization of a gene of interest to the housekeeping genes *Gapdh* or *Actb* was calculated by the $2^{-\Delta Ct}$ method. All reactions were run in triplicates, and the mean $2^{-\Delta Ct}$ was calculated for each gene. Genes with a Ct-values > 35 were considered to be below the detection limit. The smallest possible $2^{-\Delta Ct}$ value of the detection limit of an experiment was used for the graphical presentation of gene expression data on a logarithmic scale. This value is defined as ΔCt (detection limit) = ΔCt_{max} (gene of interest) – ΔCt_{min} (housekeeping gene), where ΔCt_{max} (gene of interest) equals 35, and where ΔCt_{min} (housekeeping gene) is the smallest Ct value of a housekeeping gene observed in the specific experiment.

2.28. Single-cell RNA-sequencing

For single-cell RNA-seq, lamina propria cells positive for Ccr2 and/or Cd64 were sorted from 4 control mice and 4 induced CD98hc$^{\Delta CX3CR1}$ mice and counted. Cell suspensions volumes aiming at a targeted recovery of ~ 3,000 cells were loaded on the wells of a 10× Genomics Chromium Single Cell Controller (one well per mouse replicate). Single-cell capture, and cDNA and library preparation were performed with a Single Cell 3' v2 Reagent Kit (10× Genomics) according to manufacturer's instructions. Sequencing was performed on one flow-cell of an Illumina NexSeq 500 machine at the Genomics Facility Basel of the ETH Zurich. Paired-end reads were obtained, and their quality was assessed with the FastQC tool (version 0.11.5). The length of the first read was 26-mers, composed of individual cells barcodes (16nt) and molecular barcodes (unique molecular identifiers; 10nt). The length of the second read, composed of the transcript sequence, was 58-mers. The samples in the different wells were identified using sample barcodes of 8nt. Sequencing files were processed with the Cell Ranger software (version 2.1.0, provided by 10× Genomics and available at https://support.10xgenomics.com/single-cell-gene-expression/software/downloads/latest) to perform sample and cell demultiplexing, read alignment to the mouse mm10 genome assembly with STAR, and to generate read count table. Default settings and parameters were used, except for the version of STAR updated to 2.5.3a, and the STAR parameters *outSAMmultNmax* set to 1 and *alignIntronMax* set to 10000. The reference transcriptome "refdata-cellranger-mm10-1.2.0", provided by 10× Genomics and based on Ensembl release 84 (Zerbino et al., 2018), was used (available at c http://cf.10xgenomics.com/supp/cell-exp/refdata-cellranger-mm10-1.2.0.tar.gz). Because the mouse strain includes a fluorescent reporter gene, a generic EYFP sequence obtained from https://www.addgene.org/browse/sequence_vdb/6394/ was added to the reference transcriptome before mapping. Samples were merged with the "cellranger aggregate" procedure without downsampling.

Further analysis was performed starting from the unique molecular identifiers (UMI) counts matrix using the scran (version 1.8.4) and scater (version 1.8.4)(McCarthy et al., 2017) Bioconductor packages, following mostly the steps illustrated in the simpleSingleCell Bioconductor workflow (version 1.2.1) (Lun et al., 2016).

Based on the clearly bimodal distributions observed across cells, cells with $\log_{10}$ library sizes less than 2.8 (i.e., a minimum of 630 reads), with $\log_{10}$ total number of features detected less than 2.6 (i.e., a minimum of 399 genes detected), with more than 5% of UMI counts attributed to the mitochondrial genes (Ilicic et al., 2016), or with any read attributed to the Hemoglobin genes were filtered out. Low-abundance genes with average $\log_2$ CPM (counts per million reads) values lower than 0.005 were filtered out. The resulting filtered dataset included expression values for 11,947 genes for 3,213 cells, ranging from 83 to 724 cells per sample, for a total of 1,863 control cells, and 1,350 CD98 cKO cells. An average of 1,645 genes was detected per cell.

The raw UMI counts were normalized with the size factors estimated from pools of cells to avoid the dominance of zeros in the matrix (Lun et al., 2016; Vallejos et al., 2017). A mean-dependent trend was fitted to the variances of the log expression values of endogenous genes to distinguish between genuine biological variability and technical noise (Brennecke et al., 2013), under the assumption that most genes are not differentially expressed across cells, and their variance is mainly technical (*trendVar* function of the scran package with loess trend and span of 0.05 to better fit the sparse data). The fitted technical noise was subtracted, and the residual "biological" component of the gene variance was used to denoise the PCA with the *denoisePCA* function of the scran package. A t-stochastic neighbor embedding (t-SNE) was built with a perplexity of 30 using the top 500 most variable genes and the denoised expression matrix as input.

Clustering of cells into putative subpopulations was done on normalized log-counts values using hierarchical clustering on the Euclidean distances between cells (with Ward's criterion to minimize the total variance within each cluster; package cluster version 2.0.7-1). The clusters of cells were identified

by applying a dynamic tree cut (package dynamicTreeCut, version 1.63-1), which resulted in 9 clusters. Marker genes specific for each cluster were identified with the *findMarkers* function of the scran package, which fits a linear model to the expression values for each gene using the limma framework. Differential expression between cKO and control cells stratified by differentiation stage was performed by summing the UMI counts of cells from each sample in each cluster when at least 20 cells could be aggregated. This resulted in a total of 32 aggregated samples, and at least 3 replicates per condition for each cluster. The genes were filtered to keep those with CPM (counts per million reads sequenced) values higher than 1 in at least 3 samples and detected in at least 20 individual cells. The aggregated samples were then treated as bulk RNA-seq samples (Lun and Marioni, 2017): the package edgeR (version 3.24.2) (Robinson et al., 2010) was used to perform TMM normalization (Robinson and Oshlack, 2010), and to test for differential expression with the Generalized Linear Model (GLM) framework. Genes with a false discovery rate lower than 5% were considered differentially expressed. Gene set enrichment analysis was performed with the function camera (Wu and Smyth, 2012) using the default parameter value of 0.01 for the correlations of genes within gene sets, on gene sets from the Hallmark collection (Liberzon et al., 2015) of the Molecular Signature Database (MSigDB, version 6.0) (Subramanian et al., 2005). We considered only sets containing more than 10 genes and gene sets with a false discovery rate lower than 5% were considered significant.

Following (Duò et al., 2018) the building of a self-organizing map (SOM) and its minimal spanning tree was performed using the FlowSOM Bioconductor package (version 1.14.0) (Van Gassen et al., 2015), using the 30 first principal components of the denoised PCA as input, and a 9×9 grid.

Two-dimensional cell densities were calculated with the kde2d function of the MASS package (version 7.3-50). Differential cell densities on pairs of principal components were calculated as the $\log_2$ of the ratio of the density of cKO cells over the density of control cells (after a prior count of 1e-03 was added to the density estimates)

Remaining statistical analysis on the expression dataset analysis and plotting were performed using the R software (version 3.5.1).

The scRNA-seq dataset is available in the GEO database under accession GSE126574. The data are available under the following link: https://www.ncbi.nlm.nih.gov/geo/query/acc.cgi?acc=GSE126574 Data will be private until the submitted manuscript is accepted.

2.29.   Quantitative determination of nitrite and nitrate

The Nitric Oxide Assay Kit (Invitrogen) was used to determine nitrite and nitrate in BMDMs culture supernatant of non-stimulated, LPS + IFNγ, and IL-4 + IL-13 stimulated macrophages. The procedure has been done according to the companies recommended user manual. Data were acquired with the BioTek™ Synergy™ H1 Hybrid Multi-Mode All Detection Modes Microplate Readers.

2.30.   Statistics

The data were analyzed with GraphPad Prism software (version 7.03) and are presented as dot plots in which the median of each experimental group is presented in addition to the individual samples. Statistical significance was calculated using the Mann–Whitney U test for two groups or using the Kruskal–Wallis test followed by the Dunn's correction test for multiple comparisons. When the data are presented as a time course, the arithmetic means ± standard deviation (SD) is shown. Statistical significance was calculated using two-way ANOVA with the Sidak's correction. Outliers were identified with the Grubb test during the analysis of data acquired from samples from the Swiss IBD Cohort only. The p-values are indicated as follows: $*p \leq 0.05$, $**p \leq 0.01$, $***p \leq 0.001$, and $****p \leq 0.0001$.

3.1.   High CD98hc expression by colonic lamina propria macrophages and their progenitors

Recent reports suggested that the overexpression of CD98hc by intestinal epithelial cells leads to more severe colitis and colitis-associated cancer (Nguyen et al., 2011), and the oral administration of nanoparticles loaded with CD98 small interfering RNA attenuates the severity of colitis. The cellular uptake of these nanoparticles leads to a decreased CD98 expression by intestinal macrophages and epithelial cells (Xiao et al., 2014). Nevertheless, the expression levels of CD98 by intestinal macrophages and their progenitors have not been studied to date in detail. The first aim of the study was to define CD98 expression levels by the monocyte-macrophage dendritic cell progenitors (MDP), the common monocyte progenitors (cMoP), and the monocytes (Mo) in the bone marrow (BM) (Hettinger et al., 2013). Therefore, flow cytometry was used to analyze BM cells from unmanipulated mice. The BM cells could be distinguished in Lin^- (CD3, CD19, NK1.1, Ly6G, Ter119) $CD115^+$ $CD117^+$ $CD135^+$ $Ly6C^-$ $CD11b^-$ MDPs, in Lin^- $CD115^+$ $CD117^+$ $CD135^-$ $Ly6C^+$ $CD11b^-$ cMoPs, and in Lin^- $CD115^+$ $CD117^+$ $CD135^+$ $CD11b^+$ monocytes, which could be further discriminated in $Ly6C^{high}$, $Ly6C^{mid}$, and $Ly6C^{low}$ monocytes (**Figure 3.1A**). About all the cells of MDPs, cMoPs, and $Ly6C^{high}$ monocytes were CD98 positive. The $Ly6C^{mid}$ and $Ly6C^{low}$ monocytes reveal a slight decrease in CD98 positive cells, which is also shown by the median fluorescence intensity (MFI) (**Figure 3.1B and 3.1C**). Furthermore, t-distributed stochastic neighbor embedding (t-SNE) analysis visualizing the highly complex multi-dimensional flow cytometry dataset, showed the distribution of the different characterized cell populations in the BM. These different t-SNE clusters were also positive for the CD98 (**Figure 3.1D**). The major cLP macrophages originate from the extravasation of $Ly6C^{high}$ blood monocytes into the cLP. These cells pass through the well described 'monocyte waterfall' during the differentiation phase into intestinal macrophages (Schridde et al., 2017). The cLP cells can be distinguished in Lin^- $CD11b^+$ $CCR2^+$, and in Lin^- $CD11b^+$ $CD64^+$ populations. The $CCR2^+$ population exhibit the 'monocyte waterfall' from $Ly6C^{high}$ MHC II^- via $Ly6C^{mid}$ MHC II^+, towards to $Ly6C^{low}$ MHC II^+ subpopulations, which correspond to extravasated blood monocytes. The $CD64^+$ population exhibit two subpopulations, which are either $Ly6C^{low}$ MHC II^- or $Ly6C^{low}$ MHC II^+. These subpopulations have typical features of tissue

macrophages (Tamoutounour et al., 2012) (**Figure 3.1E**). The distinct subpopulations of the cLP showed high CD98 expression level and the CD98 MFI was not significantly impaired (**Figure 3.1F and 3.1G**). Also, the t-SNE clusters of the colonic mononuclear cells could confirm the high CD98 expression of the monocyte and macrophage subpopulations (**Figure 3.1H**).
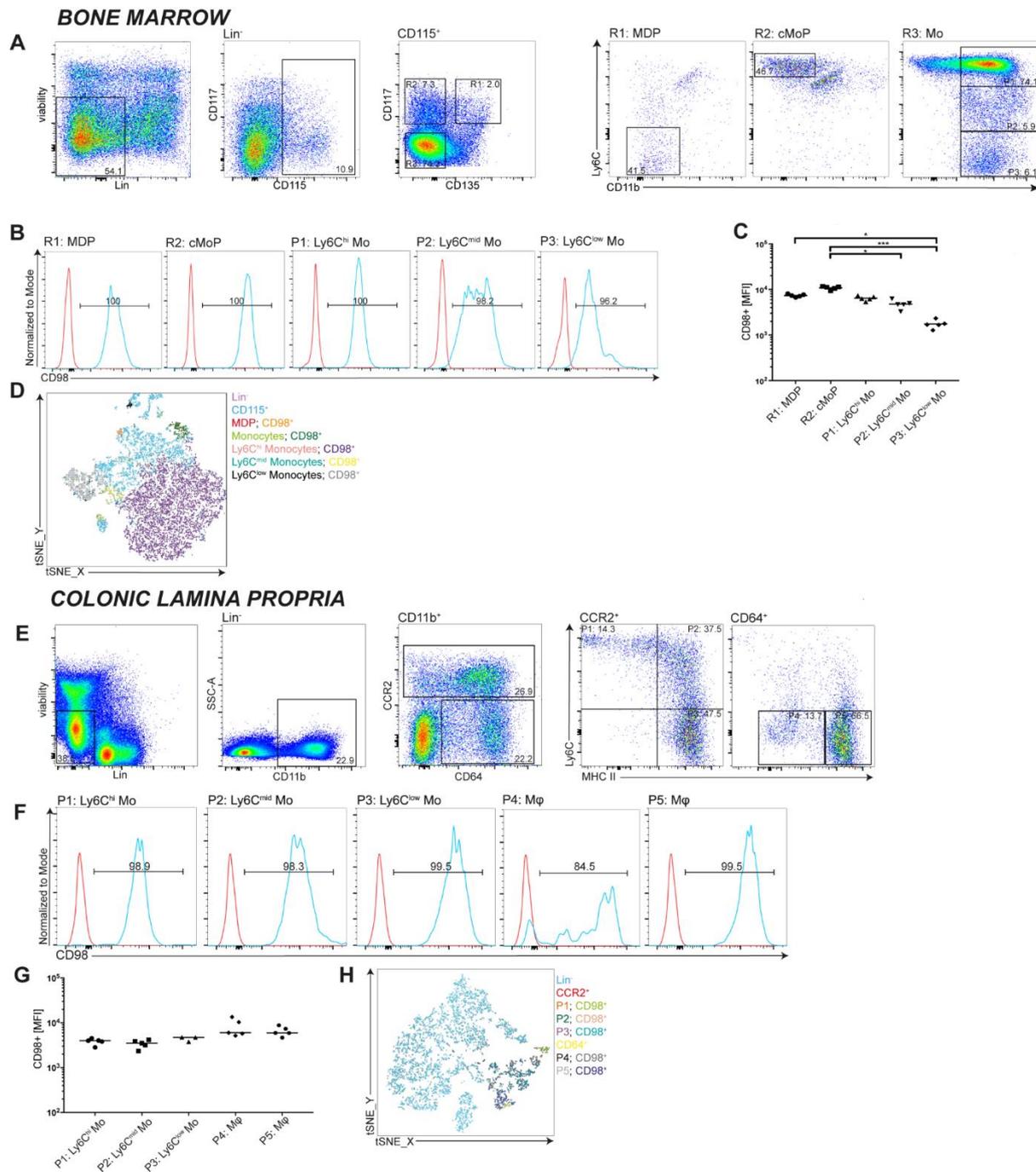

Figure 3.1: Monocytes, Macrophages, and their progenitors express CD98. Bone marrow cells were isolated from C57Bl/6 wild type (WT) mice. Monocyte and dendritic cell progenitors (MDP), common monocyte progenitors (cMoP) and monocytes were analyzed for CD98 expression. (**A**) After gating on viable, and lineage negative cells (CD3, CD19, NK1.1, Ly6G, Ter119),

MDPs were identified as CD115^{+}, CD117^{+}, CD135^{+}, Ly6C^{-}, and CD11b^{-} cells. cMoPs were defined as CD115^{+}, CD117^{+}, CD135^{-}, Ly6C^{+}, and CD11b^{-} cells, and monocytes characterized as CD115^{+}, CD117^{-}, CD135^{-}, and CD11b^{+} cells with Ly6C^{high}, Ly6C[mid], and Ly6C^{low} expression. (**B**) Expression and (**C**) median fluorescence intensity (MFI) of the glycoprotein CD98 by indicated monocytes and their progenitors. Red histograms represent the fluorescence minus one (FMO) control, blue histograms represent CD98 stained cells. Numbers in histogram plots indicated the percentage of CD98^{+} cells. Each dot represents one animal; the mean is indicated. The data were analyzed by Kruskal-Wallis test followed by Dunn's correction. *$p < 0.05$, ***$p < 0.001$. (**D**) t-distributed stochastic neighbor embedding (t-SNE) of CD98 expression by indicated bone marrow cells. Colonic lamina propria cells were isolated from WT animals, and CD98 expression determined by monocytes, their intermediates, and macrophages. (**E**) After gating of viable cells and lineage exclusion (CD3, CD19, NK1.1, Ly6G, Ter119), CD11b^{+} cells were identified. CCR2/CD64 dot plots were obtained by gating on CD11b^{+} cells to discriminate CCR2^{+} monocytes (Mo) from CD64^{+}/CCR2^{-} macrophages (Mφ), which were further distinguished by Ly6C and MHC class II staining. (**F**) Expression and (**G**) MFI of CD98 of indicated populations. FMO controls are indicated by red histograms, blue histograms indicate CD98 stained cells. Numbers in histogram plots indicated the percentage of CD98^{+} cells. Each dot represents one animal; the mean is indicated. (**H**) t-SNE shows the distribution of CD98^{+} clusters in colonic lamina propria.

The glycoprotein CD98 is a disulfide-bonded heterodimeric complex composed of the genes *SLC3A2* for human and *Slc3a2* for mice and *SLC7A5/Slc7a5* which is also known as the large neutral amino acid transporter (LAT1). The 4F2hc/CD98 heavy chain of the LAT1 is encoded by the SLC3A2 and the CD98 light chain by the SLC7A5. This membrane transporter protein preferentially transports branched-chain (valine, leucine, isoleucine) and aromatic (tryptophan, tyrosine) amino acids (Nicklin et al., 2009). Thus, the expression levels of the amino acid transporters in the cLP of unmanipulated as well as colitic mice were assessed. Consequently, chosen known amino acid transporters such as *Slc7a5, Slc7a6, Slc7a7, Slc7a8, Slc7a10,* and *Slc7a11* were analyzed. The amino acid transporters *Slc7a5, Slc7a7,* and *Slc7a10* carry neutral branched and aromatic amino acids into the cell, the *Slc7a6* and *Slc7a8* transport cationic amino acids through the cell membrane, and the *Slc7a11* is an antiporter of cysteine and glutamate. All amino acid transporters are highly expressed in the cLP of unmanipulated mice as well as in dextran sodium sulfate (DSS)-induced colitis mice, where only reduced expression of *Slc7a6* was observed. However, no significant expression levels of *Slc7a5, Slc7a7, Slc7a8, Slc7a10,* and *Slc7a11* between unmanipulated and DSS-treated mice were found (**Figure 3.2A**). Moreover, immunofluorescence revealed that CX3CR1[+]/GFP[+] mononuclear phagocytes and IECs of the cLP

express CD98 (**Figure 3.2B**). Additionally, to determine the expression level of CD98 *in vitro,* BM was isolated and bone marrow-derived macrophages (BMDM) were generated in the presence of M-CSF. Afterward, the differentiated BMDMs were either non-stimulated or stimulated with LPS and IFN-γ or with IL-4 and IL-13 to polarize the cells into pro-inflammatory or anti-inflammatory. Flow cytometric analysis of non-stimulated and stimulated BMDMs showed that LPS and IFN-γ, as well as the IL-4 and IL-13 stimulation of the BMDMs, did not have any influence on CD98 expression compared to the non-stimulated BMDMs (**Figure 3.2C and 3.2D**).
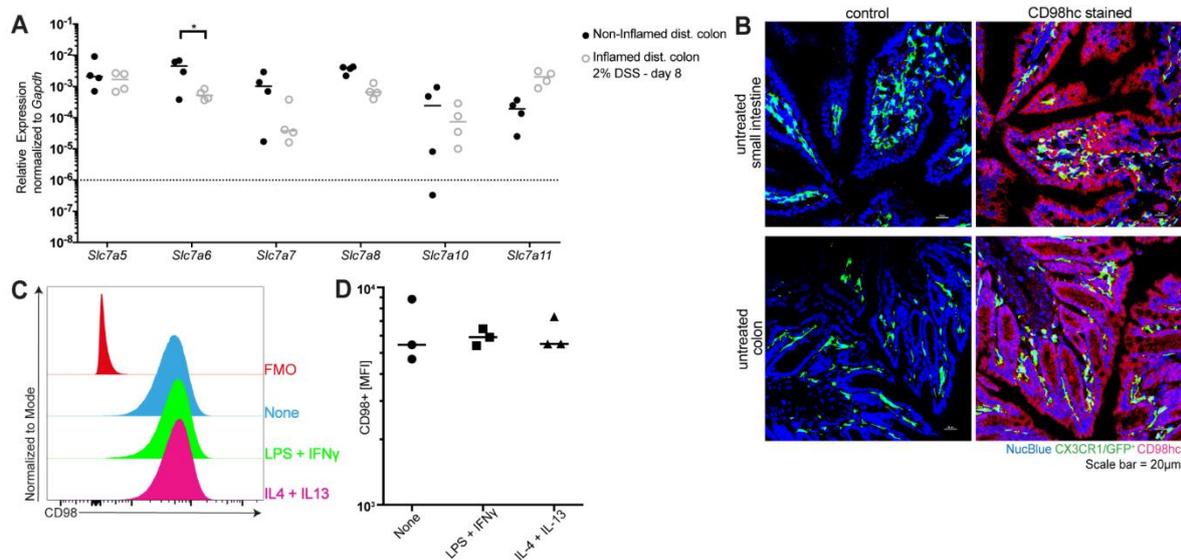
Figure 3.2: CD98 is expressed in small and large intestine. (**A**) RNA was isolated, and reverse transcribed from non-inflamed C57BL/6 WT mice and from inflamed WT mice on day 7, after receiving 2% DSS in the drinking water for 5 days which was exchanged to normal drinking water for another 2 days. The expression level of *Slc7a5, Slc7a6, Slc7a7, Slc7a8, Slc7a10,* and *Slc7a11* was determined by RT-qPCR. Each dot indicates one individual animal; dotted line shows the detection limit. Data were analyzed by two-way ANOVA followed by Sidak's correction; *$p<0.05$. (**B**) The small intestine and the colon of unmanipulated Cx3cr1-GFP mice were stained for CD98hc and counterstained with NucBlue. (**C and D**) Bone marrow-derived macrophages (BMDM) were stimulated either with LPS + IFN-γ or with IL-4 + IL-13 and surface CD98 expression measured by flow cytometry. Histogram and mean fluorescence intensity (MFI) are shown.

Further, as tissue-resident macrophages may originate from an early stage of embryonic development, the CD98 expression was determined in the embryonic yolk sac (E8.5), liver Kupffer cells and epidermal Langerhans cells. The macrophages of the yolk sac revealed a significant lower CD98 expression

compared to the tissue-resident macrophages such as Kupffer cells and Langerhans cells which exhibit CD98 of more than 95% (**Figure 3.3A – 3.3C**). Taken together, our results show that mononuclear phagocytes and their progenitors express CD98 in steady state as well as under inflammatory conditions.
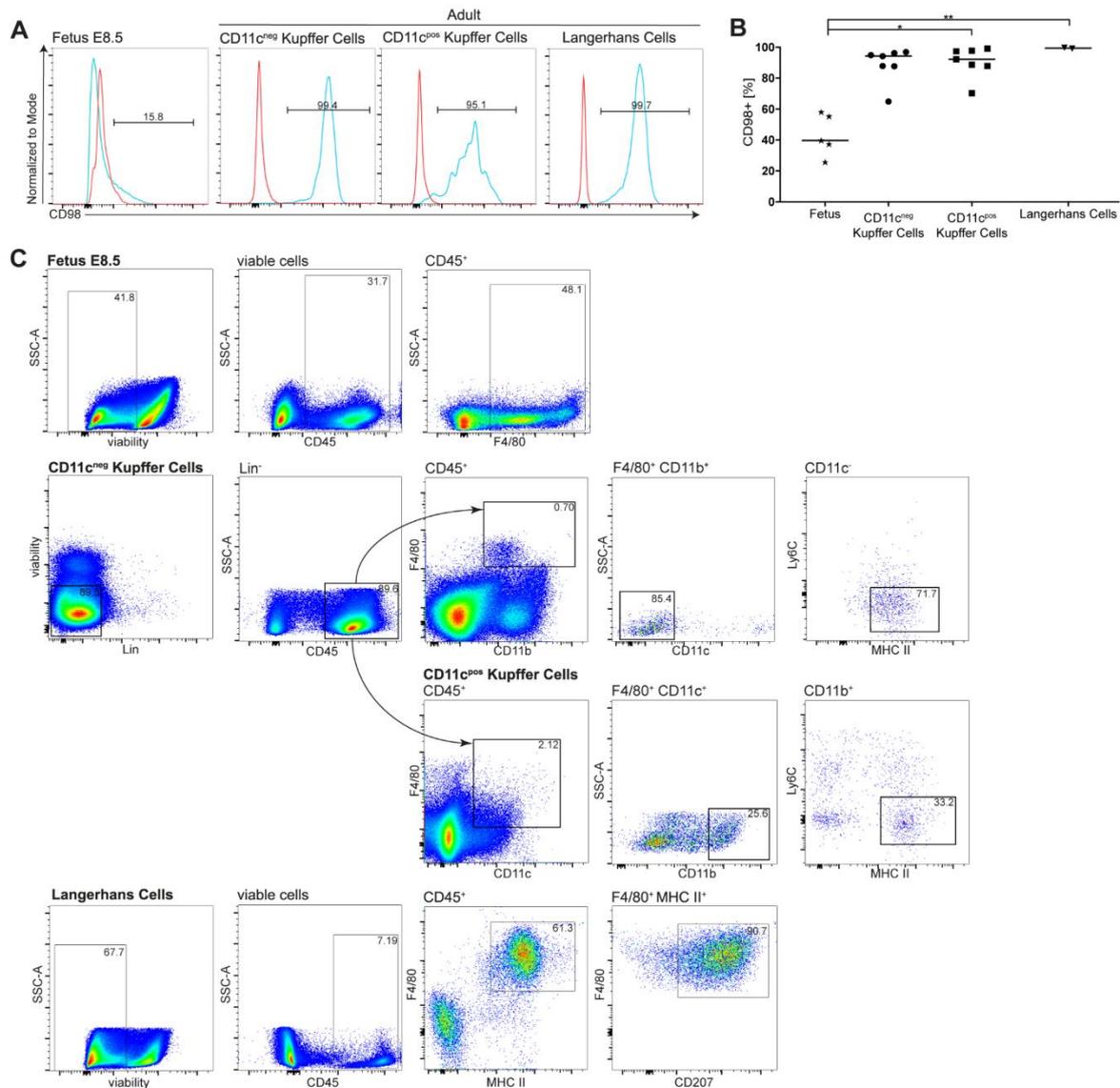
Figure 3.3: CD98 is expressed in tissue-resident macrophages. (**A**) Histogram and (**B**) MFI of yolk sac macrophages from embryos (E8.5), CD11c^{neg} and CD11c^{pos} liver Kupffer cells and epidermal Langerhans cells isolated from unmanipulated adult mice and stained for CD98. Red histograms show FMO control, blue histograms cells stained for CD98. Number within plots indicated the percentage of CD98$^+$ macrophages, Kupffer cells, and Langerhans cells. (**C**) Gating strategy for the identification of the yolk sac macrophages, CD11c^{neg}, and CD11c^{pos} liver Kupffer cells and epidermal Langerhans cells. Statistical significance was analyzed with a Kruskal-Wallis test followed by Dunn's correction; *p<0.05, **p<0.01.

3.2.   Excision of CD98 in colonic macrophages in CD98hc$^{\Delta CX3CR1}$ mice

Given that mononuclear phagocytes express CD98 in steady state as well as in inflamed conditions, we next wanted to establish a mouse model, which allows silencing of CD98hc specifically in CX3CR1$^+$ mononuclear phagocytes. The colonic macrophages are characterized by high expression levels of the chemokine receptor CX3CR1, whose corresponding ligand fractalkine/CX3CL1 is expressed by intestinal epithelial cells (Muehlhoefer et al., 2000; Niess et al., 2005). Therefore, CD98hc$^{\Delta CX3CR1}$ mice were generated by breeding Cx3cr1^{CreER} mice with CD98hc$^{flox/flox}$ mice to delete the expression of CD98 in intestinal CX3CR1$^+$ mononuclear phagocytes. Of note, the injection of tamoxifen into pregnant CD98hc$^{\Delta CX3CR1}$ mice was intrauterine lethal to the offspring (data not shown), which elucidated that a complete knock-out is embryonic lethal. Tamoxifen was administered every 24 hours for a total of five consecutive days, and the CD98 expression level by the 'monocyte waterfall' subpopulations as well as the tissue macrophage subpopulations was determined for 21 days. On day 2 after the first tamoxifen injection, a decreased percentage of CD98$^+$ cells in the subpopulations of the cLP was observed (**Figure 3.4A and 3.4B**). The lowest percentage of CD98$^+$ monocytes and macrophages in the cLP appeared at day 7 which indicates the optimal timeframe of CD98 silencing. Within 14 days after the first tamoxifen injection, the percentage of CD98$^+$ Ly6C^{high} and Ly6C^{mid} monocytes normalized, whereas the percentage of CD98$^+$ Ly6C^{low} monocytes recovered within 21 days. By contrast, the CD98 expression of MHC II$^-$ and MHC II$^+$ macrophages in the cLP did not fully recover within 21 days after the first i.p. injection of tamoxifen. Of note, histogram plots of macrophages obtained 14 days after tamoxifen injection shows a biphasic distribution suggesting that CD98 silenced macrophages are replaced with newly recruited CD98$^+$ precursor cells (**Figure 3.4B**).

As yolk-sac-derived myeloid progenitors (Gomez Perdiguero et al., 2015), fetal-liver-derived monocytes, and hematopoietic stem cell (HSC)-derived myeloid precursors contribute to the development of tissue-resident macrophages such as Kupffer cells, the CD98 expression by CD11c^{neg} and CD11c^{pos} Kupffer cells was also determined after tamoxifen-induced CD98 deletion. The tamoxifen treatment led to a significant reduction of CD98 expression by CD11c^{neg} and CD11c^{pos} Kupffer cells already on day 2 after the first i.p. injection. Interestingly, this CD98 silencing induced by tamoxifen

treatment over five consecutive days recovered again within 28 days, indicating that Kupffer cells are partially replenished by extravasated blood monocytes (Scott et al., 2016) (**Figure 3.4C and 3.4E**). The decrease in CD98 expression at day 7 was notably less pronounced in Kupffer cells compared to the 'monocyte waterfall' subsets and the MHC II$^+$ macrophage in the cLP. Moreover, injection of tamoxifen did not affect the CD98 expression by epidermal Langerhans cells (**Figure 3.4D and 3.4E**).
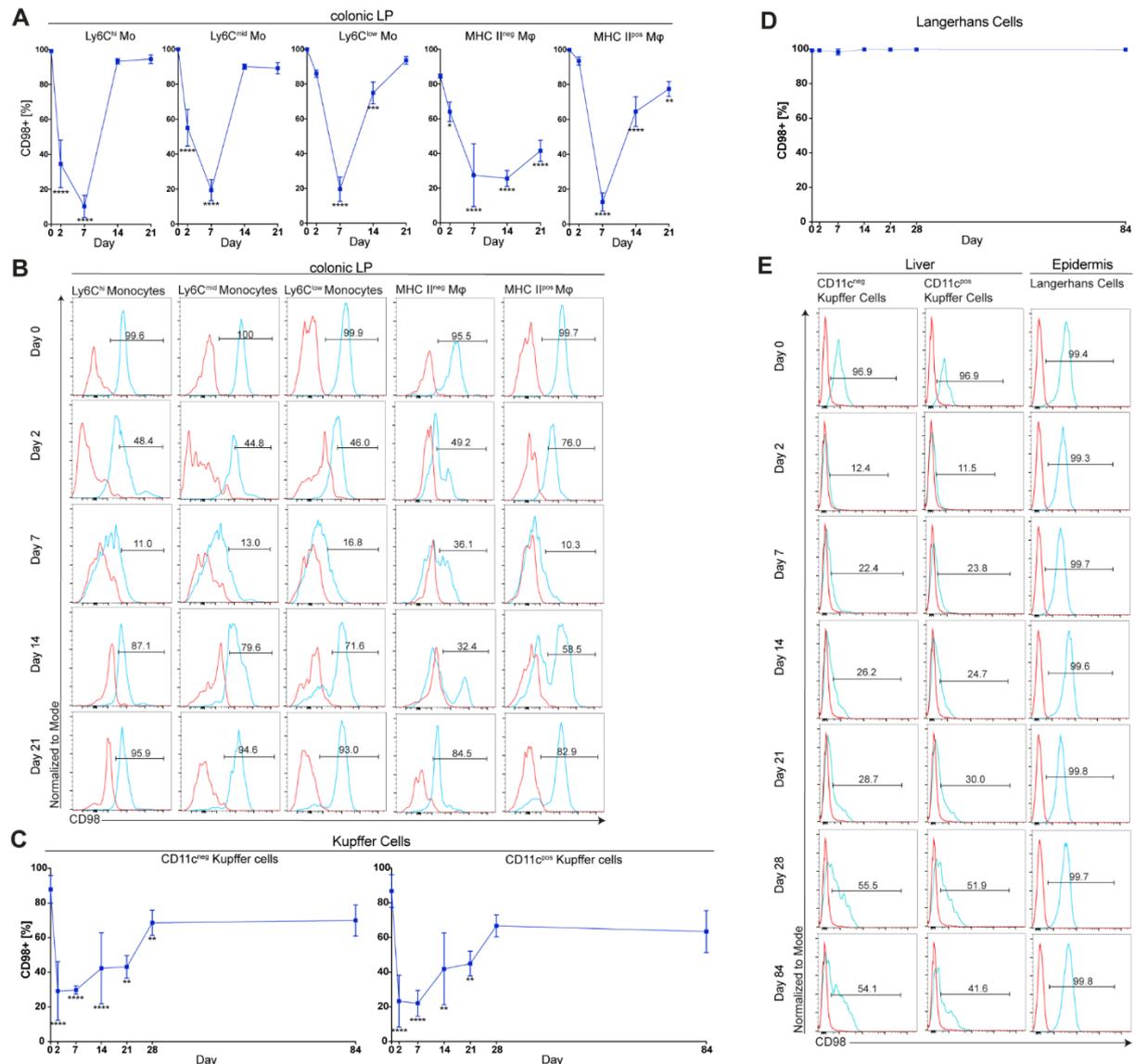
Figure 3.4: Tamoxifen injection into CD98hc$^{\Delta CX3CR1}$ animals leads to the excision of CD98 in monocytes and macrophages. Monocytes and macrophages were isolated from the colonic lamina propria (cLP) and analyzed for CD98 expression by flow cytometry after intraperitoneal tamoxifen injection into CD98hc$^{\Delta CX3CR1}$ animals. (**A**) Percentage of CD98$^+$ monocytes (Mo) and macrophages (Mφ) at indicated time points (n=3). The data is shown as the mean (±SD) and analyzed by two-way ANOVA followed by Sidak's correction; *p<0.05, **p<0.01, ***p<0.001, ****p<0.0001. (**B**) Histogram plots of

indicated monocytes and macrophages from the colonic lamina propria at indicated time points after tamoxifen injection into CD98hc$^{\Delta CX3CR1}$ mice. FMO control is represented by red histograms, CD98 stained cells by blue histograms. Numbers in histogram plots indicated the percentage of CD98^{+} cells. (**C**) Mean (±SD) percentage of CD98^{+} CD11c^{neg}, and CD11c^{pos} liver Kupffer cells and (**D**) epidermal Langerhans cells at indicated days after intraperitoneal tamoxifen injection into CD98hc$^{\Delta CX3CR1}$ animals (n=3). The results were analyzed by two-way ANOVA followed by Sidak's correction; *$p<0.05$, **$p<0.01$, ***$p<0.001$, ****$p<0.0001$. (**E**) Histogram plots of CD11c^{neg} and CD11c^{pos} liver Kupffer cells and of epidermal Langerhans cells at indicated time points after tamoxifen injection into CD98hc$^{\Delta CX3CR1}$ mice. Red histograms display FMO controls, blue histograms CD98^{+} cells; Numbers in histograms show the percentage of CD98^{+} cells.

Macrophages, monocytes, T cell subsets, NK cells, dendritic cells (DC), and platelets also express the fractalkine receptor, CX3CR1 (Gerlach et al., 2016). Therefore, to investigate the effect of tamoxifen treatment on other CX3CR1^{+} cell populations found in the intestine, flow cytometry analysis was performed to determine the CD98 expression of cLP macrophages, B cells, CD4^{+} and CD8^{+} T cells, DCs, neutrophils, and NK cells. Interestingly, cLP macrophages but not B cells, CD4^{+} and CD8^{+} T cells, DCs, neutrophils, and NK cells showed a significant decrease of CD98 expression after the tamoxifen treatment (**Figure 3.5A**). Furthermore, as CD98hc also binds to integrin β1 (CD29) and mediates the integrin activation, cell spreading, cell survival, and cell growth, the CD98 silencing did not affect the CD29 expression of the 'monocyte waterfall' and macrophage subpopulations in the cLP of DSS-induced colitic mice (**Figure 3.5B**). These results suggest that tamoxifen injection in CD98hc$^{\Delta CX3CR1}$ animals silenced the expression of the glycoprotein CD98. Thus, we have established a mouse model which allows successful silencing of CD98 in monocytes and macrophages.
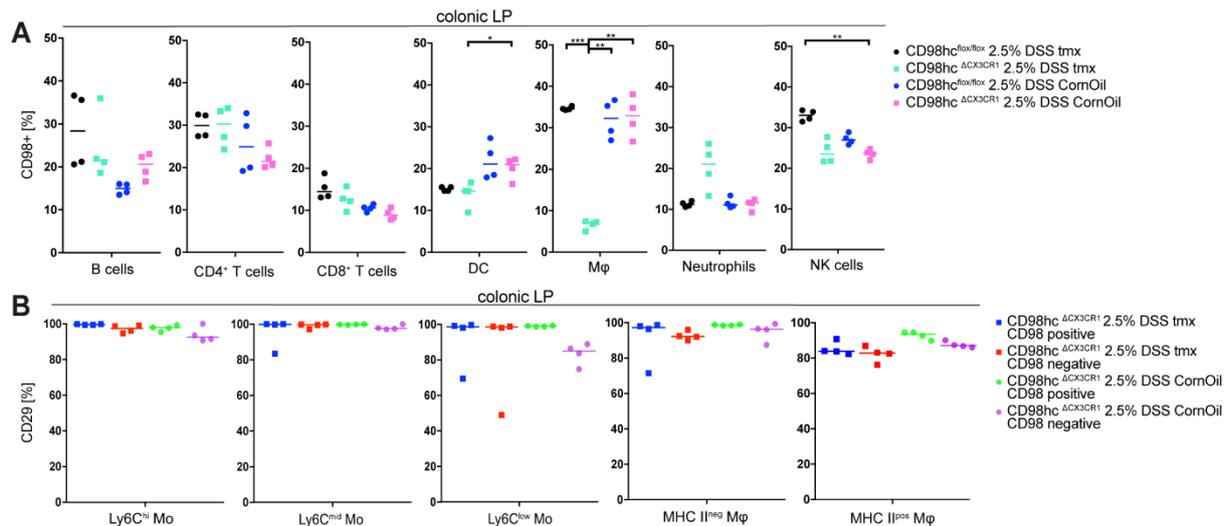
Figure 3.5: Tamoxifen-induced Cre-mediated excision of CD98 in CD98hc$^{\Delta CX3CR1}$ animals deletes CD98 in monocytes and macrophages but not in T cells. (**A**) Percentage of CD98 expression by B cells, CD4$^+$ and CD8$^+$ T cells, dendritic cells (DC), macrophages (Mφ), and neutrophils isolated from the colonic lamina propria of corn oil- or tamoxifen-treated C57BL/6 WT or CD98hc$^{\Delta CX3CR1}$ animals. (**B**) Percentage of integrin β1/CD29$^+$ monocytes and macrophages in indicated mouse lines treated with corn oil or tamoxifen. Data were analyzed by two-way ANOVA followed by Sidak's correction; *p<0.05, ****p<0.0001.

3.3. Loss of CD98 by macrophages leads to attenuated colitis

We next determined whether the silencing of CD98 by 'monocyte waterfall' subsets and macrophage subset of the cLP affects the development of DSS-induced colitis. Both CD98hc$^{\Delta CX3CR1}$ and CD98hc$^{flox/flox}$ animals were treated either with tamoxifen or the tamoxifen carrier corn oil. As a result, tamoxifen-treated CD98hc$^{\Delta CX3CR1}$ mice showed significantly reduced clinical signs such as body weight loss (**Figure 3.6A**) and reduced disease activity index (**Figure 3.6B**), reduced histological signs of colitis (**Figure 3.6C and 3.7B**), and decreased colon shortening (**Figure 3.6D and 3.6F**). Further, the flow cytometry analysis and immunofluorescence staining confirmed the successful silencing of CD98 by tamoxifen treatment in CD98hc$^{\Delta CX3CR1}$ animals (**Figure 3.6E and 3.7A**).
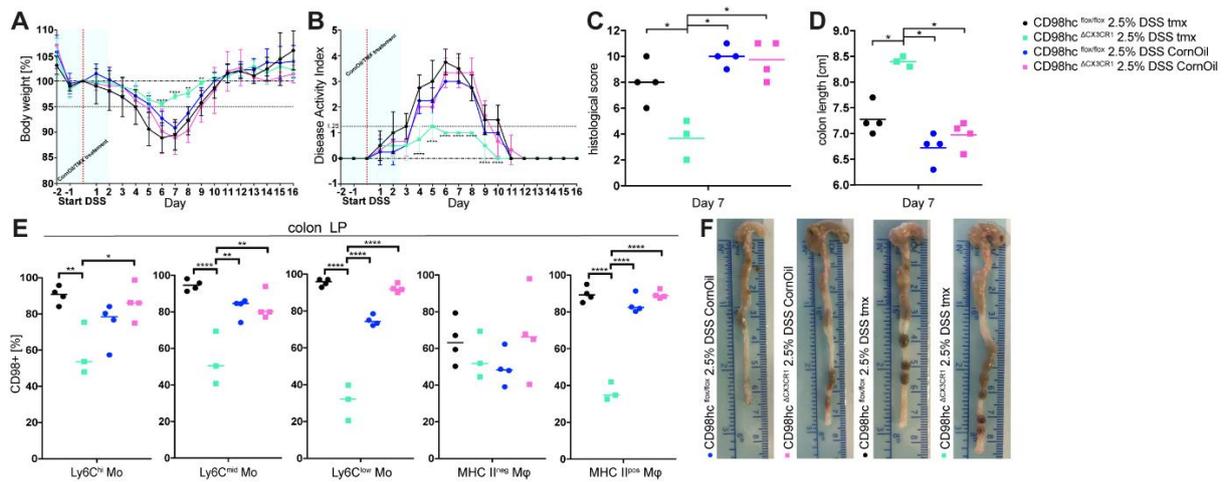
Figure 3.6: Attenuated colitis after CD98 silencing by monocytes and macrophages. Colitis was induced by adding 2.5% dextran sodium sulfate (DSS) to CD98hc$^{flox/flox}$ and CD98hc$^{\Delta CX3CR1}$ mice which were treated either with corn oil or with tamoxifen. (**A**) The mean percentage of body weight change (±SD) and (**B**) disease activity index are shown. The data were analyzed by two-way ANOVA followed by Sidak's correction; ***$p < 0.001$. (**C**) Histological scores were assessed in a blinded fashion by two independent investigators. The mean histological score was determined for each animal after H&E staining of colonic tissues, presented as individual dot and analyzed with a Mann-Whitney U test; *$p < 0.05$. (**D**) The colon length was determined at day 7 after the start of DSS administration, colon length is shown for each individual animal, the mean indicated and analyzed with a Mann-Whitney U test; *$p < 0.05$. (**E**) Percentage of CD98$^+$ monocytes (Mo) and macrophages (Mφ) of indicated groups 7 days after start of DSS administration. Each dot represents one animal. Data were analyzed by two-way ANOVA followed by Sidak's correction; *$p < 0.05$, **$p < 0.01$, ***$p < 0.001$. (**F**) A representative image of the colon from each group is shown.

The immunofluorescence staining of colon sections obtained from CD98hc$^{\Delta CX3CR1}$ and CD98hc$^{flox/flox}$ mice treated either with tamoxifen or corn oil during DSS-induced colitis depict that mononuclear phagocytes and epithelial cells express CD98 with a reduced staining intensity in tamoxifen-treated CD98hc$^{\Delta CX3CR1}$ mice (**Figure 3.7A**). Hematoxylin and eosin (H&E) staining (**Figure 3.7B**) and colonoscopy (**Figure 3.7C**) confirmed the decreased severity of DSS-induced colitis in tamoxifen-treated CD98hc$^{\Delta CX3CR1}$ mice, compared to mice treated with the carrier corn oil.
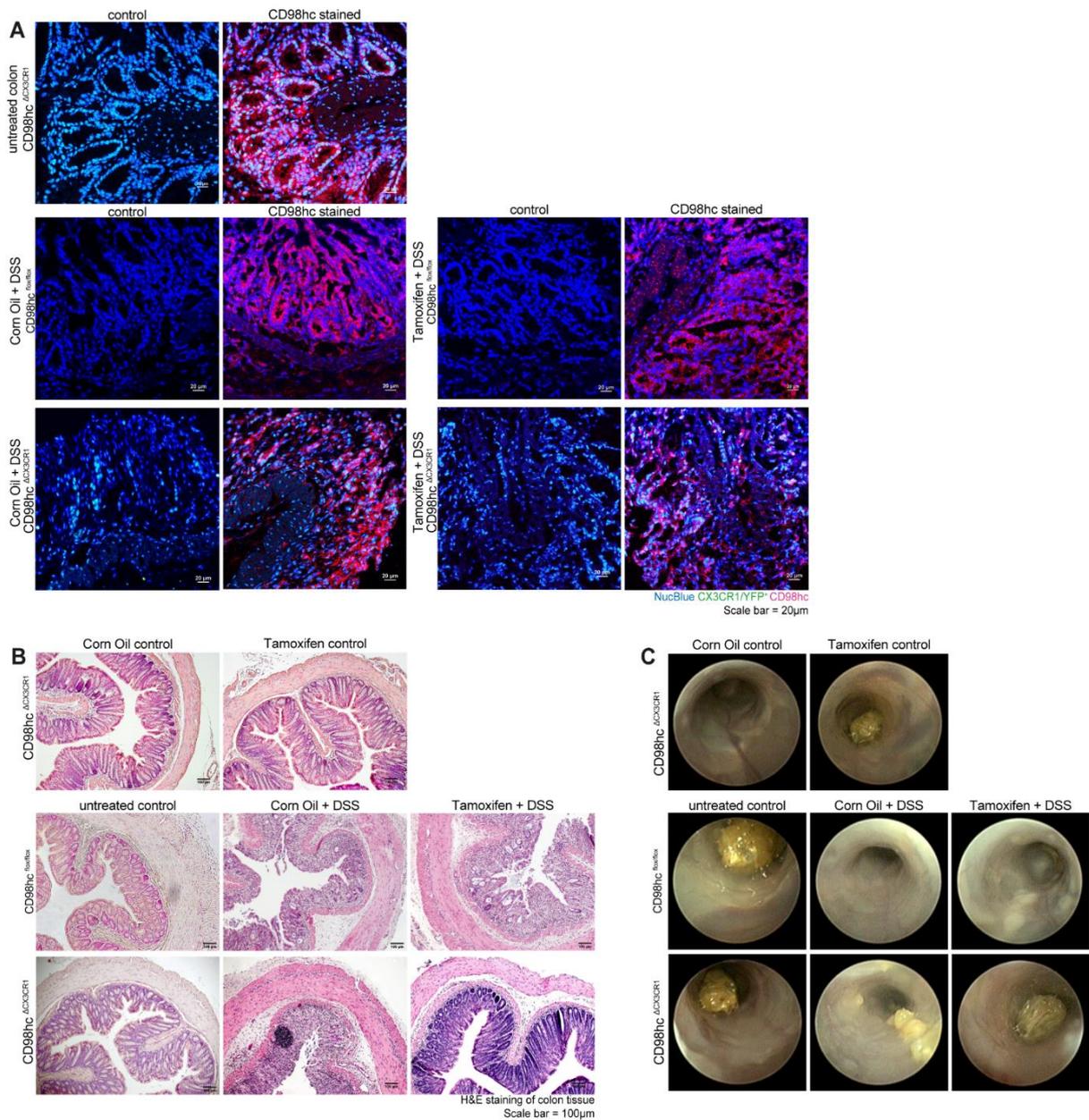
Figure 3.7: Reduced CD98 staining intensity and attenuated colitis in tamoxifen-treated CD98hc$^{\Delta CX3CR1}$ mice. (**A**) CD98 staining, (**B**) H&E staining of colonic tissues, and (**C**) endoscopic images from indicated groups.

Furthermore, the CD98hc$^{flox/flox}$ and CD98hc$^{\Delta CX3CR1}$ animals were fed with 10% higher amino acid chow (5% more L-leucine and 5% more L-isoleucine) to induce an increased inflammation on a CD98 dependent manner compared to conventional chow. The disease activity index (DAI) showed an increased inflammation in untreated, tamoxifen- or corn-oil-treated CD98$^{flox/flox}$ mice, and corn-oil-treated CD98hc$^{\Delta CX3CR1}$ mice (all control groups), whereas silencing of CD98 attenuated the severity of DSS-induced colitis in CD98hc$^{\Delta CX3CR1}$ mice fed with control diet as shown before (**Figure 3.8A left**

panel). The control groups fed with enriched amino acid diet revealed similar DAI as those fed with the control diet. Interestingly, tamoxifen-treated CD98hc$^{\Delta CX3CR1}$ mice which were fed with amino acid enriched diet had a significantly increased DAI compared to tamoxifen-treated CD98hc$^{\Delta CX3CR1}$ mice fed with control diet likely due to an increased amino acid influx in a CD98 dependent manner, which results in a rapidly upregulation and probably higher expression of the CD98hc as shown by Yan and Lamb in 2010. Thus, infiltrating immune cells such as neutrophils or DCs might be more activated due to the higher amino acid influx or compensate the arbitrary immunological behavior of CD98 deleted monocytes and macrophages which leads to increased inflammatory response and a more severe clinical sign of colonic inflammation.

Further, the control groups, as well as the tamoxifen-treated CD98hc$^{\Delta CX3CR1}$ mice, fed with amino acid enriched diet showed tendentially colon shortening compared to the mice fed with control diet (**Figure 3.8A middle panel**) which is additionally indicated by representative images (**Figure 3.8B**). Furthermore, the histological score revealed an increased inflammation in tamoxifen-treated CD98hc$^{\Delta CX3CR1}$ mice fed with the enriched amino acid diet compared to the tamoxifen-treated CD98hc$^{\Delta CX3CR1}$ mice fed with the control diet. However, the control groups, fed either with control diet or amino acid diet, showed similar increased histological scores (**Figure 3.8 A right panel**), which is additionally indicated by H&E staining (**Figure 3.8C**). Hence, histological signs of colitis showed increased disruption of the mucosal architecture in untreated CD98hc$^{flox/flox}$ mice fed with both control and amino acid enriched diet, and in tamoxifen- and corn-oil-treated CD98hc$^{flox/flox}$ mice, as well as in corn-oil-treated CD98hc$^{\Delta CX3CR1}$ mice fed with amino acid enriched diet. In contrast, histological analysis of tamoxifen-treated CD98hc$^{\Delta CX3CR1}$ mice fed with control diet did not show DSS-induced severity of colitis in that extent. Further, compared to the control diet, tamoxifen-treated CD98hc$^{\Delta CX3CR1}$ mice fed with amino acid-enriched diet revealed a tendentially increased histological sign of colonic inflammation (**Figure 3.8**). Taken together, these results elucidate that the loss of CD98 in monocytes and macrophages of the cLP attenuated the severity of chemically induced colitis in mice. Moreover, the increased influx of amino acids by amino acid-enriched diet leads to a tendentially elevated colonic inflammation by infiltrating immune cells such as granulocytes and DCs.
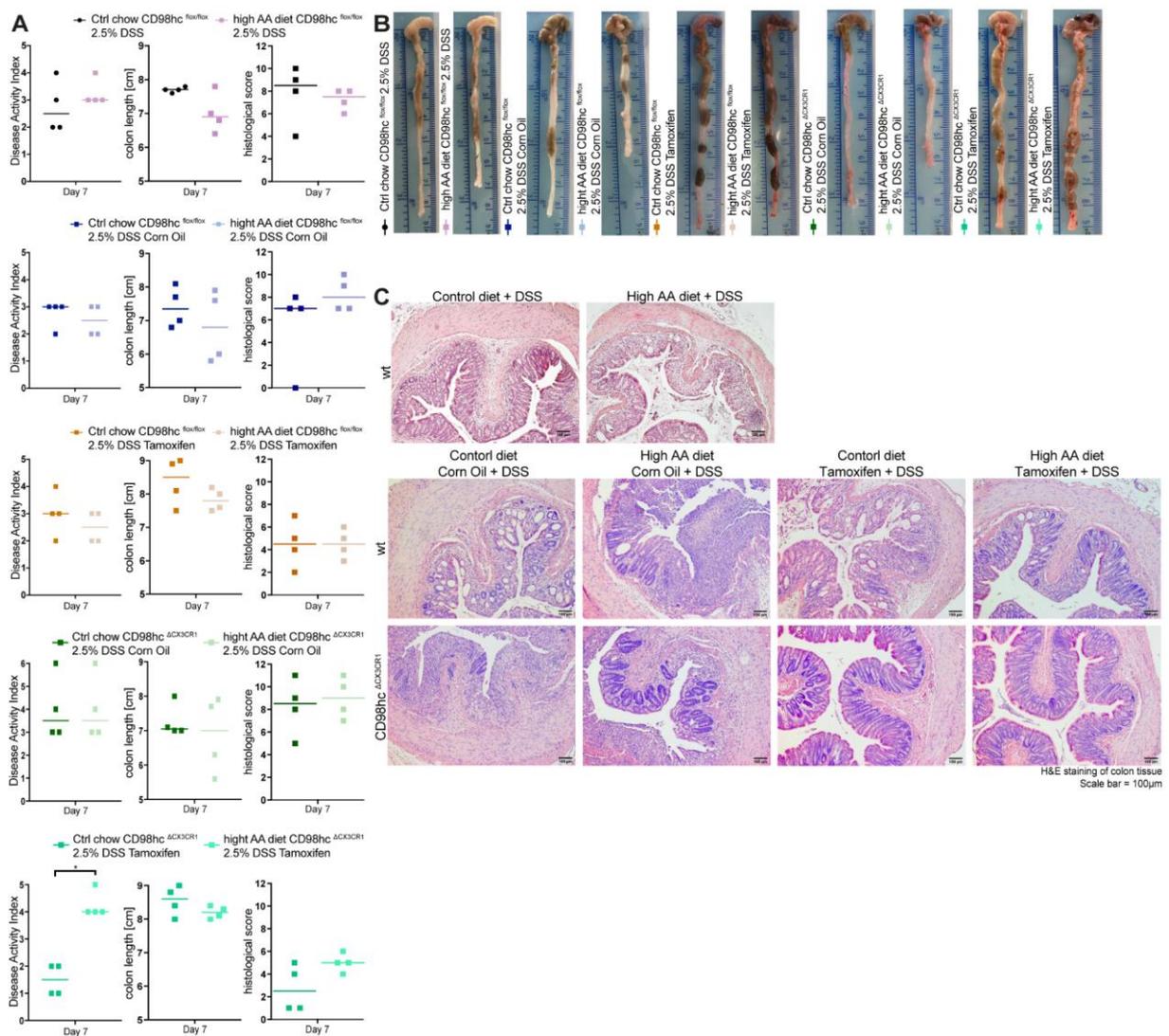
Figure 3.8: Amino acid enriched diet potentially increased DSS-induced colitis in a CD98 dependent manner. Tamoxifen- or corn-oil-treated CD98hc^flox/flox and CD98hc^ΔCX3CR1 mice were fed with control or amino acid chow following 2.5% DSS-induced colitis. (**A**) Disease activity index (DAI), colon length, and histological scores are shown. Each dot presents an individual animal. (**B**) A representative image of the colon from each group is shown. (**C**) H&E staining of colonic biopsies.

3.4. Single-cell RNA sequencing suggests a developmental trajectory of monocytes to macrophages in the colonic lamina propria

Unmanipulated and healthy female mice were used for transcriptomic investigations to analyze the behavior of colonic monocytes and macrophages on a CD98 dependent manner. Therefore, CCR2$^+$ and CD64$^+$ cell populations were sorted together from CD98hc$^{\Delta CX3CR1}$ mice after the treatment with tamoxifen or corn oil which were further analyzed by single-cell RNA sequencing (scRNA-seq).

Cell suspensions volumes aiming at a targeted recovery of ~ 3,000 cells were loaded on the wells of a 10× Genomics Chromium Single Cell Controller (one well per mouse replicate by at least 3 mice per condition). The resulting filtered dataset included expression values for 11,947 genes for 3,213 cells, ranging from 83 to 724 cells per sample, for a total of 1,863 control cells, and 1,350 CD98 cKO cells. An average of 1,645 genes was detected per cell. Differential expression between control and cKO cells stratified by differentiation stage when at least 20 cells could be aggregated. This resulted in a total of 32 aggregated samples, and at least 3 replicates per condition for each cluster. The genes were filtered to keep those with CPM (counts per million reads sequenced) values higher than 1 in at least 3 samples and detected in at least 20 individual cells. We considered only sets containing more than 10 genes and gene sets with a false discovery rate of lower than 5% as significant.

The scRNA-seq data analysis of unsupervised hierarchical clustering of specific genes (**Figure 3.9A**) as well as hypervariable genes (**Figure 3.9B**) revealed the presence of nine distinct clusters. Further, the data analysis suggested a hierarchically structured lineage tree from cluster 2, via cluster 1 and 4, towards to cluster 6 and 3. Moreover, the t-SNE analysis indicated a close relationship between clusters 1 to 4, whereas cluster 5, 7, 8, and 9 seem to be distinctly separated from every single cluster and are not related to the lineage tree clusters (**Figure 3.9C**). In addition to that, cluster 6 seems to be also separated. Nevertheless, cluster 6 corresponds to the CD64$^+$ MHC class II-negative cells described by flow cytometry.
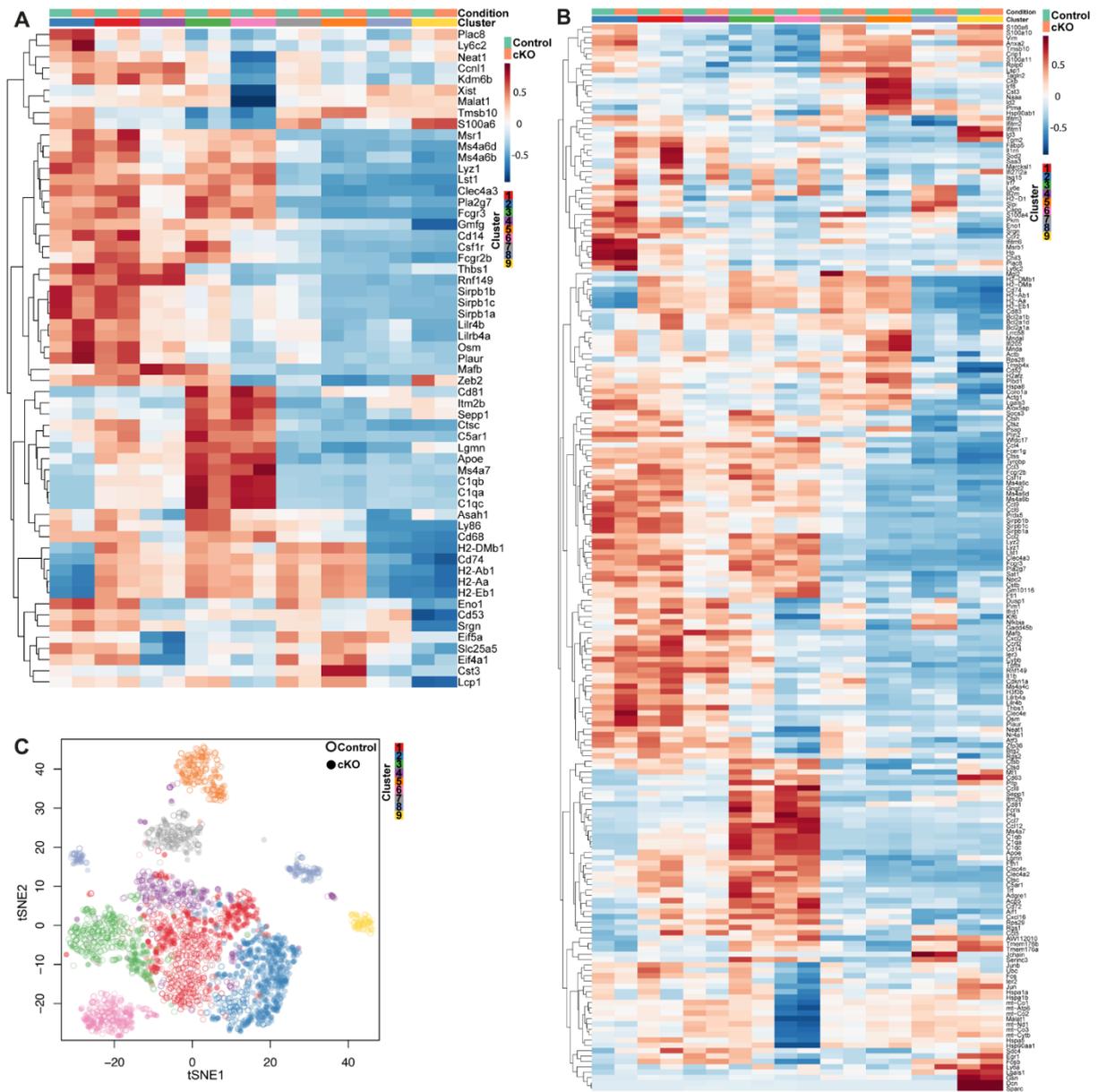
Figure 3.9: Single-cell RNA sequencing suggests a developmental trajectory from monocytes to macrophages in the colonic lamina propria. CCR2+ and CD64+ colonic lamina propria cells that include the 'monocyte waterfall' intermediates and macrophages from CD98hc$^{\Delta CX3CR1}$ mice treated with corn oil or with tamoxifen were sorted after gating on viable, lineage negative (CD3, CD19, NK1.1, Ly6G, Ter119), and CD11b+ cells and further analyzed by single-cell RNA-sequencing (scRNA-seq). scRNA-seq was performed in quadruples. (**A**) Heatmap of cluster-specific genes and (**B**) heatmap of hypervariable genes by cells from corn oil (control) and tamoxifen (cKO) treated animals. Nine individual clusters were identified and shown in different colors. (**C**) The t-SNE analysis depicts the distribution of the nine different clusters and indicates their relationship.

For the identification of the individual clusters of the lineage tree clusters, genes were selected that are allocated expressed by monocytes or macrophages. Genes like *Ccr2, Cd14,* and *Ly6c2* are expressed by cluster 1, 2, and in a lower extent in cluster 4 suggesting that these clusters are monocyte subpopulations of the cLP. *Cd72, Cd74, Cd81, Cx3cr1,* and *Adgre1* (EMR1, F4/80) are prominently expressed by cluster 3 and 6 indicating that cluster 3 and 6 are the macrophage subpopulations (**Figure 3.10A**). The non-related clusters 5, 7, 8, and 9 expresses in a higher extent the genes *Cd63, Ly6a, Ly6c1,* and *Cst3* suggesting a possible 'contamination' with granulocytes and dendritic cells (**Figure 3.9B**). Consequently, the 'contaminating' clusters 5, 7, 8, and 9 were excluded and neglected for the specific analysis of cLP monocytes and macrophages. Flow cytometry analysis of chosen genes from the heatmap of genes characteristic for monocytes and macrophages (**Figure 3.10A**) confirmed that MHC II$^-$ and MHC II$^+$ macrophages have higher CD81 expression compared to Ly6C^{high} and Ly6C^{mid} monocytes. Additionally, monocytes and macrophages expressed CD14 and CD72 (**Figure 3.10B and 3.10C**). The deletion of CD98 in monocytes and macrophage of the cLP did not significantly affect the expression of CD14, CD72, and CD81. Merely CD98 silenced Ly6C^{high} monocytes showed lower CD14 expression and CD98 silenced Ly6C^{low} monocytes increased CD81 expression (**Figure 3.10B and 3.10C**). Further, the principal component analysis (PCA) suggested the development of monocytes to macrophages via intermediates within these nine different clusters (**Figure 3.11A**). Relative density plots generated by overlying the transcriptome of control and CD98-deficient clusters indicated a block in the 'monocyte waterfall'-development to mature colonic macrophages in tamoxifen-treated CD98hc$^{\Delta CX3CR1}$ mice. In these animals, CD98-deficient cells accumulated in the first two clusters of the 'monocyte waterfall' whereas the control cells showed higher density in cluster 3 (**Figure 3.11B**). The FlowSOM analysis also suggested a developmental trajectory from monocytes towards macrophages of the lineage tree clusters (**Figure 3.11C**). The calculation of the relative proportion of cells per cluster indicated an enrichment of CD98-deficient cells in cluster 2 compared to the control cells which are more concentrated in the clusters 1 and 3 (**Figure 3.10D**). Further, FlowSOM analysis with pie charts that depict the relative proportion of CD98-deficient cells from tamoxifen-treated CD98hc$^{\Delta CX3CR1}$ mice and control cells from corn-oil-treated CD98hc$^{\Delta CX3CR1}$ mice indicated that CD98-deficient cells are

enriched in the early developmental stages of monocytes to gut macrophages in the colonic lamina propria whereas control cells are concentrated in cluster 3 (**Figure 3.11D**).
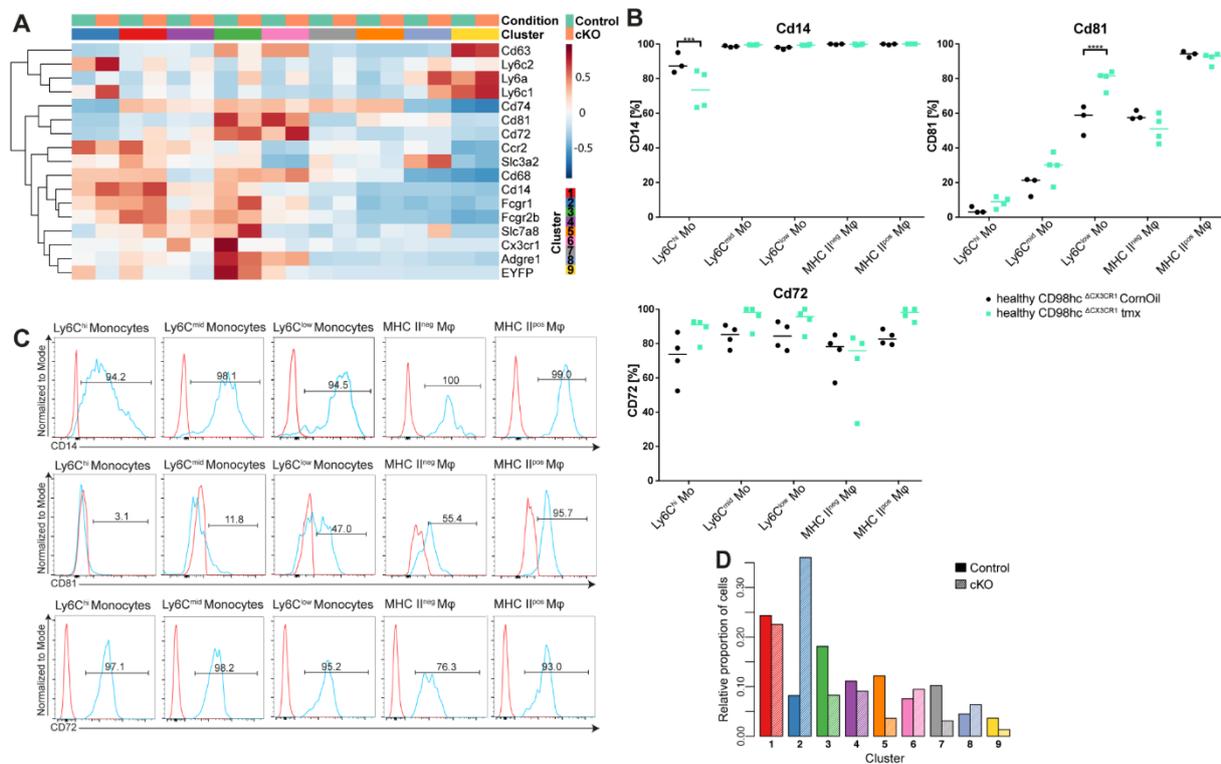
Figure 3.10: Identification of the individual clusters. (**A**) Genes that are characteristic for monocytes and macrophages were depicted and presented as a heatmap. The heatmap of top cluster-specific genes consists of the union of the top 10 genes from each between-clusters pairwise comparison. (**B**) Percentage of CD14$^+$, CD81$^+$, and CD72$^+$ colonic lamina propria monocytes (Mo) and macrophages (Mφ) determined by flow cytometry. One individual dot represents an individual animal in the dot plots. Data were analyzed by two-way ANOVA followed by Sidak's correction; ***p<0.001, ****p<0.0001. (**C**) Histogram of monocytes (Mo) and macrophages (Mφ) after CD14, CD81, and CD72 staining. Red histograms are the FMO control, blue histograms the CD14$^+$, CD81$^+$, or CD72$^+$ cells. Numbers in histograms indicate the percentage of CD14$^+$, CD81$^+$, and CD72$^+$ monocytes and macrophages. (**D**) Relative frequency of control and cKO cells within the different clusters in the scRNA-seq experiment.
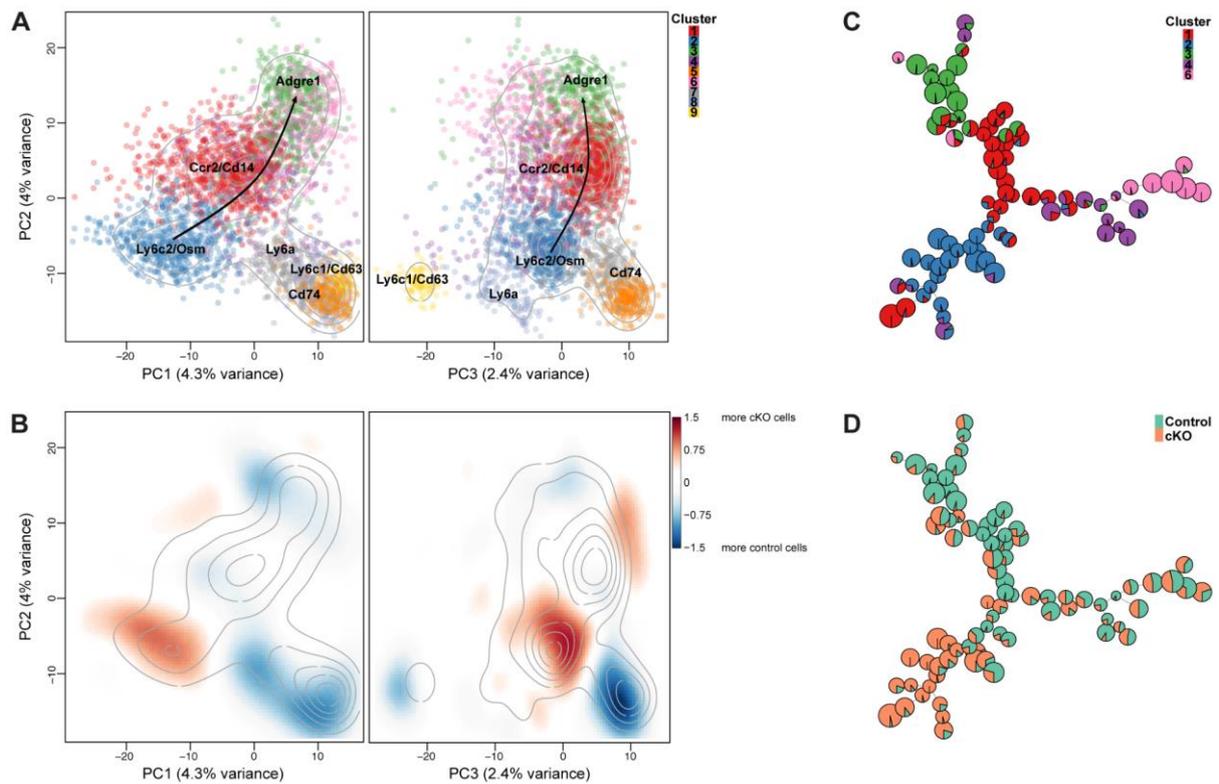
Figure 3.11: Trajectory from monocytes towards macrophages of the lineage tree clusters. (**A**). Principal component analysis (PCA) of single-cells is based on the 500 most variable genes across all cells. The colors represent cells from different clusters. Contour lines indicate the density of the cells in the PCA space. (**B**) The color of the differential 2D density plot represents the log2 ratio of 2D densities of cKO cells over control cells. (**C**) FlowSOM analysis shows also the distribution of the 6 individual clusters. Clusters 5, 7, 8, and 9, which are possible granulocyte and DC contaminants, were omitted from the FlowSOM analysis. (**D**) Pie charts within the FlowSOM tree indicate the relative enrichment of cKO cells over control cells.

3.5.   Increased apoptotic signatures after silencing of CD98

To further gain insights into the molecular mechanisms involved in the developmental arrest in CD98 deficient macrophages, genes which were differentially expressed between tamoxifen- or corn oil-treated CD98hc$^{\Delta CX3CR1}$ mice within each cluster along the developmental trajectory were analyzed in detail (Lun and Marioni, 2017). For this analysis, the "pseudo-bulk" samples were used. These samples were first controlled on a PCA. Next, the first principal components separated the samples according to their differentiation stage. Interestingly, on principal components 3 and 4 the control and CD98 cKO samples within each cluster are clearly separated (**Figure 3.12**). **Table S7** lists the genes in each

individual cluster that were significantly up- or down-regulated (absolute log2 fold-change > |1| and FDR < 0.05) between tamoxifen- or corn oil-treated CD98hc$^{\Delta CX3CR1}$ mice.
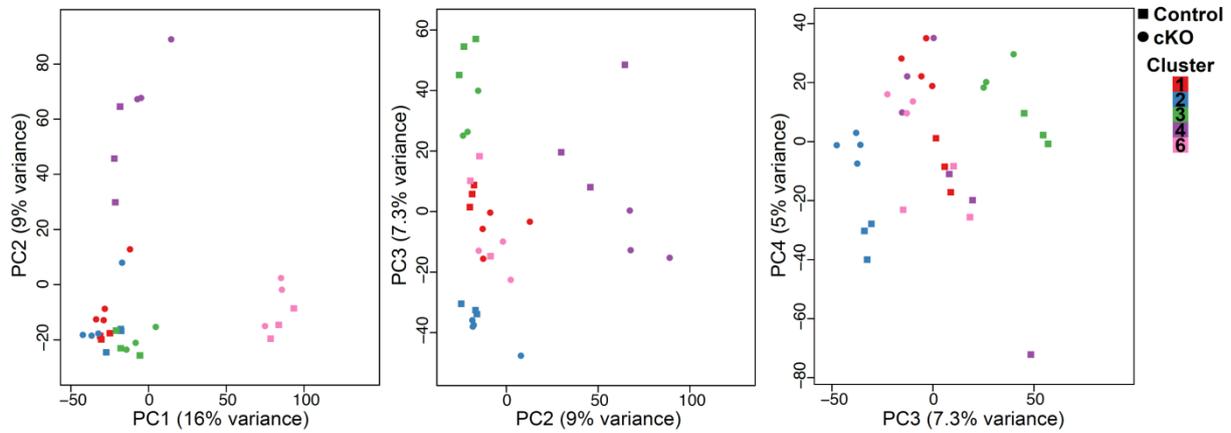
Figure 3.12: Clusters distribution of tamoxifen- or corn oil-treated CD98hc$^{\Delta CX3CR1}$. Per cluster different expressed genes between control and cKO animals were retrospectively analyzed and presented in a principal component analysis (PCA) plots.

Further, a heatmap of genes which are involved in apoptosis pathways was generated. The heatmap depicts apoptosis genes which were chosen from the heatmap of hypervariable genes. The analysis indicates increased expression of the significant differential expressed genes *Osm, Bcl2l11,* and *Tnf* in clusters 1 and 2 correspondings to CD98 silenced monocyte populations (**Figure 3.13A**). Additionally, Gene Set Enrichment Analysis (GSEA) shows apoptosis-related up- or down-regulated genes in cluster 2 but not in cluster 1 and clusters 3, 4, and 6 of tamoxifen-treated CD98hc$^{\Delta CX3CR1}$ mice (**Figure 3.13B**). Monocytes of cluster 1 and 2 had higher expression levels of selected apoptosis-related genes compared to monocytes of cluster 4 and macrophages of cluster 3 and 6. Cells of cluster 2 had an increased *Osm* expression after excision of CD98 (**Figure 3.13C**).
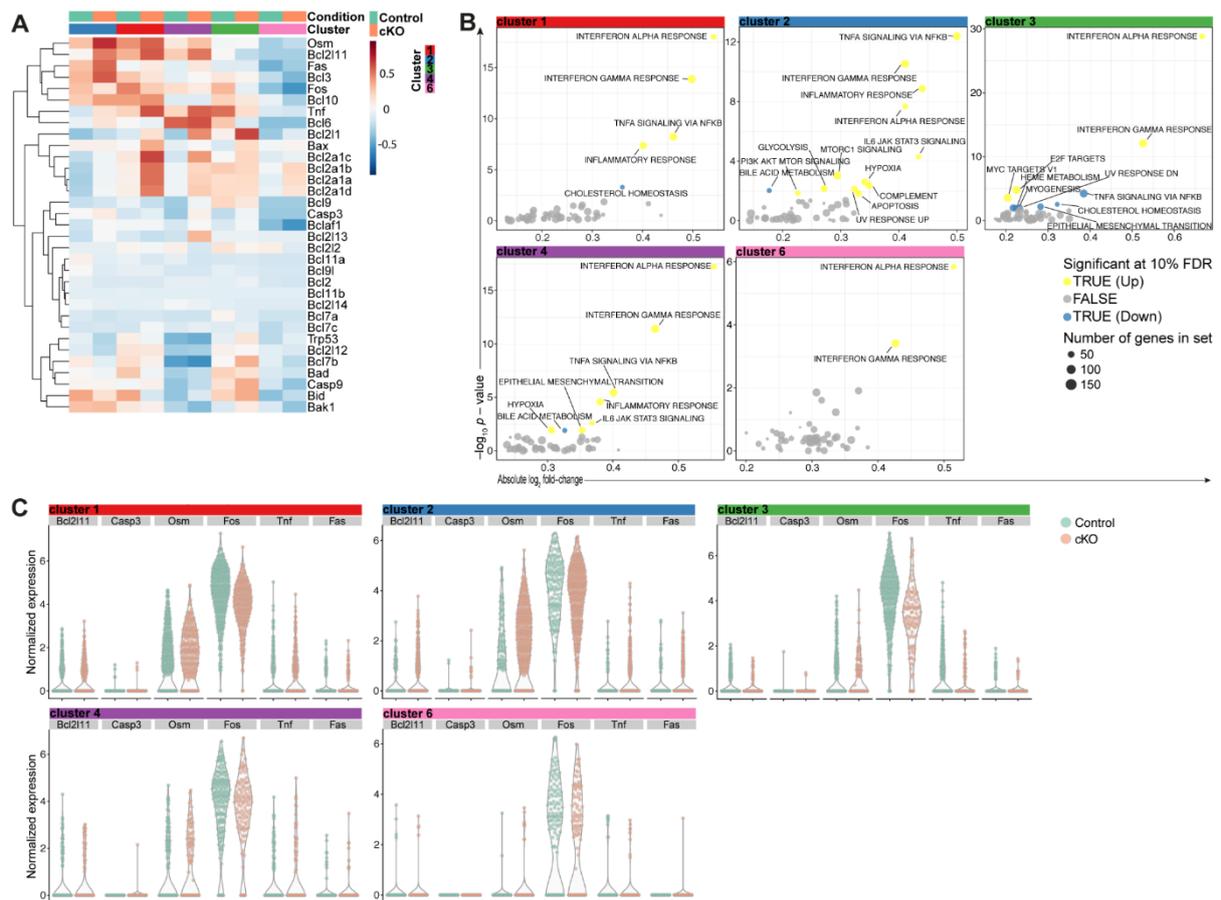
Figure 3.13: Enrichment of apoptosis-related genes in CD98 cKO cells. (**A**) Regulation of genes associated with apoptosis was displayed. (**B**) Gene Set Enrichment Analysis (GSEA) indicates enrichment of differential expresses genes in CD98 cKO cells over control cells in indicated signatures per cluster. (**C**) Expression of *Bcl2l11*, *Casp3*, *Osm*, *Fos*, *Tnf* and *Fas by* CD98 cKO cells and control cells per individual cluster.

Furthermore, flow cytometry analysis of an independent experiment in mice using the DSS-induced colitis model indicated increased apoptosis after CD98 deletion (**Figure 3.14A and 3.14B**). According to that, the excision of CD98 by injection of tamoxifen over five consecutive days resulted in reduced Ly6C^{low} monocyte and MHC class II-positive macrophage cell numbers on day 2 and day 7 after the first tamoxifen injection (**Figure 3.15A and 3.15B**).
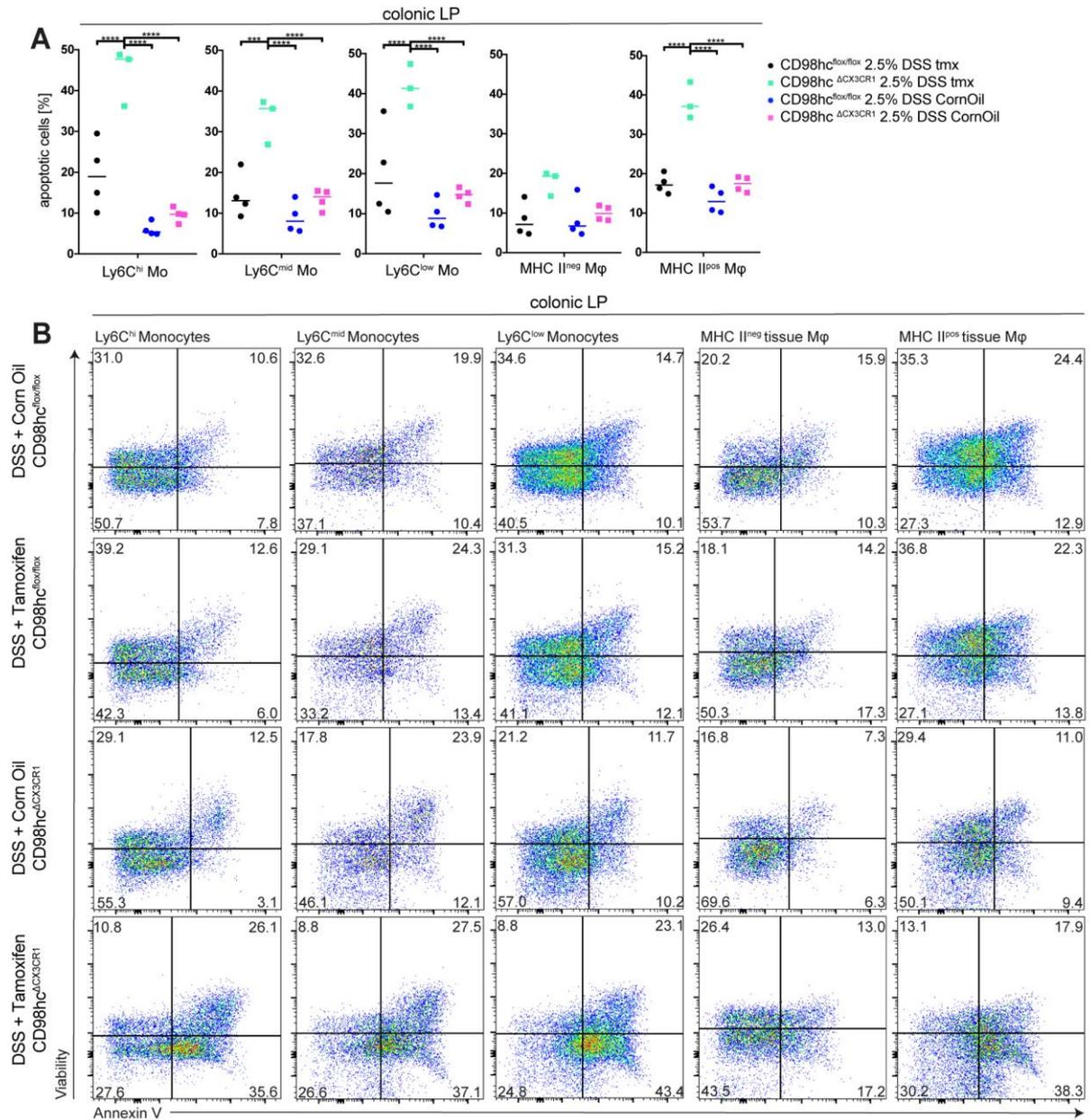
Figure 3.14: Deletion of CD98 leads to increased apoptosis in colonic macrophages. (**A**) Percentage of apoptotic cells determined by flow cytometry after Annexin V/viability staining by indicated monocytes (Mo) and macrophages (Mφ) after treatment of CD98hc$^{flox/flox}$ or CD98hc$^{\Delta CX3CR1}$ animals with corn oil- or tamoxifen. (**B**) Flow cytometry dot plots indicated experimental groups after Annexin V/viability staining. Each dot represents one animal. Data was analyzed by two-way ANOVA followed by Sidak's correction; **p<0.01, ***p<0.001, ****p<0.0001.
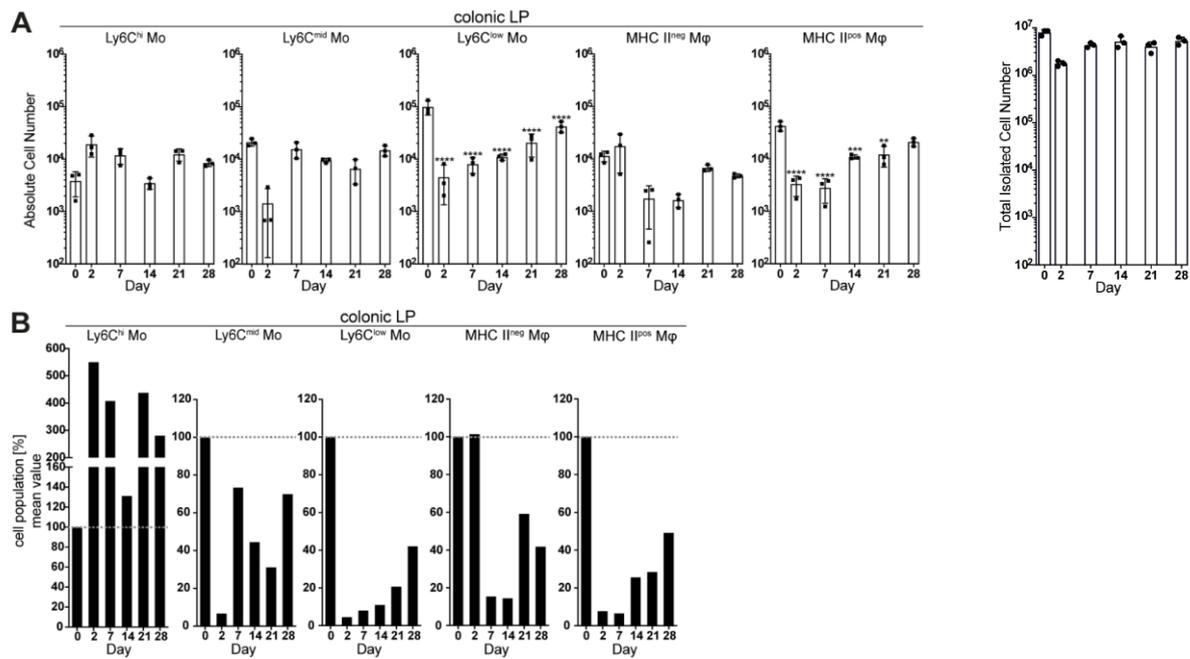
Figure 3.15: Deletion of CD98 leads to reduced cell number in colonic macrophages. (**A**) Absolute cell numbers of monocytes (Mo) and macrophages (Mφ) at indicated time points after tamoxifen injection in CD98hc$^{\Delta CX3CR1}$ mice. Monocyte and macrophage cell numbers in the colonic lamina propria (LP) of CD98hc$^{\Delta CX3CR1}$ animals (n=3) is shown as the mean (±SD) and analyzed by two-way ANOVA followed by Sidak's correction; **p<0.01, ***p<0.001, ****p<0.0001. The variability in total isolated cell numbers from colonic digests of CD98hc$^{\Delta CX3CR1}$ animals (n=3) is shown as the mean (±SD) and analyzed by Kurskal-Wallis test followed by Dunn's correction; **p<0.01. (**B**) Ratios of colonic lamina propria monocytes (Mo) and macrophages (Mφ) between CD98hc$^{\Delta CX3CR1}$ animals before tamoxifen treatment, during tamoxifen treatment, and after tamoxifen treatment at indicated time points.

3.6. Reduced macrophage numbers after silencing of CD98 in the cLP

The scRNA-seq revealed an impaired 'monocyte waterfall'-development into mature gut macrophages in the cLP. Therefore, daily intraperitoneal injection of tamoxifen into CD98hc$^{\Delta CX3CR1}$ animals throughout 28 days was performed. The experiment aimed to silence CD98 constantly in the monocyte and macrophage subpopulations without being replenished by BM-derived cells newly entering the cLP (**Figure 3.16A**). Interestingly, extravasated Ly6C^{high} monocytes and Ly6C^{mid} monocytes showed a significant CD98 silencing over time. However, the absolute cell number of Ly6C^{high} monocytes and Ly6C^{mid} monocytes was not decreased. Similar results are observed of the MHC II$^-$ macrophages which show also a significantly reduced expression of CD98 but no impaired cell number. In contrast, Ly6C^{low}

54

monocytes and MHC II$^+$ macrophages showed a significant CD98 silencing as well as prominent decreased cell number of both Ly6C^{low} monocytes by day 14 and MHC II$^+$ macrophages by day 7 after the first tamoxifen injection (**Figure 3.16B and 3.16C**).
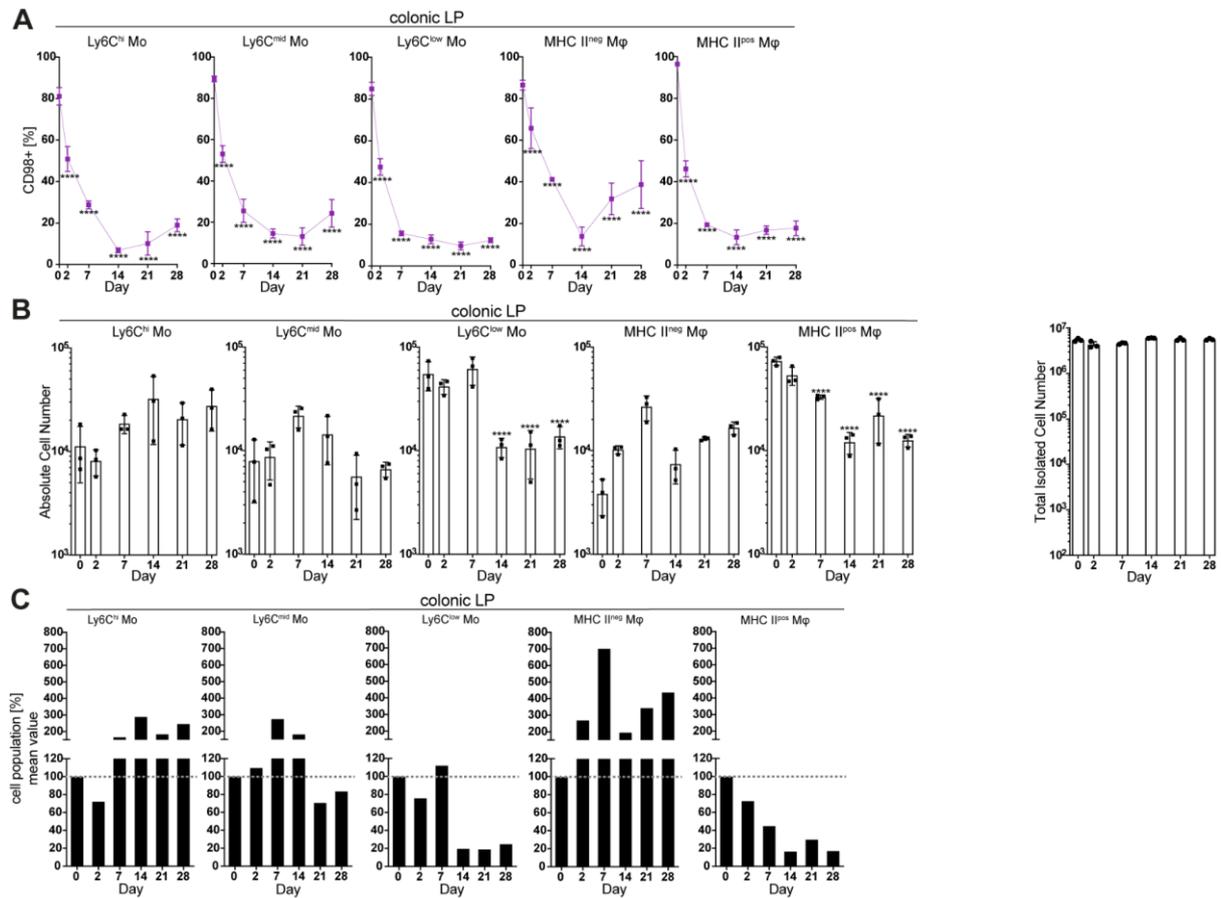
Figure 3.16: Deletion of CD98 in monocytes and macrophages leads to reduced macrophage numbers in the colonic lamina propria. Percentage of monocytes and macrophages that express CD98 and total monocyte and macrophage number in the colonic lamina propria of CD98hc$^{\Delta CX3CR1}$ mice was determined after receiving tamoxifen for 28 days. (**A**) Percentage of CD98$^+$ monocytes (Mo) and macrophages (Mφ), and (**B**) total monocyte (Mo) and macrophage (Mφ) numbers in the colonic lamina propria of CD98hc$^{\Delta CX3CR1}$ animals (n=3) is shown as the mean (±SD) and analyzed by two-way ANOVA followed by Sidak's correction; ****$p < 0.0001$. The variability in total isolated cell numbers from colonic digests of CD98hc$^{\Delta CX3CR1}$ animals (n=3) is shown as the mean (±SD) and analyzed by Kurskal-Wallis test followed by Dunn's correction; not significant. (**C**) Ratios of colonic lamina propria monocytes (Mo) and macrophages (Mφ) between CD98hc$^{\Delta CX3CR1}$ animals before tamoxifen treatment and during tamoxifen treatment at indicated time points.

Additionally, BMDMs obtained from CD98hc$^{\Delta CX3CR1}$ mice were generated to investigate the effect of CD98 deletion *in vitro*. Therefore, tamoxifen was administered into M-CSF differentiated BMDMs. Astonishingly, *in vitro* silencing of CD98 ultimately resulted in cell death on day 7 of differentiation of non-stimulated, LPS + IFNγ, or IL-4 + IL-13 stimulated BMDMs (**Figure 3.17A**). Furthermore, nitric oxide synthetase and arginase-I are prototypic markers of pro-inflammatory and anti-inflammatory macrophages (Coburn et al., 2016; Tsumura et al., 2012). Additionally, a further characteristic of pro-inflammatory and anti-inflammatory macrophages is the metabolism of arginine (Ginhoux et al., 2016; Hesse et al., 2001; Mosser and Zhang, 2008). Measurement of nitric oxide indicates the impact of CD98 silencing on macrophage metabolism of arginine by the administration of 10 mM D-phenylalanine, a natural inhibitor of SLC3A2-SLC7A5 activity (Schuster et al., 2015), into M-CSF differentiated and non-stimulated, LPS + IFNγ, or IL-4 + IL-13 stimulated BMDMs. The *in vitro* treatment of BMDMs with D-phenylalanine revealed in a slight increase of nitrate production in the culture supernatant of non-stimulated and pro-inflammatory BMDMs (**Figure 3.17B**). Taken together, our data confirm that the silencing of CD98 leads to an impairment of the 'monocyte waterfall'-development into tissue-resident macrophages in the cLP. Thus, the cell numbers of Ly6C^{low} monocytes and mature MHC II$^+$ macrophages were significantly diminished. Furthermore, *in vitro* inhibition of the SLC3A2-SLC7A5 activity indicates stimulation of pro-inflammatory macrophages.
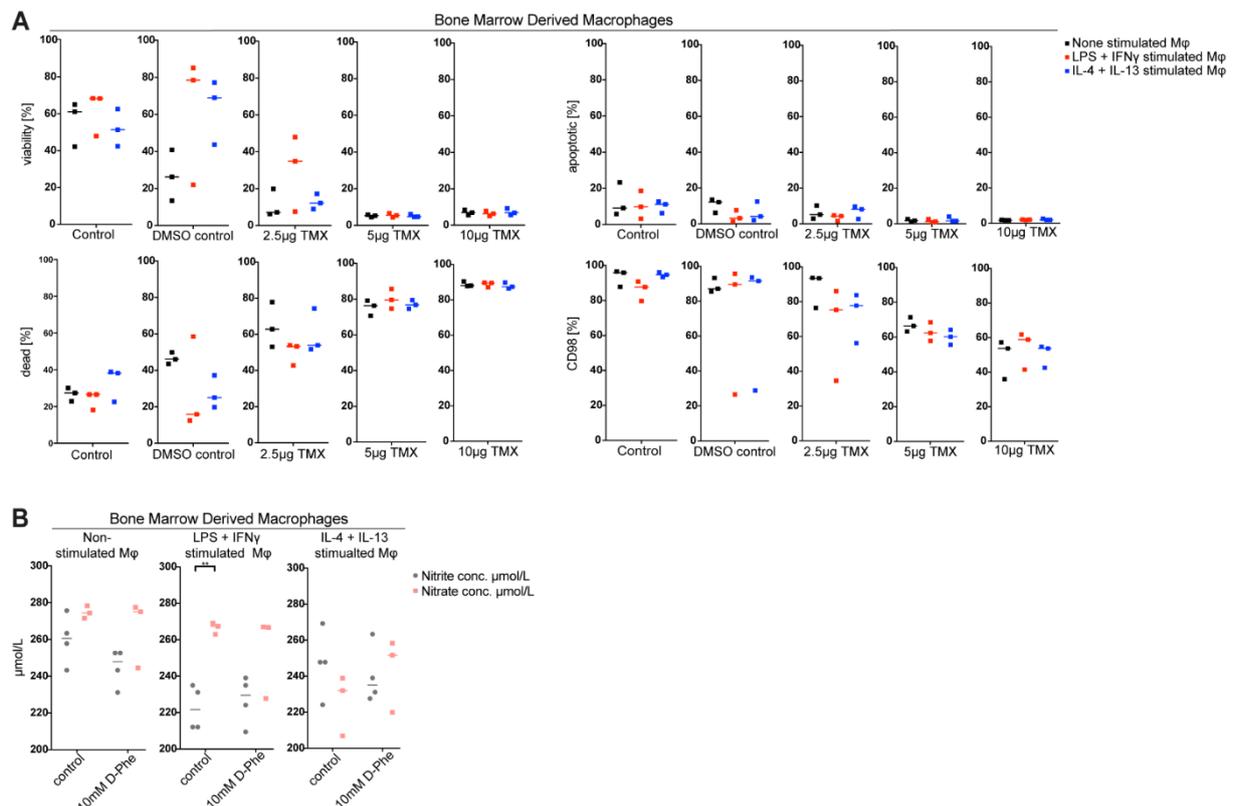
Figure 3.17: *In vitro* **deletion of CD98 results in cell death.** (**A**) Non-stimulated, LPS + IFNγ, or IL-4 + IL-13 stimulated bone marrow-derived macrophages (BMDM) were cultured in RPMI 1640 medium containing: none (control), 100 µg dimethyl sulfoxide (DMSO control), 2.5 µg, 5 µg, and 10 µg tamoxifen dissolved in DMSO. Viability, cell death, apoptotic cells, and percentage of CD98 expression was determined by flow cytometry after Annexin V/ viability staining and CD98 staining. (**B**) Slc3a2-Slc7a5 activity in BMDMs was inhibited with 10 mM D-phenylalanine and nitrite/nitrate production measured.

3.7. High CD98 expression in patients with inflammatory bowel disease (IBD)

The chronic intestinal inflammatory disease has two main known forms: (1) Crohn's disease (CD), and (2) ulcerative colitis (UC) (Uhlig and Powrie, 2018), in which CD98 might play a crucial role (Laroui et al., 2014; Nguyen et al., 2011). Therefore, the Swiss IBD Cohort provided biopsies from patients with quiescent and active UC and patients with quiescent and active CD which were taken from the inflamed regions of the intestine to determine the expression level of CD98 heavy chain (*CD98hc/SLC3A2*) and CD98 light chain (*CD98lc/SLC7A5*). Interestingly, RT-qPCR analysis revealed a very high CD98hc as well as CD98lc expression in both UC and CD patients without any significant difference between quiescent or active disease. (**Figure 3.18A**). Furthermore, immunofluorescence staining was realized to

investigate the CD98hc expression in human intestinal tissue of both UC and CD patients. The immunofluorescence staining in non-inflamed and inflamed tissue confirmed the expression of CD98hc by intestinal epithelial cells as well as lamina propria cells (**Figure 3.18B and 3.18C**). The CD98 staining intensity underpins the bright CD98hc expression of IECs and lamina propria cells of non-inflamed and inflamed biopsies of both UC and CD patient (**Figure 3.18B and 3.18C**). Therefore, these results implicated that CD98 is highly expressed in steady state as well as under inflamed conditions in human cLP.
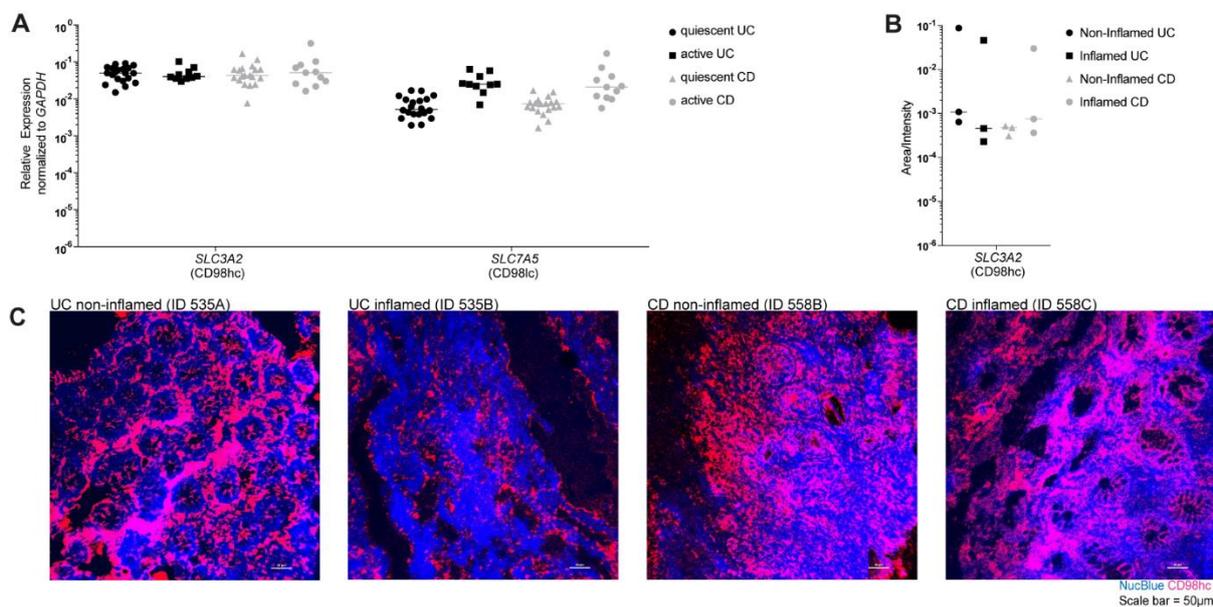
Figure 3.18: Inflammatory bowel disease patients express CD98. The Swiss IBD cohort provided colonic or ileal biopsies from Crohn's disease (CD) or ulcerative colitis (UC) patients which were in remission (quiescent) or with active disease. (**A**) *CD98hc*/*SLC3A2* and *CD98lc/SLC7A5* expression was determined by RT-qPCR. (**B**) CD98hc fluorescence intensity of staining of biopsies from CD and UC patients. (**C**) Cryosections of inflamed and non-inflamed regions of the same CD and UC patients (patient identification numbers in brackets) were stained for CD98 and counterstained with NucBlue.

4   *DISCUSSION*

In this study, we show that the CD98 is highly expressed by BM progenitor cells as well as by intestinal mononuclear phagocytes in the steady state. Additionally, CD98 is also highly expressed under inflammatory conditions. In the gut, monocytes and macrophages survey the intestinal content by clearing apoptotic cell bodies and microorganisms that have crossed the epithelial barrier (Mowat et al., 2017), and that extravasated blood monocytes give rise to gut macrophages through different intermediate stages (Schridde et al., 2017). Our results show the intestinal 'monocyte waterfall'-development on a transcriptomic level by scRNA-seq. Further, macrophages are essential for tissue repair and restoration of intestinal homeostasis during intestinal inflammation (Arnold et al., 2016; Joeris et al., 2017). Interestingly, the deletion of the CD98hc in intestinal mononuclear phagocytes resulted in attenuated severity of DSS-induced colitis. Additionally, the expression level of CD29 was not affected by the tamoxifen-induced CD98 deletion. The transcriptomic analysis revealed that the silencing of CD98 results in a block of the 'monocyte waterfall'-development into gut macrophages. Thus, the impaired monocyte-macrophage-development is associated with increased apoptosis signature in the CD98hc deleted monocytes and macrophages. Consequently, the absolute cell number of Ly6C^{low} monocytes (P3) and MHC II^{pos} macrophages (P5) is significantly reduced. Furthermore, as CD98 correlates with IBD (Laroui et al., 2014; Nguyen et al., 2011), CD98hc is highly expressed in colonic tissue of patients with CD and UC. Therefore, targeting the glycoprotein CD98, which is associated with gut homeostasis and the intestinal innate immune responses (Yadav et al., 2016), represents a potential therapeutic target for the treatment of IBD.

4.1.   CD98 expression of mononuclear phagocytes and their progenitors

The expression levels of CD98 by intestinal macrophages and their progenitors have not been studied to date in detail. Therefore, we characterized first the progenitors in the bone marrow (BM) and elucidated their CD98 expression, as the glycoprotein 4F2/CD98, encoded by the genes *SLC3A2/Slc3a2* in human/mice, is ubiquitously expressed in many cell types and in almost all cell lines (Cantor and

Ginsberg, 2012; Haynes et al., 1981). We could show, in accordance with the previous findings that the MDPs, cMoPs, and monocytes of the BM (Hettinger et al., 2013) also express CD98. Moreover, these cells show more than 96% CD98 positivity. Further, analysis of the mononuclear phagocytes in the colonic lamina propria revealed a high expression level of CD98. Merely the immature $CD64^+$ MHC II^- subpopulation showed less CD98 positive cells (~ 85%), which might be due to the differentiation and in this way, shape-changing development from the $CCR2^+$ $Ly6C^{low}$ MHC II^+ monocytes towards to $CD64^+$ MHC II^+ tissue macrophages. Additionally, chosen CD98lc were also highly expressed in the colonic tissue in steady state as well as under inflammatory conditions. Moreover, high CD98 expression levels of BMDMs did not show any differences by stimulating with pro- or anti-inflammatory cytokines. Interestingly, analysis of the ontogeny of tissue-resident macrophages and their CD98 expression showed, that embryonic macrophages have very low CD98 expression. The amino acid transporter is increased expressed in adult tissue-resident macrophages such as Kupffer cells and Langerhans cells. Here, we could show that CD98 is highly expressed in mononuclear phagocytes in the gut, liver, and epidermis.

4.2.   'Monocyte waterfall'-development and the effect of CD98 deletion

The expression of CD98 is required for the development of $Ly6C^{high}$ monocytes into gut-resident macrophages because the deletion of CD98 had three main impacts:

First, extravasated $Ly6C^{high}$ monocytes are impaired in their genetic development into tissue-resident macrophages. Additionally, the blockage of monocyte differentiation is associated with increased expression of apoptosis-related genes, which indicates an earlier cell death of $Ly6C^{high/mid}$ monocytes in the cLP.

Second, the impairment of $Ly6C^{high}$ monocytes to differentiate into macrophages resulted in significantly reduced numbers of $Ly6C^{low}$ monocytes and mature macrophages in $CX3CR1^+$ cells.

Third, deletion of CD98 by addition of tamoxifen into *in vitro* culture of BMDMs resulted in increased cell death.

The deletion of CD98 specifically in monocytes and macrophages leads to attenuated colitis in mice. Whether this is due to genetic varieties or not, had not been investigated before. In this study, we analyzed the 'monocyte waterfall'-development into gut-resident macrophages by single-cell RNA sequencing (scRNA-seq). For that, CD98hc$^{\Delta CX3CR1}$ mice treated with tamoxifen versus the carrier corn oil were compared. The results suggest nine different clusters of immune cell types in the cLP. Further, a developmental trajectory of monocytes to gut-resident macrophages on a single-cell transcriptome level is suggested by the expression of genes allocated to monocytes (cluster 1, 2, and 4 expressing *Ly6c2, Ccr2, Cd14*) or to macrophages (cluster 3 and 6 expressing *Cd63, Cd72, Cd74, Cd81, Cx3cr1, Adgre1* (EMR1, F4/80)). The chronology of the lineage tree: cluster 2 (Population 1 (P1)), cluster 1 (P2), cluster 4 (P3), cluster 6 (P4), and cluster 3 (P5). Moreover, the t-SNE analysis indicated a close relationship between the clusters characterized as monocytes and macrophages, whereas the remaining clusters 5, 7, 8, and 9 are not related to the lineage tree clusters. These clusters express *Cd63, Ly6a, Ly6c1,* and *Cst3* suggesting a possible 'contamination' with granulocytes and DCs (Varol et al., 2010), which is likely that these cell types are detected due to contaminating GALT. As this study is focusing on monocytes and macrophages in the cLP, the 'contaminating' clusters were excluded and neglected. Flow cytometry was used to confirm chosen genes (CD14, CD72, and CD81) expressed by monocytes and/or macrophages. Unlike on the transcriptomic level which revealed a high expression of CD14 in monocytes and CD72 in macrophages, flow cytometry analysis indicated that CD14 and CD72 are at the same extent expressed on the cell surface of monocytes and macrophages. Merely CD81 was increasingly expressed from monocytes towards to macrophages. Additionally, the deletion of CD98 did not interfere with the cell surface expression of CD14, CD72, and CD81. Interestingly, relative density plots and the relative proportion of cells indicated an accumulation of Ly6C^{high} monocytes in CD98hc$^{\Delta CX3CR1}$ animals treated with tamoxifen compared to the CD98hc$^{\Delta CX3CR1}$ animals treated with corn oil. These findings indicate that the expression of CD98 is required for the differentiation of Ly6C^{high} monocytes into gut-resident macrophages. Thus, in CD98 deleted mice the 'monocyte

waterfall'-development in the gut is significantly impaired. Given that the Ly6C^{high} monocytes are blocked in their development, we investigated in more detail the expression of genes associated with apoptosis. Therefore, selected genes were analyzed and revealed an increased expression of *Fas, Bcl2l11, Tnf,* and *Osm* in clusters 1 and 2 correspondings to CD98 deleted monocytes. Moreover, Gene Set Enrichment Analysis (GSEA) shows apoptosis-related up- or down-regulated genes which are more prominent expressed in cluster 2 but not in cluster 1, 3, 4, and 6 of tamoxifen-treated CD98hc$^{\Delta CX3CR1}$ mice. Further, these selected apoptosis-related genes are highly expressed in monocytes of cluster 1 and 2. Especially *Osm* is more pronounced expressed in cluster 2 after the excision of CD98. Cluster 4, 3, and 6 do not show significantly distinguishable apoptosis-related gene expression. Thus, the impairment of the 'monocyte waterfall'-development might be due to increased apoptotic gene expression in CD98 deficient cells.

Because of increased apoptosis-related genes in CD98 deleted cells, flow cytometry analysis was carried out to explore apoptotic cells in the subpopulations of intestinal monocytes and macrophages. Indeed, our investigations indicated also that CD98 deletion not only leads to increased apoptotic gene expression, but also to increased apoptosis of the colonic monocytes and macrophages. Further, analysis of the cell numbers indicated a significantly reduced Ly6c^{low} monocyte and MHC II$^+$ macrophage numbers after silencing CD98. This effect accompanies with the kinetics of CD98 silencing in which day 7 revealed the optimum of CD98 deletion. Consequently, the lowest cell population number of MHC II$^+$ macrophages occurred on day 7. In addition, the silencing of CD98 over 28 days by daily tamoxifen treatment in CD98hc$^{\Delta CX3CR1}$ mice revealed a permanent decreased cell number of Ly6C^{low} monocytes and MHC II$^+$ macrophages. Moreover, Ly6C^{high} monocytes showed a tendency of accumulation over the time of CD98 deletion. Besides, the *in vitro* model could show that the addition of different concentrations of tamoxifen into cultures of M-CSF differentiated BMDMs obtained from CD98hc$^{\Delta CX3CR1}$ mice resulted in cell death. Furthermore, *in vitro* treatment of BMDMs with 10 mM D-phenylalanine, which is a natural inhibitor of the SLC3A2-SLC7A5 activity (Schuster et al., 2015), revealed in a slight increase of non-stimulated 'resting' BMDMs into pro-inflammatory BMDMs indicated by elevated nitrate expression. Hence, *in vitro* CD98 deletion by D-phenylalanine changed the

metabolism of arginine in 'resting' macrophages to the metabolism of pro-inflammatory macrophages. Thus, arginine is metabolized to nitric oxide. However, D-phenylalanine did not show any impairment of the metabolism of anti-inflammatory BMDMs, which metabolize arginine to ornithine (Ginhoux et al., 2016; Hesse et al., 2001; Martinez and Gordon, 2014; Mosser and Zhang, 2008).

4.3. Deletion of CD98hc

Given that CD98 is highly expressed in monocytes and macrophages of the cLP, we next deleted specifically CD98hc in CX3CR1$^+$ mononuclear phagocytes. For that, we used the inducible Cre-*loxP* system that controls the Cre system by the temporal inducer tamoxifen, which is systemically administered by intraperitoneal injection. In this system, tamoxifen modifies Cre protein which fuses with estrogen receptor containing a mutated ligand binding domain (also known as CreERT). Usually, the CreERT binds to the heat shock protein 90 (HSP90), which is disrupted when it binds to the synthetic steroid tamoxifen. Furthermore, this nuclear translocation leads to the interaction of CreERT with *loxP* sites (Kim et al., 2018). The use of the CrERT system led us to delete CD98hc only in CX3CR1$^+$ monocytes and macrophages of CD98hc$^{\Delta CX3CR1}$ animals. The i.p. injection of tamoxifen over five consecutive days led to decreased CD98hc expression of colonic mononuclear phagocytes as well as Kupffer cells, which primarily seed from fetal liver-derived monocytes and maintain through self-renewal (Hoeffel et al., 2015), in a time-dependent manner. However, i.p. injection of tamoxifen did not affect the CD98 expression of Langerhans cells which develop prenatally independent of the monocyte pool (Yona et al., 2013). This might be due to several reasons:

Half-life of the active metabolites of tamoxifen (Jahn et al., 2018)
Tamoxifen is a prodrug with little affinity for the estrogen receptor. It is metabolized in the liver by the cytochrome P450 isoform CYP2D6 and CYP3A4 into the active metabolites afimoxifene (4-hydroxytamoxifen; 4-OHT), N-desmethyl-tamoxifen (NDM-TAM) and endoxifen (N-desmethyl-4-hydroxytamoxifen), with a 30-100 times greater affinity for the estrogen receptor. The half-life of i.p.

injected TAM and its metabolites are ~ 40h in the serum after a single dose of TAM with TAM (9.9 h), 4-OH-TAM (15.8 h), NMD-TAM (19.9 h), and END (33.2 h).

Application and distribution of tamoxifen (Bosenberg et al., 2006; Vasioukhin et al., 1999).

Tamoxifen can be applied by different routes: orally, intraperitoneally, or by topical application on the skin. Thus, in the mouse organism, the active metabolites of tamoxifen are systemically distributed. Moreover, Vasioukhin and co-workers showed that TAM is detectable in all layers of the skin epidermis. Hence, the inhibition of CD98 silencing by the tamoxifen injection in Langerhans cells might be due to another mechanism.

Embryonic development of mononuclear phagocytes (Yona et al., 2013).

Myeloid cells, including mononuclear phagocytes, are known to arise by a series of waves from primitive hematopoiesis (early embryogenesis) to definitive hematopoiesis (late fetal stages). Macrophages from the primitive origin (e.g., microglia) maintain themselves throughout adult life by limited self-renewal as well as longevity without any input from definitive hematopoiesis. The fractalkine gene *Cx3cr1* is broadly expressed within the mononuclear phagocyte system. Epidermal Langerhans cells derive from primitive macrophages and fetal liver cells. Indeed, during adulthood, this compartment maintains itself independent from bone marrow-derived blood monocyte input compared to Kupffer cells, which are partially replenished by blood monocytes shown by Scott and co-workers in 2016. Further, the expression of the fractalkine receptor/CX3CR1 is discontinued during maturation. Thus, in adulthood, epidermal Langerhans cells are CX3CR1 negative.

Therefore, due to the lack of CX3CR1 in epidermal Langerhans cells, CD98hc is not deleted by the i.p. injection of tamoxifen, signifying the high CD98hc expression. Additionally, analysis of other cell types like B cells, CD4$^+$ and CD8$^+$ T cells, DCs, neutrophils, and NK cells for their CD98 expression elucidated that the specific deletion of CD98hc only occurs in colonic macrophages and not in other immune cells harbored in the cLP. Further, the optimal silencing revealed around day 7 after the first injection of tamoxifen. However, as in the cLP the CD98 expression could be restored within 14 to 21

days, tissue-resident Kupffer cells needed up to 28 days. These findings suggest that CX3CR1[+] macrophages in the cLP are constantly replenished by circulating blood monocytes. Nevertheless, blood monocytes might replenish Kupffer cells, which stay in this niche usually as long-lived self-renewing cells (David et al., 2016; Scott et al., 2016). Possibly, the silencing of CD98 in CX3CR1 expressing mononuclear phagocytes inhibits the restoration of gut macrophages and Kupffer cells due to cell death of monocyte intermediates. CD98 mediates not only the uptake of branched-chain amino acids (BCAA), it also binds to the cytoplasmic tail of integrin tails such as β1A and β3 integrins to regulate the integrin signaling (Cantor and Ginsberg, 2012). Investigation for the expression of integrin β1 (CD29) during tamoxifen treatment showed no alteration of the CD29 expression. Therefore, we did not investigate the CD98 and CD29 interaction in detail.

4.4. Deletion of CD98 protects mice from DSS induced colitis

The overexpression of CD98 in epithelial cells leads to an increased proliferation of IECs combined with an impaired barrier function. Further, the overexpression of CD98 leads also to a more severe colitis and colitis-associated cancer (Nguyen et al., 2011). It has been shown, that the treatment of animals with nanoparticles carrying small interfering RNAs directed against CD98 could reduce the CD98 expression in macrophages and colonic epithelial cells *in vitro*. In mice, the application of single chain CD98 (scCD98)-functionalized small interfering CD98 RNA (siCD98)-loaded nanoparticles by hydrogels reduced colon expression of CD98. Thus, colitis severity has been reduced (Xiao et al., 2014). In this study, we used a genetically engineered cKO mouse in which the floxed CD98 sequence is cut out by the tamoxifen-induced Cre activation. Thus, CD98hc is specifically deleted in CX3CR1[+] monocytes and macrophages. In contrast, Xiao and co-workers used scCD98-functionalized siCD98-loaded nanoparticles which have an affinity for CD98-overexpressing cells to significantly reduce the CD98 expression. In comparison to our specific tamoxifen-induced CD98 deletion, the siCD98-loaded nanoparticles reduce the CD98 expression not only in CD98-overexpressing colonic epithelial cells and macrophages but also in all other cell types harbored in the cLP. Further, previous work showed also that the silencing of CD98 in regulatory T cells (Treg) leads to reduced Treg cell number and an impaired

suppressive function in the gut, which is likely due to reduced uptake of BCAA and not by CD29-mediated adhesion (Ikeda et al., 2017). As the optimal time frame of CD98 silencing was given, DSS-induced colitis experiment was realized. Our results showed, that the deletion of CD98 in CD98hc$^{\Delta CX3CR1}$ animals leads to attenuation of colitis indicated by the clinical signs of body weight loss, disease activity index (DAI), colon shortening, histological signs, and endoscopically. Further, the decreased severity of colitis indicates that the expression of CD98 by intestinal epithelial cells (Nguyen et al., 2011) and macrophages mediates colitis. Moreover, as the reduced uptake of BCAA attenuates the severity of colitis, feeding mice with 10% higher amino acid chow (5% more L-leucine and 5% more L-isoleucine) compared to conventional chow revealed a tendency of increased intestinal inflammation in tamoxifen-treated CD98hc$^{\Delta CX3CR1}$ mice. Thus, the influx of BCAA leads to a rapidly higher expression of the amino acid transporter CD98hc (Yan and Lamb, 2010) supporting the inflammatory response of intestinal immune cells which might compensate the impaired immunological behavior of CD98 deficient colonic monocytes and macrophages.

4.5.   CD98 in human inflammatory bowel disease

CD98 is highly expressed in steady state as well as under inflammatory conditions in the mouse intestine. Thus, the high CD98hc expression might be due to the ingestion of amino acids which results in a rapid and transient upregulation of the amino acid transporter CD98 (Yan and Lamb, 2010). As CD98 strongly correlates with IBD (Laroui et al., 2014; Nguyen et al., 2011), we investigated the expression levels of *SLC3A2* and *SLC7A5* in human IBD patients. Therefore, biopsies from patients with quiescent and active UC and patients with quiescent and active CD were taken by the Swiss Inflammatory Bowel Disease Cohort Study. The results indicated also in humans that *SLC3A2* and *SLC7A5* are highly expressed in patients with quiescent and active UC or in patients with quiescent and active CD. Further, immunofluorescence staining additionally showed that CD98hc is ubiquitously expressed by IECs as well as lamina propria cells of the colon. The intensity per area showed no significant difference between non-inflamed or inflamed colon samples of UC or CD patients. Thus,

RT-qPCR analysis, as well as immunofluorescence staining, support mutually the high CD98 expression in human.

4.6.   Concluding remarks

In conclusion, this study indicates that monocytes develop into gut-resident macrophages through different intermediates. These intermediates are characterized as two main population which express either CCR2 or CD64. The CCR2$^+$ population is further distinguished into Ly6C^{high} monocytes (P1), Ly6C^{mid} monocytes (P2), and Ly6C^{low} monocytes (P3), and the CD64$^+$ population into immature MHC II$^-$ macrophages (P4) and mature MHC II$^+$ macrophages (P5).

It has been shown that the conditional deletion of CD98 inhibits the clonal proliferation of T cells in response to antigens and prevent the establishment of autoimmune disease (Cantor et al., 2011) or to abrogate the ability of B cells to respond to mitogens which leads to defects in plasma cell formation (Cantor et al., 2009). We observed that the conditional deletion of CD98 impairs the differentiation of monocytes into macrophages in the colonic lamina propria. Moreover, the cell numbers of Ly6C^{low} monocytes, as well as MHC II$^+$ macrophages, were significantly reduced *in vivo*. Thus, the development of resident intestinal macrophages partially depends on the expression of CD98 (**Figure 4.1**). As a consequence, DSS-induced colitis was significantly attenuated in CD98hc$^{\Delta CX3CR1}$ animals treated with tamoxifen.

In the future, targeting the glycoprotein CD98, which is associated with gut homeostasis and the intestinal innate immune responses (Yadav et al., 2016), as well as strongly correlates with IBD (Laroui et al., 2014; Nguyen et al., 2011), represents a potential therapeutic target for the treatment of IBD. Moreover, molecular pathways that are involved in the 'monocyte waterfall'-development but also in the maturation of gut macrophages need to be better described. Additionally, understanding the mechanism of development of macrophages in the intestinal lamina propria may also provide attractive molecular therapeutic targets for the treatment of IBD.
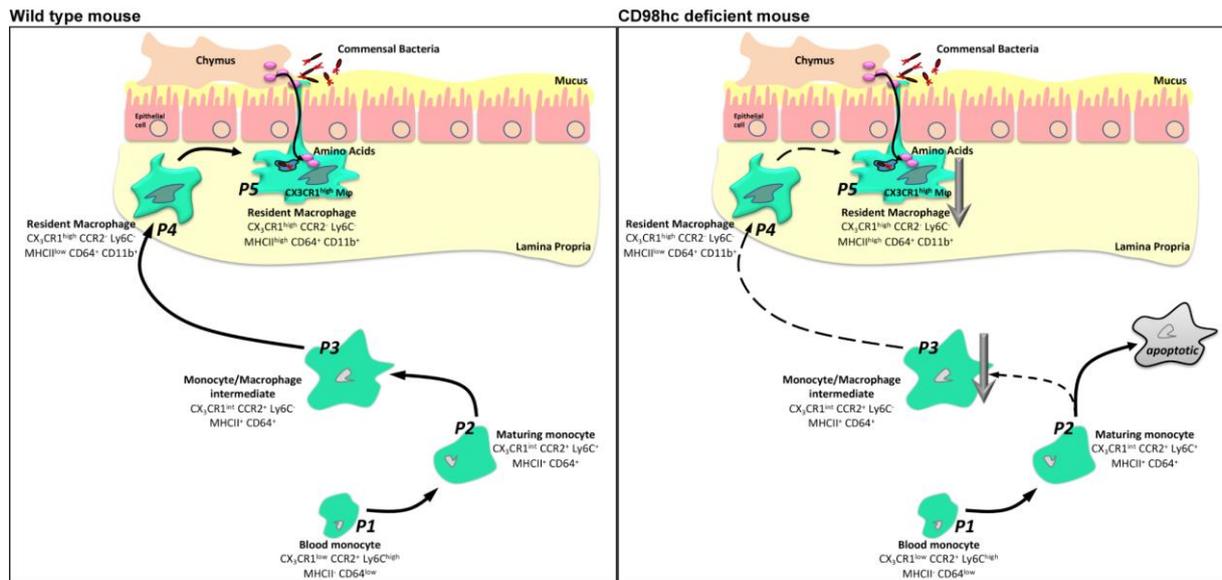
Figure 4.1: Schematic representation. The 'monocyte waterfall'-development into gut macrophages in C57BL/6 WT and CD98hc deficient mouse.

5   REFERENCES

Abraham, C., and Cho, J.H. (2009). Inflammatory bowel disease. N Engl J Med *361*, 2066–2078.

Alexander, D.E. (2008). Multiple functions of the herpes simplex virus type 1 encoded protein ICP34. 5 combat the host anti-viral response. (Washington University in St. Louis).

Ananthakrishnan, A.N. (2015). Epidemiology and risk factors for IBD. Nature Reviews Gastroenterology &Amp; Hepatology *12*, 205.

Aoki, R., Shoshkes-Carmel, M., Gao, N., Shin, S., May, C.L., Golson, M.L., Zahm, A.M., Ray, M., Wiser, C.L., Wright, C.V., and Kaestner, K.H. (2016). Foxl1-expressing mesenchymal cells constitute the intestinal stem cell niche. Cell Mol Gastroenterol Hepatol *2*, 175-188.

Arnold, I.C., Mathisen, S., Schulthess, J., Danne, C., Hegazy, A.N., and Powrie, F. (2016). CD11c(+) monocyte/macrophages promote chronic Helicobacter hepaticus-induced intestinal inflammation through the production of IL-23. Mucosal Immunol *9*, 352-363.

Arques, J.L., Hautefort, I., Ivory, K., Bertelli, E., Regoli, M., Clare, S., Hinton, J.C., and Nicoletti, C. (2009). Salmonella induces flagellin- and MyD88-dependent migration of bacteria-capturing dendritic cells into the gut lumen. Gastroenterology *137*, 579-587, 587 e571-572.

Asano, K., Takahashi, N., Ushiki, M., Monya, M., Aihara, F., Kuboki, E., Moriyama, S., Iida, M., Kitamura, H., Qiu, C.H.*, et al.* (2015). Intestinal CD169(+) macrophages initiate mucosal inflammation by secreting CCL8 that recruits inflammatory monocytes. Nat Commun *6*, 7802.

Atreya, R., Zimmer, M., Bartsch, B., Waldner, M.J., Atreya, I., Neumann, H., Hildner, K., Hoffman, A., Kiesslich, R., and Rink, A.D. (2011). Antibodies against tumor necrosis factor (TNF) induce T-cell apoptosis in patients with inflammatory bowel diseases via TNF receptor 2 and intestinal CD14+ macrophages. Gastroenterology *141*, 2026-2038.

Bain, C.C., Bravo-Blas, A., Scott, C.L., Perdiguero, E.G., Geissmann, F., Henri, S., Malissen, B., Osborne, L.C., Artis, D., and Mowat, A.M. (2014). Constant replenishment from circulating monocytes maintains the macrophage pool in the intestine of adult mice. Nat Immunol *15*, 929-937.

Bain, C.C., and Schridde, A. (2018). Origin, Differentiation, and Function of Intestinal Macrophages. Front Immunol *9*, 2733.

Bain, C.C., Scott, C.L., Uronen-Hansson, H., Gudjonsson, S., Jansson, O., Grip, O., Guilliams, M., Malissen, B., Agace, W.W., and Mowat, A.M. (2013). Resident and pro-inflammatory macrophages in the colon represent alternative context-dependent fates of the same Ly6Chi monocyte precursors. Mucosal Immunol *6*, 498–510.

Bajaj, J., Konuma, T., Lytle, N.K., Kwon, H.Y., Ablack, J.N., Cantor, J.M., Rizzieri, D., Chuah, C., Oehler, V.G., Broome, E.H.*, et al.* (2016). CD98-Mediated Adhesive Signaling Enables the Establishment and Propagation of Acute Myelogenous Leukemia. Cancer Cell *30*, 792-805.

Baumgart, D.C., and Sandborn, W.J. (2012). Crohn's disease. Lancet *380*, 1590–1605.

Bosenberg, M., Muthusamy, V., Curley, D.P., Wang, Z., Hobbs, C., Nelson, B., Nogueira, C., Horner, J.W., 2nd, Depinho, R., and Chin, L. (2006). Characterization of melanocyte-specific inducible Cre recombinase transgenic mice. Genesis *44*, 262-267.

Boulter, E., Estrach, S., Tissot, F.S., Hennrich, M.L., Tosello, L., Cailleteau, L., de la Ballina, L.R., Pisano, S., Gavin, A.C., and Feral, C.C. (2018). Cell metabolism regulates integrin mechanosensing via an SLC3A2-dependent sphingolipid biosynthesis pathway. Nat Commun *9*, 4862.

Brennecke, P., Anders, S., Kim, J.K., Kolodziejczyk, A.A., Zhang, X., Proserpio, V., Baying, B., Benes, V., Teichmann, S.A., Marioni, J.C., and Heisler, M.G. (2013). Accounting for technical noise in single-cell RNA-seq experiments. Nature methods *10*, 1093-1095.

Burada, F., Mirea, C.S., Cucu, M.G., Vilcea, I.D., Cimpoeru, A., and Ioana, M. (2018). The Association between Nod2 R702w Polymorphism and Susceptibility to Colorectal Cancer in Romanian Patients. Curr Health Sci J *44*, 135-139.

Camacho-Barquero, L., Villegas, I., Sánchez-Calvo, J.M., Talero, E., Sánchez-Fidalgo, S., Motilva, V., and de la Lastra, C.A. (2007). Curcumin, a Curcuma longa constituent, acts on MAPK p38 pathway modulating COX-2 and iNOS expression in chronic experimental colitis. International immunopharmacology *7*, 333-342.

Cantor, J., Browne, C.D., Ruppert, R., Feral, C.C., Fassler, R., Rickert, R.C., and Ginsberg, M.H. (2009). CD98hc facilitates B cell proliferation and adaptive humoral immunity. Nat Immunol *10*, 412–419.

Cantor, J., Slepak, M., Ege, N., Chang, J.T., and Ginsberg, M.H. (2011). Loss of T cell CD98 H chain specifically ablates T cell clonal expansion and protects from autoimmunity. J Immunol *187*, 851–860.

Cantor, J.M., and Ginsberg, M.H. (2012). CD98 at the crossroads of adaptive immunity and cancer. J Cell Sci *125*, 1373–1382.

Coburn, L.A., Horst, S.N., Allaman, M.M., Brown, C.T., Williams, C.S., Hodges, M.E., Druce, J.P., Beaulieu, D.B., Schwartz, D.A., and Wilson, K.T. (2016). L-Arginine Availability and Metabolism Is Altered in Ulcerative Colitis. Inflamm Bowel Dis *22*, 1847-1858.

Coskun, M. (2014). Intestinal Epithelium in Inflammatory Bowel Disease. Frontiers in Medicine *1*.

David, B.A., Rezende, R.M., Antunes, M.M., Santos, M.M., Freitas Lopes, M.A., Diniz, A.B., Sousa Pereira, R.V., Marchesi, S.C., Alvarenga, D.M., Nakagaki, B.N.*, et al.* (2016). Combination of Mass Cytometry and Imaging Analysis Reveals Origin, Location, and Functional Repopulation of Liver Myeloid Cells in Mice. Gastroenterology *151*, 1176–1191.

De Schepper, S., Verheijden, S., Aguilera-Lizarraga, J., Viola, M.F., Boesmans, W., Stakenborg, N., Voytyuk, I., Smidt, I., Boeckx, B., Dierckx de Casterle, I.*, et al.* (2018). Self-Maintaining Gut Macrophages Are Essential for Intestinal Homeostasis. Cell *175*, 400-415 e413.

Deves, R., and Boyd, C.J.J.o.M.B. (2000). Surface antigen CD98 (4F2): not a single membrane protein, but a family of proteins with multiple functions. *173*, 165-177.

Duò, A., Robinson, M.D., and Soneson, C. (2018). A systematic performance evaluation of clustering methods for single-cell RNA-seq data. F1000Research *7*, 1141-1141.

Eckmann, L. (2006). Animal models of inflammatory bowel disease: lessons from enteric infections. Ann N Y Acad Sci *1072*, 28-38.

Eri, R., McGuckin, M.A., and Wadley, R. (2012). T cell transfer model of colitis: a great tool to assess the contribution of T cells in chronic intestinal inflammation. Methods Mol Biol *844*, 261-275.

Fenczik, C.A., Zent, R., Dellos, M., Calderwood, D.A., Satriano, J., Kelly, C., and Ginsberg, M.H. (2001). Distinct domains of CD98hc regulate integrins and amino acid transport. Journal of Biological Chemistry *276*, 8746-8752.

Feral, C.C., Nishiya, N., Fenczik, C.A., Stuhlmann, H., Slepak, M., and Ginsberg, M.H. (2005). CD98hc (SLC3A2) mediates integrin signaling. Proceedings of the National Academy of Sciences *102*, 355-360.

Gerlach, C., Moseman, E.A., Loughhead, S.M., Alvarez, D., Zwijnenburg, A.J., Waanders, L., Garg, R., de la Torre, J.C., and Andrian, U.H. (2016). The Chemokine Receptor CX3CR1 Defines Three Antigen-Experienced CD8 T Cell Subsets with Distinct Roles in Immune Surveillance and Homeostasis. Immunity *45*, 1270–1284.

Ginhoux, F., Schultze, J.L., Murray, P.J., Ochando, J., and Biswas, S.K. (2016). New insights into the multidimensional concept of macrophage ontogeny, activation and function. Nat Immunol *17*, 34-40.

Gomez Perdiguero, E., Klapproth, K., Schulz, C., Busch, K., Azzoni, E., Crozet, L., Garner, H., Trouillet, C., Bruijn, M.F., Geissmann, F., and Rodewald, H.R. (2015). Tissue-resident macrophages originate from yolk-sac-derived erythro-myeloid progenitors. Nature *518*, 547–551.

Gren, S.T., and Grip, O. (2016). Role of Monocytes and Intestinal Macrophages in Crohn's Disease and Ulcerative Colitis. Inflamm Bowel Dis *22*, 1992-1998.

Hausmann, M., Kiessling, S., Mestermann, S., Webb, G., Spottl, T., Andus, T., Scholmerich, J., Herfarth, H., Ray, K., Falk, W., and Rogler, G. (2002). Toll-like receptors 2 and 4 are up-regulated during intestinal inflammation. Gastroenterology *122*, 1987–2000.

Haynes, B., Hemler, M., Mann, D., Eisenbarth, G., Shelhamer, J., Mostowski, H., Thomas, C.A., Strominger, J., and Fauci, A.J.T.J.o.I. (1981). Characterization of a monoclonal antibody (4F2) that binds to human monocytes and to a subset of activated lymphocytes. *126*, 1409-1414.

Hesse, M., Modolell, M., La Flamme, A.C., Schito, M., Fuentes, J.M., Cheever, A.W., Pearce, E.J., and Wynn, T.A. (2001). Differential regulation of nitric oxide synthase-2 and arginase-1 by type 1/type 2 cytokines in vivo: granulomatous pathology is shaped by the pattern of L-arginine metabolism. The Journal of Immunology *167*, 6533-6544.

Hettinger, J., Richards, D.M., Hansson, J., Barra, M.M., Joschko, A.C., Krijgsveld, J., and Feuerer, M. (2013). Origin of monocytes and macrophages in a committed progenitor. Nat Immunol *14*, 821–830.

Hoeffel, G., Chen, J., Lavin, Y., Low, D., Almeida, F.F., See, P., Beaudin, A.E., Lum, J., Low, I., Forsberg, E.C.*, et al.* (2015). C-Myb(+) erythro-myeloid progenitor-derived fetal monocytes give rise to adult tissue-resident macrophages. Immunity *42*, 665–678.

Ikeda, K., Kinoshita, M., Kayama, H., Nagamori, S., Kongpracha, P., Umemoto, E., Okumura, R., Kurakawa, T., Murakami, M., Mikami, N.*, et al.* (2017). Slc3a2 Mediates Branched-Chain Amino-Acid-Dependent Maintenance of Regulatory T Cells. Cell Rep *21*, 1824–1838.

Ilicic, T., Kim, J.K., Kolodziejczyk, A.A., Bagger, F.O., McCarthy, D.J., Marioni, J.C., and Teichmann, S.A. (2016). Classification of low quality cells from single-cell RNA-seq data. Genome Biol *17*, 29.

Imhann, F., Vich Vila, A., Bonder, M.J., Fu, J., Gevers, D., Visschedijk, M.C., Spekhorst, L.M., Alberts, R., Franke, L., van Dullemen, H.M.*, et al.* (2018). Interplay of host genetics and gut microbiota underlying the onset and clinical presentation of inflammatory bowel disease. Gut *67*, 108-119.

Italiani, P., and Boraschi, D. (2014). From Monocytes to M1/M2 Macrophages: Phenotypical vs. Functional Differentiation. Front Immunol *5*, 514.

Jahn, H.M., Kasakow, C.V., Helfer, A., Michely, J., Verkhratsky, A., Maurer, H.H., Scheller, A., and Kirchhoff, F. (2018). Refined protocols of tamoxifen injection for inducible DNA recombination in mouse astroglia. Scientific Reports *8*, 5913.

Jobin, C., Bradham, C.A., Russo, M.P., Juma, B., Narula, A.S., Brenner, D.A., and Sartor, R.B. (1999). Curcumin blocks cytokine-mediated NF-κB activation and proinflammatory gene expression by inhibiting inhibitory factor I-κB kinase activity. The Journal of Immunology *163*, 3474-3483.

Joeris, T., Müller-Luda, K., Agace, W.W., and Mowat, A.M. (2017). Diversity and functions of intestinal mononuclear phagocytes. Mucosal Immunology *10*, 845.

Kamada, N., Hisamatsu, T., Okamoto, S., Chinen, H., Kobayashi, T., Sato, T., Sakuraba, A., Kitazume, M.T., Sugita, A., Koganei, K.*, et al.* (2008). Unique CD14 intestinal macrophages contribute to the pathogenesis of Crohn disease via IL-23/IFN-gamma axis. J Clin Invest *118*, 2269–2280.

Kim, H., Kim, M., Im, S.-K., and Fang, S. (2018). Mouse Cre-LoxP system: general principles to determine tissue-specific roles of target genes. Laboratory animal research *34*, 147-159.

Koelink, P.J., Wildenberg, M.E., Stitt, L.W., Feagan, B.G., Koldijk, M., van 't Wout, A.B., Atreya, R., Vieth, M., Brandse, J.F., Duijst, S.*, et al.* (2018). Development of Reliable, Valid and Responsive Scoring Systems for Endoscopy and Histology in Animal Models for Inflammatory Bowel Disease. J Crohns Colitis *12*, 794-803.

Komada, H., Imai, A., Hattori, E., Ito, M., Tsumura, H., Onoda, T., Kuramochi, M., Tani, M., Yamamoto, K., and Yamane, M. (2006). Possible activation of murine T lymphocyte through CD98 is independent of interleukin 2/interleukin 2 receptor system. Biomedical Research *27*, 61-67.

Laroui, H., Geem, D., Xiao, B., Viennois, E., Rakhya, P., Denning, T., and Merlin, D. (2014). Targeting intestinal inflammation with CD98 siRNA/PEI-loaded nanoparticles. Mol Ther *22*, 69-80.

Lawrance, I.C., Rogler, G., Bamias, G., Breynaert, C., Florholmen, J., Pellino, G., Reif, S., Speca, S., and Latella, G. (2017). Cellular and Molecular Mediators of Intestinal Fibrosis. J Crohns Colitis *11*, 1491-1503.

Leonardi, I., Li, X., Semon, A., Li, D., Doron, I., Putzel, G., Bar, A., Prieto, D., Rescigno, M., McGovern, D.P.B.*, et al.* (2018). CX3CR1(+) mononuclear phagocytes control immunity to intestinal fungi. Science *359*, 232-236.

Liberzon, A., Birger, C., Thorvaldsdottir, H., Ghandi, M., Mesirov, J.P., and Tamayo, P. (2015). The Molecular Signatures Database (MSigDB) hallmark gene set collection. Cell Syst *1*, 417-425.

Lim, H.Y., Müller, N., Herold, M.J., Van Den Brandt, J., and Reichardt, H.M. (2007). Glucocorticoids exert opposing effects on macrophage function dependent on their concentration. Immunology *122*, 47-53.

Limketkai, B.N., Wolf, A., and Parian, A.M. (2018). Nutritional Interventions in the Patient with Inflammatory Bowel Disease. Gastroenterol Clin North Am *47*, 155-177.

Linard, C., Grémy, O., and Benderitter, M. (2008). Reduction of peroxisome proliferation-activated receptor γ expression by γ-irradiation as a mechanism contributing to inflammatory response in rat colon: modulation by the 5-aminosalicylic acid agonist. Journal of Pharmacology and Experimental Therapeutics *324*, 911-920.

Loddo, I., and Romano, C. (2015). Inflammatory Bowel Disease: Genetics, Epigenetics, and Pathogenesis. Front Immunol *6*, 551.

Lun, A.T., McCarthy, D.J., and Marioni, J.C. (2016). A step-by-step workflow for low-level analysis of single-cell RNA-seq data with Bioconductor. F1000Res *5*, 2122.

Lun, A.T.L., and Marioni, J.C. (2017). Overcoming confounding plate effects in differential expression analyses of single-cell RNA-seq data. Biostatistics *18*, 451-464.

Maeda, S., Nakazato, Y., Hayashi, K., Nishihira, M., Inoue, T., Araki, O., Karube, Y., Kobayashi, S., and Chida, M. (2018). L-Type Amino Acid Transporter 1 Immunoreactivity as a Possible Diagnostic and Prognostic Marker of Thymic Carcinoma. Tohoku J Exp Med *246*, 167-174.

Martinez, F.O., and Gordon, S. (2014). The M1 and M2 paradigm of macrophage activation: time for reassessment. F1000Prime Rep *6*, 13.

McCarthy, D.J., Campbell, K.R., Lun, A.T., and Wills, Q.F. (2017). Scater: pre-processing, quality control, normalization and visualization of single-cell RNA-seq data in R. Bioinformatics *33*, 1179-1186.

Mifflin, R.C., Pinchuk, I.V., Saada, J.I., and Powell, D.W. (2011). Intestinal myofibroblasts: targets for stem cell therapy. Am J Physiol Gastrointest Liver Physiol *300*, G684-696.

Mizoguchi, A. (2012). Animal models of inflammatory bowel disease. Prog Mol Biol Transl Sci *105*, 263-320.

Mizoguchi, A., Takeuchi, T., Himuro, H., Okada, T., and Mizoguchi, E. (2016). Genetically engineered mouse models for studying inflammatory bowel disease. J Pathol *238*, 205-219.

Mori, K., Miyamoto, N., Higuchi, Y., Nanba, K., Ito, M., Tsurudome, M., Nishio, M., Kawano, M., Uchida, A., and Ito, Y.J.C.i. (2001). Cross-talk between RANKL and FRP-1/CD98 Systems: RANKL-mediated osteoclastogenesis is suppressed by an inhibitory anti-CD98 heavy chain mAb and CD98-mediated osteoclastogenesis is suppressed by osteoclastogenesis inhibitory factor. *207*, 118-126.

Mori, K., Nishimura, M., Tsurudome, M., Ito, M., Nishio, M., Kawano, M., Kozuka, Y., Yamashita, Y., Komada, H., Uchida, A.J.M.m., and immunology (2004). The functional interaction between CD98 and CD147 in regulation of virus-induced cell fusion and osteoclast formation. *193*, 155-162.

Mosser, D.M., and Zhang, X. (2008). Activation of murine macrophages. Curr Protoc Immunol *Chapter 14*, Unit 14 12.

Mowat, A.M., Scott, C.L., and Bain, C.C. (2017). Barrier-tissue macrophages: functional adaptation to environmental challenges. Nat Med *23*, 1258–1270.

Muehlhoefer, A., Saubermann, L.J., Gu, X., Luedtke-Heckenkamp, K., Xavier, R., Blumberg, R.S., Podolsky, D.K., MacDermott, R.P., and Reinecker, H.C. (2000). Fractalkine is an epithelial and endothelial cell-derived chemoattractant for intraepithelial lymphocytes in the small intestinal mucosa. J Immunol *164*, 3368–3376.

Nakamura, E., Sato, M., Yang, H., Miyagawa, F., Harasaki, M., Tomita, K., Matsuoka, S., Noma, A., Iwai, K., and Minato, N.J.J.o.B.C. (1999). 4F2 (CD98) heavy chain is associated covalently with an amino acid transporter and controls intracellular trafficking and membrane topology of 4F2 heterodimer. *274*, 3009-3016.

Nguyen, H.T., Dalmasso, G., Torkvist, L., Halfvarson, J., Yan, Y., Laroui, H., Shmerling, D., Tallone, T., D'Amato, M., Sitaraman, S.V., and Merlin, D. (2011). CD98 expression modulates intestinal homeostasis, inflammation, and colitis-associated cancer in mice. J Clin Invest *121*, 1733–1747.

Nguyen, T.L., Vieira-Silva, S., Liston, A., and Raes, J. (2015). How informative is the mouse for human gut microbiota research? Dis Model Mech *8*, 1-16.

Nicklin, P., Bergman, P., Zhang, B., Triantafellow, E., Wang, H., Nyfeler, B., Yang, H., Hild, M., Kung, C., Wilson, C.*, et al.* (2009). Bidirectional transport of amino acids regulates mTOR and autophagy. Cell *136*, 521–534.

Niess, J.H., Brand, S., Gu, X., Landsman, L., Jung, S., McCormick, B.A., Vyas, J.M., Boes, M., Ploegh, H.L., Fox, J.G.*, et al.* (2005). CX3CR1-mediated dendritic cell access to the intestinal lumen and bacterial clearance. Science *307*, 254–258.

Ordas, I., Eckmann, L., Talamini, M., Baumgart, D.C., and Sandborn, W.J. (2012). Ulcerative colitis. Lancet *380*, 1606–1619.

Perlman, R.L. (2016). Mouse models of human disease: An evolutionary perspective. Evol Med Public Health *2016*, 170-176.

Peterson, L.W., and Artis, D. (2014). Intestinal epithelial cells: regulators of barrier function and immune homeostasis. Nature Reviews Immunology *14*, 141.

Pittet, V., Juillerat, P., Mottet, C., Felley, C., Ballabeni, P., Burnand, B., Michetti, P., Vader, J.P., and Swiss, I.B.D.C.S.G. (2009). Cohort profile: the Swiss Inflammatory Bowel Disease Cohort Study (SIBDCS). Int J Epidemiol *38*, 922–931.

Prager, G.W., Féral, C.C., Kim, C., Han, J., and Ginsberg, M.H. (2007). CD98hc (SLC3A2) interaction with the integrin β subunit cytoplasmic domain mediates adhesive signaling. Journal of Biological Chemistry *282*, 24477-24484.

Reynolds, B., Laynes, R., Ögmundsdóttir, M.H., Boyd, C.R., and Goberdhan, D.C. (2007). Amino acid transporters and nutrient-sensing mechanisms: new targets for treating insulin-linked disorders? (Portland Press Limited).

Robinson, M.D., McCarthy, D.J., and Smyth, G.K. (2010). edgeR: a Bioconductor package for differential expression analysis of digital gene expression data. Bioinformatics *26*, 139-140.

Robinson, M.D., and Oshlack, A. (2010). A scaling normalization method for differential expression analysis of RNA-seq data. Genome Biol *11*, R25.

Rogler, G. (2015). Where are we heading to in pharmacological IBD therapy? Pharmacol Res *100*, 220-227.

Rogler, G., Andus, T., Aschenbrenner, E., Vogl, D., Falk, W., Scholmerich, J., and Gross, V. (1997). Alterations of the phenotype of colonic macrophages in inflammatory bowel disease. Eur J Gastroenterol Hepatol *9*, 893–899.

Sands, B.E. (2014). New drugs on the horizon for IBD. Dig Dis *32 Suppl 1*, 74-81.

Schirmer, M., Franzosa, E.A., Lloyd-Price, J., McIver, L.J., Schwager, R., Poon, T.W., Ananthakrishnan, A.N., Andrews, E., Barron, G., Lake, K.*, et al.* (2018). Dynamics of metatranscription in the inflammatory bowel disease gut microbiome. Nat Microbiol *3*, 337-346.

Schridde, A., Bain, C.C., Mayer, J.U., Montgomery, J., Pollet, E., Denecke, B., Milling, S.W.F., Jenkins, S.J., Dalod, M., Henri, S.*, et al.* (2017). Tissue-specific differentiation of colonic macrophages requires TGFbeta receptor-mediated signaling. Mucosal Immunol *10*, 1387–1399.

Schuster, A.T., Homer, C.R., Kemp, J.R., Nickerson, K.P., Deutschman, E., Kim, Y., West, G., Sadler, T., Stylianou, E., Krokowski, D.*, et al.* (2015). Chromosome-associated protein D3 promotes bacterial clearance in human intestinal epithelial cells by repressing expression of amino acid transporters. Gastroenterology *148*, 1405-1416 e1403.

Scott, C.L., Zheng, F., Baetselier, P., Martens, L., Saeys, Y., Prijck, S., Lippens, S., Abels, C., Schoonooghe, S., Raes, G.*, et al.* (2016). Bone marrow-derived monocytes give rise to self-renewing and fully differentiated Kupffer cells. Nat Commun *7*, 10321.

Seo, S.U., Kuffa, P., Kitamoto, S., Nagao-Kitamoto, H., Rousseau, J., Kim, Y.G., Nunez, G., and Kamada, N. (2015). Intestinal macrophages arising from CCR2(+) monocytes control pathogen infection by activating innate lymphoid cells. Nat Commun *6*, 8010.

Shaw, T.N., Houston, S.A., Wemyss, K., Bridgeman, H.M., Barbera, T.A., Zangerle-Murray, T., Strangward, P., Ridley, A.J.L., Wang, P., Tamoutounour, S.*, et al.* (2018). Tissue-resident macrophages in the intestine are long lived and defined by Tim-4 and CD4 expression. J Exp Med *215*, 1507–1518.

Smythies, L.E., Sellers, M., Clements, R.H., Mosteller-Barnum, M., Meng, G., Benjamin, W.H., Orenstein, J.M., and Smith, P.D. (2005). Human intestinal macrophages display profound inflammatory anergy despite avid phagocytic and bacteriocidal activity. J Clin Invest *115*, 66–75.

Souza, A.L., Fiorini Aguiar, S.L., Goncalves Miranda, M.C., Lemos, L., Freitas Guimaraes, M.A., Reis, D.S., Vieira Barros, P.A., Veloso, E.S., Carvalho, T.G., Ribeiro, F.M.*, et al.* (2017). Consumption of Diet Containing Free Amino Acids Exacerbates Colitis in Mice. Front Immunol *8*, 1587.

Steinert, A., Linas, I., Kaya, B., Ibrahim, M., Schlitzer, A., Hruz, P., Radulovic, K., Terracciano, L., Macpherson, A.J., and Niess, J.H. (2017). The Stimulation of Macrophages with TLR Ligands Supports Increased IL-19 Expression in Inflammatory Bowel Disease Patients and in Colitis Models. J Immunol *199*, 2570–2584.

Subramanian, A., Tamayo, P., Mootha, V.K., Mukherjee, S., Ebert, B.L., Gillette, M.A., Paulovich, A., Pomeroy, S.L., Golub, T.R., Lander, E.S., and Mesirov, J.P. (2005). Gene set enrichment analysis: A

knowledge-based approach for interpreting genome-wide expression profiles. Proc Natl Acad Sci U S A *102*, 15545-15550.

Tamoutounour, S., Guilliams, M., Montanana Sanchis, F., Liu, H., Terhorst, D., Malosse, C., Pollet, E., Ardouin, L., Luche, H., Sanchez, C*., et al.* (2013). Origins and functional specialization of macrophages and of conventional and monocyte-derived dendritic cells in mouse skin. Immunity *39*, 925-938.

Tamoutounour, S., Henri, S., Lelouard, H., Bovis, B., Haar, C., van der Woude, C.J., Woltman, A.M., Reyal, Y., Bonnet, D., Sichien, D*., et al.* (2012). CD64 distinguishes macrophages from dendritic cells in the gut and reveals the Th1-inducing role of mesenteric lymph node macrophages during colitis. Eur J Immunol *42*, 3150–3166.

Torres, J., Mehandru, S., Colombel, J.F., and Peyrin-Biroulet, L. (2017). Crohn's disease. Lancet *389*, 1741–1755.

Tsumura, H., Ito, M., Li, X.K., Nakamura, A., Ohnami, N., Fujimoto, J., Komada, H., and Ito, Y. (2012). The role of CD98hc in mouse macrophage functions. Cell Immunol *276*, 128–134.

Tsurudome, M., and Ito, Y.J.C.R.i.I. (2000). Function of fusion regulatory proteins (FRPs) in immune cells and virus-infected cells. *20*.

Uhlig, H.H., and Powrie, F. (2018). Translating Immunology into Therapeutic Concepts for Inflammatory Bowel Disease. Annu Rev Immunol *36*, 755-781.

Ungaro, R., Mehandru, S., Allen, P.B., Peyrin-Biroulet, L., and Colombel, J.F. (2017). Ulcerative colitis. Lancet *389*, 1756–1770.

Vallejos, C.A., Risso, D., Scialdone, A., Dudoit, S., and Marioni, J.C. (2017). Normalizing single-cell RNA sequencing data: challenges and opportunities. Nat Meth *14*, 565-571.

Van Gassen, S., Callebaut, B., Van Helden, M.J., Lambrecht, B.N., Demeester, P., Dhaene, T., and Saeys, Y. (2015). FlowSOM: Using self-organizing maps for visualization and interpretation of cytometry data. Cytometry Part A *87*, 636-645.

Varol, C., Zigmond, E., and Jung, S. (2010). Securing the immune tightrope: mononuclear phagocytes in the intestinal lamina propria. Nat Rev Immunol *10*, 415-426.

Vasioukhin, V., Degenstein, L., Wise, B., and Fuchs, E. (1999). The magical touch: genome targeting in epidermal stem cells induced by tamoxifen application to mouse skin. Proceedings of the National Academy of Sciences *96*, 8551-8556.

Verrey, F. (2003). System L: heteromeric exchangers of large, neutral amino acids involved in directional transport. Pflügers Archiv *445*, 529-533.

Villablanca, E.J., De Calisto, J., Paredes, P.T., Cassani, B., Nguyen, D.D., Gabrielsson, S., and Mora, J.R. (2014). β7 integrins are required to give rise to intestinal mononuclear phagocytes with tolerogenic potential. Gut *63*, 1431-1440.

Wirtz, S., Popp, V., Kindermann, M., Gerlach, K., Weigmann, B., Fichtner-Feigl, S., and Neurath, M.F. (2017). Chemically induced mouse models of acute and chronic intestinal inflammation. Nat Protoc *12*, 1295–1309.

Wu, D., and Smyth, G.K. (2012). Camera: a competitive gene set test accounting for inter-gene correlation. Nucleic Acids Res *40*, e133.

Xiao, B., Laroui, H., Viennois, E., Ayyadurai, S., Charania, M.A., Zhang, Y., Zhang, Z., Baker, M.T., Zhang, B., Gewirtz, A.T., and Merlin, D. (2014). Nanoparticles with surface antibody against CD98 and carrying CD98 small interfering RNA reduce colitis in mice. Gastroenterology *146*, 1289-1300 e1281-1219.

Yadav, V., Varum, F., Bravo, R., Furrer, E., Bojic, D., and Basit, A.W. (2016). Inflammatory bowel disease: exploring gut pathophysiology for novel therapeutic targets. Transl Res *176*, 38-68.

Yan, L., and Lamb, R.F. (2010). mTOR Signaling by amino acid nutrients: involvement of MAP4K3. In The Enzymes (Elsevier), pp. 77-97.

Yona, S., Kim, K.W., Wolf, Y., Mildner, A., Varol, D., Breker, M., Strauss-Ayali, D., Viukov, S., Guilliams, M., Misharin, A.*, et al.* (2013). Fate mapping reveals origins and dynamics of monocytes and tissue macrophages under homeostasis. Immunity *38*, 79-91.

Zerbino, D.R., Achuthan, P., Akanni, W., Amode, M.R., Barrell, D., Bhai, J., Billis, K., Cummins, C., Gall, A., Giron, C.G.*, et al.* (2018). Ensembl 2018. Nucleic Acids Res *46*, D754-D761.

Zigmond, E., and Jung, S. (2013). Intestinal macrophages: well educated exceptions from the rule. Trends Immunol *34*, 162-168.

Zigmond, E., Varol, C., Farache, J., Elmaliah, E., Satpathy, A.T., Friedlander, G., Mack, M., Shpigel, N., Boneca, I.G., Murphy, K.M.*, et al.* (2012). Ly6C hi monocytes in the inflamed colon give rise to proinflammatory effector cells and migratory antigen-presenting cells. Immunity *37*, 1076-1090.

6 APPENDIX

6.1. Supplementary Data

Table S1: IBD patient characteristics used for expression analysis

Baseline Group characteristics				
	Crohn' disease		**Ulcerative colitis**	
	Quiescent (n=20)	**Active (n=11)**	**Quiescent (n=20)**	**Active (n=11)**
Gender, male/female, n (%)	60/40 % 12 male, 8 females	36/64% 4 m, 7 f	35/65% 12 m, 8 f	54/45% 6 m, 5 f
Median age (range), yr	56 (32-81)	39 (31-71)	58 (31-81)	53 (24-68)
Mean BMI (SD), kg/m^2	24.15 (3)	25.55 (4.9)	24.70 (2.99)	23.89 (4.08)
Median age at diagnosis (range), yr	33.5 (18-60)	21 (14-34)	28.5 (14-65)	30 (16-60)
Median disease duration (range), yr	21.5 (6-45)	19 (7-37)	26 (8-44)	16 (7-38)
CD extent, n (%)				
Ileum isolated	5 (25%)	2 (18%)		
Colon isolated	2 (10%)	3 (27%)		
Ileocolonic	2 (10%)	5 (46%)		
Unknown	11 (55%)	1 (9%)		
UC extent, n (%)				
Proctitis			1 (5%)	1 (10%)
Left-sided colitis			3 (20%)	5 (45%)
Pancolitis			5 (25%)	5 (45%)
Unknown				
Current medical treatment, n (%)				
No treatment	5 (25%)		5 (25%)	1 (9%)
5-ASA	6 (30%)		13 (65%)	9 (81%)
Steroids		6 (54%)		4 (36%)
Immunosuppressants	11 (55%)	1 (9%)	4 (20%)	1 (9%)
Anti-TNF		1 (9%)		3 (27%)
Smoking status				
Non-smoker, n (%)	12 (60%)	6 (54%)	15 (75%)	9 (81%)
Active smoker, n (%)	6 (30%)	5 (46%)	1 (5%)	1 (9.5%)
Unknown	2 (10%)	0	4 (20%)	1(9.5%)

Table S2: IBD patient characteristics used for CD98hc immunofluorescence

	Ulceritive colitis			Crohn's		
Sample #	*504*	*535*	*619*	*558*	*568*	*620*
Gender	female	female	unknown	female	male	female
Age	50	71	unknown	72	68	69
BMI	25,6	27,3	unknown	19	32	21,6
Age at diagnosis	34	56	unknown	23	52	56
Smoking status	unknown	unknown	unknown	non-smoker	active	active
Localisation inflamed	(B) sigmoid/ rectum	(B) rectum/ sigmoid	(B) sigmoid/ rectum	unknown	(C) sigmoid	(B) term. Ileum
Localisation non-inflamed	(A) transversal colon	(A) colon	(A) ascendens/ trans	(B) rectum	(B) colon desc.	(A) col. ascendens
Medical treatment at time of study	none	none	none at time of study, but received Salofalk 10 days before	Quantalan, Immodium	Spiricort, Aldactone, Orfiril	unknown
Clinical disease activity index	5	6	unknown	unknown	74	70

Table S3: Primer sequences for RT-qPCR

Primer (mouse)	Sequence (5'-3')	Tm (°C)	Product size (bp)
Actβ-fwd	TTC TTT GCA GCT CCT TCG TT	56,4	149
Actβ-rev	ATG GAG GGG AAT ACA GCC C	59,5	
Il1β-fwd	TGT GAA ATG CCA CCT TTT GA	54,3	94
Il1β-rev	GGT CAA AGG TTT GGA AGC AG	58,4	
Il6-fwd	TCG AGG CT TAA TTA CAC ATG TTC T	62,5	94
Il6-rev	GCA TCA TCG TTG TTC ATA CAA TCA	60,3	
Il10-fwd	ATC GAT TTC TCC CCT GTG AA	56,4	108
Il10-rev	TGT CAA ATT CAT TCA TGG CCT	55,4	
Tnf-fwd	CCA CCA CGC TCT TCT GTC TAC	63,2	103
Tnf-rev	AGG GTC TGG GCC ATA GAA CT	60,5	
Slc7a5-fwd	ATG TGG CTC CGA TTC AAG A	56,4	61
Slc7a5-rev	GGA GGG CCA GAT TCA CCT	58,3	
Slc7a6-fwd	CTG CTG CCT GCG TAT GTC	58,6	64
Slc7a6-rev	ACT CGT GTG CCC CAC TTG	59,9	
Slc7a7-fwd	CAC CCC AGT GTG CTG CTA	60,8	91
Slc7a7-rev	GAA GAC CTT CAC CAG CTT GC	59,6	
Slc7a8-fwd	GCT GGA AGA AGC CTG ACA TT	58,2	78
Slc7a8-rev	AGG CCC AGA ACA GCA GGT A	60,5	
Slc7a10-fwd	GGG ACT ACG CCT ATG TCA CTG	59,9	75
Slc7a10-rev	TGA TGA GGA CAG CAC TCC AG	59,1	
Slc7a11-fwd	GAT TCA TGT CCA CAA GCA CAC	57,8	71
Slc7a11-rev	AGA GCA TCA CCA TCG TCA GA	58,5	
Il19-fwd	CTG GGC ATG ACG TTG ATT CT	58,3	185
Il19-rev	TCTCCAGGCTTAATGCTCCT	58,1	
IFNγ-fwd	ACA GCA AGG CGA AAA AGG AT	56,4	90
IFNγ-rev	TGA GCT CAT TGA ATG CTT GG	56,4	
Chil3-fwd	AGG AAG CCC TCC TAA GGA CA	60,5	82
Chil3-rev	CTC CAC AGA TTC TTC TCA AAG AGC	63,6	
Mgl1-fwd	TGA GAA AGG CTT AA GAA CTG GG	60,9	101
Mgl1-rev	GAC CAC CTG TAG TGA TGT GGG	63,2	

Primer (mouse)	Sequence (5'-3')	Tm (°C)	Product size (bp)
Mcp-1-fwd	AGG TCC CTG TCA TGC TTC TG	60,5	249
Mcp-1-rev	TCT GGA CCC ATT CCT TCT TG	58,4	
Mrc1-fwd	CTC TGT TCA GCT ATT GGA CGC	61,2	136
Mrc1-rev	CGG AAT TTC TGG GAT TCA GCT TC	62,9	
Retnla-fwd	CCA ATC CAG CTA ACT ATC CCT CC	64,6	188
Retnla-rev	CCA GTC AAC GAG TAA GCA CAG	61,2	
iNos-fwd	GTT CTC AGC CCA ACA ATA CAA GA	60,9	127
iNos-rev	GTG GAC GGG TCG ATG TCA C	61,6	
Kc-fwd	CTG GGA TTC ACC TCA AGA ACA TC	62,9	117
Kc-rev	CAG GGT CAA GGC AAG CCT C	61,6	
Primer (human)	**Sequence (5'-3')**	**Tm (°C)**	**Product size (bp)**
GAPDH-fwd	TCG ACA GTC AGC CGC ATC TTC TTT	65,2	104
GAPDH-rev	GCC CAA TAC GAC CAA ATC CGT TGA	65,2	
SLC3A2-fwd	GAC CCC TGT TTT CAG CTA CG	60,5	108
SLC3A2-rev	TCA GGG AAG CTG GAC TCA TC	60,5	
SLC7A5-fwd	TCC TGG ATC ATC CCC GTC TT	60,5	88
SLC7A5-rev	CCA CGA AGA AGA GCC TGG AG	62,5	

fwd – forward, rev – reverse, Tm – melting temperature

Table S4: Monoclonal antibodies for flow cytometry, surface antigens

Specificity (mouse)	Conjugated	Isotype	Clone	Company	Catalogue Number	Final Conc.
CD3	Biotin	Armenian hamster IgG	145-2C11	BioLegend	100303	0.6 µg/ml
CD19	Biotin	Rat IgG2a, κ	6D5	BioLegend	115503	5.0 µg/ml
NK1.1	Biotin	Mouse IgG2a, κ	PK136	BioLegend	108703	0.6 µg/ml
Ly6G	Biotin	Rat IgG2a, κ	1A8	BioLegend	127603	0.6 µg/ml
Ter119	Biotin	Rat IgG2b, κ	TER-119	BioLegend	116203	0.6 µg/ml
F4/80	Biotin	Rat IgG2a, κ	BM8	BioLegend	123105	5.0 µg/ml
I-A/I-E	AF700	Rat IgG2b, κ	M5/114.15.2	BioLegend	107622	2.5 µg/ml
Ly6C	PerCP/Cy5.5	Rat IgG2c, κ	HK1.4	BioLegend	128011	0.5 µg/ml
CD11b	PE/Cy7	Rat IgG2b, κ	M1/70	BioLegend	101215	2.0 µg/ml
CD98	PE	Rat IgG2a, κ	RL388	BioLegend	128207	0.25 µg/ml
CD64	BV711	Mouse IgG1, κ	X54-5/71	BioLegend	139311	1.0 µg/ml
F4/80	APC	Rat IgG2a, κ	BM8	BioLegend	123116	4.0 µg/ml
CD29	Pacific Blue	Armenian hamster IgG	HMβ1-1	BioLegend	102224	2.5 µg/ml
CD3	AF700	Rat IgG2b, κ	17A2	BioLegend	100216	5.0 µg/ml
CD4	BV510	Rat IgG2a, κ	RM4-5	BioLegend	100559	2.0 µg/ml

CD8	PerCP	Rat IgG2a, κ	53-6.7	BioLegend	100732	2.0 µg/ml
CD8	PerCP/Cy5.5	Rat IgG2a, κ	53-6.7	BioLegend	100734	2.0 µg/ml
CD11c	APC/Fire750	Armenian hamster IgG	N418	BioLegend	117352	4.0 µg/ml
Ly6G	APC	Rat IgG2a, κ	1A8	BioLegend	127613	1.0 µg/ml
CD19	BV785	Rat IgG2a, κ	6D5	BioLegend	115543	0.6 µg/ml
CD207	APC	Mouse IgG2a, κ	4C7	BioLegend	144205	2.0 µg/ml
CCR2	APC	Rat IgG2b	475301	R&D Systems	FAB5538A	10 µl/test
CD45	Super Bright 436	Rat IgG2b, κ	30-F11	Invitrogen	62-0451-82	1 µl/test
CD16/32 (FcγRII/III)	purified	Rat IgG2a, λ	93	Invitrogen	14-0161-85	5.0 µg/ml
CD117	BB515	Rat IgG2b, κ	2B8	BD Bioscience	564481	1.0 µg/ml
CD115	PE/Dazzle	Rat IgG2a, κ	AFS98	BioLegend	135528	0.5 µg/ml
CD135	APC	Rat IgG2a, κ	A2F10	BioLegend	135310	2.0 µg/ml
CD14	PE/Dazzle	Rat IgG2a, κ	Sa14-2	BioLegend	123326	2.0 µg/ml
CD72	BV786	Mouse IgG2b, κ	K10.6	BD Bioscience	740940	2.0 µg/ml
CD81	PerCP/Cy5.5	Armenian Hamster IgG	Eat-2	BioLegend	104911	2.0 µg/ml

Table S5: Monoclonal antibodies for flow cytometry, intracellular antigens

Specificity (mouse)	Conjugated	Isotype	Clone	Company	Catalogue Number	Final Conc.
IL-6	APC	Rat IgG1, κ	MP5-20F3	BioLegend	504508	2.0 µg/ml
IL-10	PE	Rat IgG2b, κ	JES5-16E3	BioLegend	505007	2.0 µg/ml
TNF	APC/Cy7	Rat IgG1, κ	MP6-XT22	BioLegend	506343	2.0 µg/ml

Table S6: Primer sequences for genotyping Cd98hc[flox/flox] and Cx3cr1[cre] animals (PCR)

Primer	Sequence (5'-3')	Tm (°C)	Product size (bp)
Slc3a2-wt-fwd	CAG ATT GTC AGT AAC AGA CA	54,3	400
Slc3a2-wt-rev	GTT ACC TCC ACT ATG AAT GC	56,4	
Slc3a2-mut-fwd	CAG ATT GTC AGT AAC AGA CA	54,3	600
Slc3a2-mut-rev	TCA TGC GTG AGC GTA ATT TT	54,3	
Cx3cr1-wt-fwd	AGG ATG TTG ACT TCC GAG TTG	59,5	695
Cx3cr1-wt-rev	AAG ACT CAC GTG GAC CTG CT	60,5	
Cx3cr1-mut-fwd	AGG ATG TTG ACT TCC GAG TTG	59,5	300
Cx3cr1-mut-rev	CGG TTA TTC AAC TTG CAC CA	56,4	

WT – wild type, Mut – mutant, fwd – forward, rev – reverse, Tm – melting temperature

Table S7: Differentially expressed genes in CD98hc cKO cells over control cells for each cluster of the scRNA-seq data.

Cluster 1: Gene ID	Symbol	Gene Name	log2FC	adj.P.Val
ENSMUSG00000028037	Ifi44	interferon-induced protein 44	1,7	5,9E-09
ENSMUSG00000091144	Phf11c	PHD finger protein 11C	2,0	5,9E-09
ENSMUSG00000073491	Pydc4	interferon activated gene 213	2,1	1,2E-08
ENSMUSG00000090231	Cfb	complement factor B	2,1	1,2E-08
ENSMUSG00000025498	Irf7	interferon regulatory factor 7	2,6	2,5E-08
ENSMUSG00000046687	Gm5424	argininosuccinate synthase pseudogene	2,6	2,5E-08
ENSMUSG00000076441	Ass1	argininosuccinate synthetase 1	2,6	2,5E-08
ENSMUSG00000030107	Usp18	ubiquitin specific peptidase 18	2,0	2,5E-08
ENSMUSG00000044703	Phf11a	PHD finger protein 11A	1,9	2,5E-08
ENSMUSG00000037849	Gm4955	signaling mucin HKR1-like	1,9	3,7E-08
ENSMUSG00000068245	Phf11d	PHD finger protein 11D	1,9	4,6E-08
ENSMUSG00000091649	Phf11b	PHD finger protein 11B	1,9	6,8E-08
ENSMUSG00000066677	Pydc3	interferon activated gene 208	1,7	6,8E-08
ENSMUSG00000075602	Ly6a	lymphocyte antigen 6 complex, locus A	2,3	2,9E-07
ENSMUSG00000035692	Isg15	ISG15 ubiquitin-like modifier	2,4	2,9E-07
ENSMUSG00000033213	AA467197	expressed sequence AA467197	2,7	3,8E-07
ENSMUSG00000020641	Rsad2	radical S-adenosyl methionine domain containing 2	1,9	6,2E-07
ENSMUSG00000089929	Bcl2a1b	B cell leukemia/lymphoma 2 related protein A1b	1,5	1,0E-06
ENSMUSG00000029561	Oasl2	2'-5' oligoadenylate synthetase-like 2	1,7	1,3E-06
ENSMUSG00000022586	Ly6i	lymphocyte antigen 6 complex, locus I	1,8	1,3E-06
ENSMUSG00000079017	Ifi27l2a	interferon, alpha-inducible protein 27 like 2A	1,5	1,9E-06
ENSMUSG00000073409	H2-Q6	histocompatibility 2, Q region locus 8	1,6	2,2E-06
ENSMUSG00000029379	Cxcl3	chemokine (C-X-C motif) ligand 3	2,2	2,4E-06
ENSMUSG00000033355	Rtp4	receptor transporter protein 4	1,5	4,1E-06
ENSMUSG00000060550	H2-Q7	histocompatibility 2, Q region locus 7	1,6	4,5E-06
ENSMUSG00000033880	Lgals3bp	lectin, galactoside-binding, soluble, 3 binding protein	1,3	5,5E-06
ENSMUSG00000091971	Hspa1a	heat shock protein 1A	-1,5	8,7E-06
ENSMUSG00000041827	Oasl1	2'-5' oligoadenylate synthetase-like 1	1,8	1,1E-05
ENSMUSG00000021208	Ifi27l2b	interferon, alpha-inducible protein 27 like 2B	1,9	1,1E-05
ENSMUSG00000054203	Ifi205	interferon activated gene 205	1,6	2,1E-05
ENSMUSG00000026536	Mnda	interferon activated gene 211	1,7	2,2E-05
ENSMUSG00000066861	Oas1g	2'-5' oligoadenylate synthetase 1G	1,4	3,0E-05
ENSMUSG00000000204	Slfn4	schlafen 4	1,5	3,0E-05
ENSMUSG00000074896	Ifit3	interferon-induced protein with tetratricopeptide repeats 3	1,8	3,0E-05
ENSMUSG00000035352	Ccl12	chemokine (C-C motif) ligand 12	1,9	3,0E-05
ENSMUSG00000024644	Cndp2	CNDP dipeptidase 2 (metallopeptidase M20 family)	1,6	3,0E-05
ENSMUSG00000034459	Ifit1	interferon-induced protein with tetratricopeptide repeats 1	1,7	3,0E-05
ENSMUSG00000021281	Tnfaip2	tumor necrosis factor, alpha-induced protein 2	1,3	3,2E-05

ENSMUSG00000062488	Ifit3b	interferon-induced protein with tetratricopeptide repeats 3B	1,5	3,5E-05
ENSMUSG00000041324	Inhba	inhibin beta-A	1,6	4,1E-05
ENSMUSG00000082976	Gm15056	predicted gene 15056	2,7	5,2E-05
ENSMUSG00000000318	Clec10a	C-type lectin domain family 10, member A	-1,5	5,5E-05
ENSMUSG00000069516	Lyz2	lysozyme 2	-1,1	6,5E-05
ENSMUSG00000027399	Il1a	interleukin 1 alpha	2,7	7,1E-05
ENSMUSG00000000957	Mmp14	matrix metallopeptidase 14 (membrane-inserted)	1,5	7,8E-05
ENSMUSG00000020407	Upp1	uridine phosphorylase 1	1,2	8,5E-05
ENSMUSG00000052776	Oas1a	2'-5' oligoadenylate synthetase 1A	1,3	1,0E-04
ENSMUSG00000093930	Hmgcs1	3-hydroxy-3-methylglutaryl-Coenzyme A synthase 1	-1,1	1,1E-04
ENSMUSG00000038156	Spon1	spondin 1, (f-spondin) extracellular matrix protein	1,4	1,3E-04
ENSMUSG00000046718	Bst2	bone marrow stromal cell antigen 2	1,1	1,3E-04
ENSMUSG00000031488	Rab11fip1	RAB11 family interacting protein 1 (class I)	1,3	1,3E-04
ENSMUSG00000028459	Cd72	CD72 antigen	1,4	1,5E-04
ENSMUSG00000102037	Bcl2a1a	B cell leukemia/lymphoma 2 related protein A1a	1,5	1,5E-04
ENSMUSG00000026875	Traf1	TNF receptor-associated factor 1	1,2	1,8E-04
ENSMUSG00000000184	Ccnd2	cyclin D2	1,3	2,2E-04
ENSMUSG00000090272	Mndal	myeloid nuclear differentiation antigen like	1,3	2,3E-04
ENSMUSG00000027514	Zbp1	Z-DNA binding protein 1	1,3	2,3E-04
ENSMUSG00000026357	Rgs18	regulator of G-protein signaling 18	-1,1	2,3E-04
ENSMUSG00000026981	Il1rn	interleukin 1 receptor antagonist	1,8	2,3E-04
ENSMUSG00000045932	Ifit2	interferon-induced protein with tetratricopeptide repeats 2	1,2	2,3E-04
ENSMUSG00000049103	Ccr2	chemokine (C-C motif) receptor 2	-1,2	2,4E-04
ENSMUSG00000022126	Irg1	aconitate decarboxylase 1	1,7	3,1E-04
ENSMUSG00000002108	Nr1h3	nuclear receptor subfamily 1, group H, member 3	1,5	3,8E-04
ENSMUSG00000038067	Csf3	colony stimulating factor 3 (granulocyte)	1,3	3,9E-04
ENSMUSG00000038393	Txnip	thioredoxin interacting protein	-1,2	4,9E-04
ENSMUSG00000099974	Bcl2a1d	B cell leukemia/lymphoma 2 related protein A1d	1,3	4,9E-04
ENSMUSG00000074743	Thbd	thrombomodulin	-1,2	6,2E-04
ENSMUSG00000035929	H2-Q4	histocompatibility 2, Q region locus 4	1,2	6,6E-04
ENSMUSG00000040950	Mgl2	macrophage galactose N-acetyl-galactosamine specific lectin 2	-1,6	8,5E-04
ENSMUSG00000027368	Dusp2	dual specificity phosphatase 2	1,1	9,3E-04
ENSMUSG00000017002	Slpi	secretory leukocyte peptidase inhibitor	2,4	1,2E-03
ENSMUSG00000045551	Fpr1	formyl peptide receptor 1	1,2	1,2E-03
ENSMUSG00000040483	Xaf1	XIAP associated factor 1	1,3	1,3E-03
ENSMUSG00000079018	Ly6c1	lymphocyte antigen 6 complex, locus C1	1,5	1,3E-03
ENSMUSG00000068631	Gm7676	NA	1,4	1,4E-03
ENSMUSG00000043263	Pyhin1	interferon activated gene 209	1,2	1,5E-03
ENSMUSG00000025383	Il23a	interleukin 23, alpha subunit p19	1,4	1,6E-03
ENSMUSG00000037580	Gch1	GTP cyclohydrolase 1	1,2	1,8E-03
ENSMUSG00000067235	H2-Q10	histocompatibility 2, Q region locus 10	1,2	2,0E-03
ENSMUSG00000070501	BC094916	interferon activated gene 214	1,1	2,4E-03

ENSMUSG00000031604	Msmo1	methylsterol monoxygenase 1	-1,1	2,6E-03
ENSMUSG00000035042	Ccl5	chemokine (C-C motif) ligand 5	2,5	2,9E-03
ENSMUSG00000042265	Trem1	triggering receptor expressed on myeloid cells 1	1,1	3,3E-03
ENSMUSG00000026193	Fn1	fibronectin 1	-1,1	3,4E-03
ENSMUSG00000001348	Acp5	acid phosphatase 5, tartrate resistant	1,2	3,5E-03
ENSMUSG00000035828	Pim3	proviral integration site 3	1,1	4,3E-03
ENSMUSG00000047945	Marcksl1	MARCKS-like 1	1,5	4,6E-03
ENSMUSG00000053820	Bcl2a1c	B cell leukemia/lymphoma 2 related protein A1c	1,2	4,6E-03
ENSMUSG00000034353	Ramp1	receptor (calcitonin) activity modifying protein 1	-1,1	4,9E-03
ENSMUSG00000075010	AW112010	expressed sequence AW112010	1,1	5,2E-03
ENSMUSG00000028214	Gem	GTP binding protein (gene overexpressed in skeletal muscle)	1,1	6,4E-03
ENSMUSG00000022584	Ly6c2	lymphocyte antigen 6 complex, locus C2	1,7	6,7E-03
ENSMUSG00000030342	Cd9	CD9 antigen	1,2	7,0E-03
ENSMUSG00000027315	Spint1	serine protease inhibitor, Kunitz type 1	1,2	7,0E-03
ENSMUSG00000030142	Clec4e	C-type lectin domain family 4, member e	1,3	7,5E-03
ENSMUSG00000029084	Cd38	CD38 antigen	1,2	7,5E-03
ENSMUSG00000034158	Lrrc58	leucine rich repeat containing 58	1,2	8,8E-03
ENSMUSG00000019970	Sgk1	serum/glucocorticoid regulated kinase 1	1,1	1,2E-02
ENSMUSG00000032487	Ptgs2	prostaglandin-endoperoxide synthase 2	1,3	1,3E-02
ENSMUSG00000019987	Arg1	arginase, liver	1,9	1,3E-02
ENSMUSG00000063234	Gpr84	G protein-coupled receptor 84	1,2	1,4E-02
ENSMUSG00000015568	Lpl	lipoprotein lipase	-1,6	2,1E-02
ENSMUSG00000035678	Tnfsf9	tumor necrosis factor (ligand) superfamily, member 9	1,1	2,3E-02
ENSMUSG00000001131	Timp1	tissue inhibitor of metalloproteinase 1	1,5	2,3E-02
ENSMUSG00000091955	Gm9844	NA	1,1	2,5E-02
ENSMUSG00000006818	Sod2	superoxide dismutase 2, mitochondrial	1,1	3,9E-02
ENSMUSG00000074115	Saa1	serum amyloid A 1	1,3	4,2E-02
ENSMUSG00000069439	Gm8444	NA	1,1	4,4E-02
ENSMUSG00000031609	Sap30	sin3 associated polypeptide	1,1	4,4E-02
ENSMUSG00000097971	Gm26917	NA	1,1	4,8E-02
ENSMUSG00000017009	Sdc4	syndecan 4	1,1	4,9E-02
Cluster 2: Gene ID	**Symbol**	**Gene Name**	**log2FC**	**adj.P.Val**
ENSMUSG00000056529	Ptafr	platelet-activating factor receptor	1,8	5,0E-07
ENSMUSG00000089929	Bcl2a1b	B cell leukemia/lymphoma 2 related protein A1b	1,8	5,0E-07
ENSMUSG00000075602	Ly6a	lymphocyte antigen 6 complex, locus A	2,6	2,1E-06
ENSMUSG00000029379	Cxcl3	chemokine (C-X-C motif) ligand 3	2,7	2,2E-06
ENSMUSG00000060550	H2-Q7	histocompatibility 2, Q region locus 7	2,0	3,6E-06
ENSMUSG00000102037	Bcl2a1a	B cell leukemia/lymphoma 2 related protein A1a	1,9	1,5E-05
ENSMUSG00000079017	Ifi27l2a	interferon, alpha-inducible protein 27 like 2A	1,4	2,0E-05
ENSMUSG00000024644	Cndp2	CNDP dipeptidase 2 (metallopeptidase M20 family)	2,1	2,9E-05
ENSMUSG00000099974	Bcl2a1d	B cell leukemia/lymphoma 2 related protein A1d	1,8	2,9E-05
ENSMUSG00000000204	Slfn4	schlafen 4	2,2	2,9E-05

ENSMUSG00000073409	H2-Q6	histocompatibility 2, Q region locus 8	1,8	3,0E-05
ENSMUSG00000031613	Hpgd	hydroxyprostaglandin dehydrogenase 15 (NAD)	-1,7	3,0E-05
ENSMUSG00000034158	Lrrc58	leucine rich repeat containing 58	1,7	7,4E-05
EYFP	EYFP	NA	-1,5	9,2E-05
ENSMUSG00000024014	Pim1	proviral integration site 1	1,5	9,8E-05
ENSMUSG00000047945	Marcksl1	MARCKS-like 1	2,3	1,3E-04
ENSMUSG00000025498	Irf7	interferon regulatory factor 7	1,9	1,3E-04
ENSMUSG00000028037	Ifi44	interferon-induced protein 44	1,5	1,3E-04
ENSMUSG00000079018	Ly6c1	lymphocyte antigen 6 complex, locus C1	2,3	1,4E-04
ENSMUSG00000090231	Cfb	complement factor B	1,7	2,8E-04
ENSMUSG00000002103	Acp2	acid phosphatase 2, lysosomal	1,3	5,5E-04
ENSMUSG00000066677	Pydc3	interferon activated gene 208	1,5	5,8E-04
ENSMUSG00000091144	Phf11c	PHD finger protein 11C	1,4	5,8E-04
ENSMUSG00000073491	Pydc4	interferon activated gene 213	1,5	7,4E-04
ENSMUSG00000030342	Cd9	CD9 antigen	1,8	7,8E-04
ENSMUSG00000046687	Gm5424	argininosuccinate synthase pseudogene	1,8	9,0E-04
ENSMUSG00000021208	Ifi27l2b	interferon, alpha-inducible protein 27 like 2B	2,1	9,7E-04
ENSMUSG00000017009	Sdc4	syndecan 4	2,0	9,7E-04
ENSMUSG00000035692	Isg15	ISG15 ubiquitin-like modifier	1,7	9,8E-04
ENSMUSG00000027315	Spint1	serine protease inhibitor, Kunitz type 1	1,6	9,8E-04
ENSMUSG00000002985	Apoe	apolipoprotein E	-1,1	1,0E-03
ENSMUSG00000029580	Actb	actin, beta	1,1	1,0E-03
ENSMUSG00000046718	Bst2	bone marrow stromal cell antigen 2	1,1	1,5E-03
ENSMUSG00000026875	Traf1	TNF receptor-associated factor 1	1,2	1,5E-03
ENSMUSG00000026981	Il1rn	interleukin 1 receptor antagonist	1,8	1,5E-03
ENSMUSG00000027399	Il1a	interleukin 1 alpha	2,7	1,7E-03
ENSMUSG00000029810	Tmem176b	transmembrane protein 176B	-1,1	1,7E-03
ENSMUSG00000018476	Kdm6b	KDM1 lysine (K)-specific demethylase 6B	1,2	1,9E-03
ENSMUSG00000091955	Gm9844	NA	1,6	1,9E-03
ENSMUSG00000019850	Tnfaip3	tumor necrosis factor, alpha-induced protein 3	1,5	2,0E-03
ENSMUSG00000029552	Tes	testis derived transcript	1,3	2,0E-03
ENSMUSG00000076441	Ass1	argininosuccinate synthetase 1	1,7	2,0E-03
ENSMUSG00000021025	Nfkbia	nuclear factor of kappa light polypeptide gene enhancer in B cells inhibitor, alpha	1,3	2,1E-03
ENSMUSG00000044703	Phf11a	PHD finger protein 11A	1,3	2,2E-03
ENSMUSG00000040552	C3ar1	complement component 3a receptor 1	1,3	2,3E-03
ENSMUSG00000034226	Rhov	ras homolog family member V	1,3	3,4E-03
ENSMUSG00000040950	Mgl2	macrophage galactose N-acetyl-galactosamine specific lectin 2	-1,1	3,7E-03
ENSMUSG00000066861	Oas1g	2'-5' oligoadenylate synthetase 1G	1,1	4,1E-03
ENSMUSG00000068245	Phf11d	PHD finger protein 11D	1,3	4,6E-03
ENSMUSG00000032691	Nlrp3	NLR family, pyrin domain containing 3	1,2	4,9E-03
ENSMUSG00000009633	G0s2	G0/G1 switch gene 2	1,9	5,3E-03
ENSMUSG00000063779	Chil4	chitinase-like 4	1,4	5,3E-03
ENSMUSG00000021281	Tnfaip2	tumor necrosis factor, alpha-induced protein 2	1,1	5,6E-03
ENSMUSG00000027533	Fabp5	fatty acid binding protein 5, epidermal	2,3	6,6E-03

ENSMUSG00000052776	Oas1a	2'-5' oligoadenylate synthetase 1A	1,1	7,4E-03
ENSMUSG00000031488	Rab11fip1	RAB11 family interacting protein 1 (class I)	1,3	7,5E-03
ENSMUSG00000070691	Runx3	runt related transcription factor 3	1,2	8,0E-03
ENSMUSG00000016496	Cd274	CD274 antigen	1,3	8,3E-03
ENSMUSG00000022895	Ets2	E26 avian leukemia oncogene 2, 3' domain	1,2	8,4E-03
ENSMUSG00000038467	Chmp4b	charged multivesicular body protein 4B	1,2	8,8E-03
ENSMUSG00000001627	Ifrd1	interferon-related developmental regulator 1	1,1	9,8E-03
ENSMUSG00000007872	Id3	inhibitor of DNA binding 3	1,2	1,1E-02
ENSMUSG00000027398	Il1b	interleukin 1 beta	1,3	1,2E-02
ENSMUSG00000032661	Oas3	2'-5' oligoadenylate synthetase 3	1,1	1,3E-02
ENSMUSG00000068631	Gm7676	NA	1,3	1,4E-02
ENSMUSG00000034855	Cxcl10	chemokine (C-X-C motif) ligand 10	1,7	1,4E-02
ENSMUSG00000037580	Gch1	GTP cyclohydrolase 1	1,2	1,6E-02
ENSMUSG00000022126	Irg1	aconitate decarboxylase 1	1,6	1,7E-02
ENSMUSG00000017002	Slpi	secretory leukocyte peptidase inhibitor	2,1	1,7E-02
ENSMUSG00000030142	Clec4e	C-type lectin domain family 4, member e	1,4	1,7E-02
ENSMUSG00000027660	Skil	SKI-like	1,1	1,8E-02
ENSMUSG00000030156	Cd69	CD69 antigen	1,1	1,8E-02
ENSMUSG00000031652	N4bp1	NEDD4 binding protein 1	1,2	1,8E-02
ENSMUSG00000026536	Mnda	interferon activated gene 211	1,1	1,9E-02
ENSMUSG00000032487	Ptgs2	prostaglandin-endoperoxide synthase 2	1,5	1,9E-02
ENSMUSG00000020869	Lrrc59	leucine rich repeat containing 59	1,1	2,0E-02
ENSMUSG00000054203	Ifi205	interferon activated gene 205	1,1	2,0E-02
ENSMUSG00000037820	Tgm2	transglutaminase 2, C polypeptide	1,4	2,1E-02
ENSMUSG00000026193	Fn1	fibronectin 1	-1,1	2,1E-02
ENSMUSG00000035929	H2-Q4	histocompatibility 2, Q region locus 4	1,1	2,1E-02
ENSMUSG00000037849	Gm4955	signaling mucin HKR1-like	1,1	2,4E-02
ENSMUSG00000001131	Timp1	tissue inhibitor of metalloproteinase 1	1,8	2,5E-02
ENSMUSG00000022584	Ly6c2	lymphocyte antigen 6 complex, locus C2	1,6	2,6E-02
ENSMUSG00000042190	Cmklr1	chemokine-like receptor 1	1,1	2,8E-02
ENSMUSG00000058427	Cxcl2	chemokine (C-X-C motif) ligand 2	1,5	3,1E-02
ENSMUSG00000043953	Ccrl2	chemokine (C-C motif) receptor-like 2	1,1	3,2E-02
ENSMUSG00000030747	Dgat2	diacylglycerol O-acyltransferase 2	1,1	3,5E-02
ENSMUSG00000022586	Ly6i	lymphocyte antigen 6 complex, locus I	1,1	3,5E-02
ENSMUSG00000035828	Pim3	proviral integration site 3	1,1	3,6E-02
ENSMUSG00000030203	Dusp16	dual specificity phosphatase 16	1,1	3,7E-02
ENSMUSG00000062742	Gm5239	NA	1,1	3,7E-02
ENSMUSG00000042265	Trem1	triggering receptor expressed on myeloid cells 1	1,1	4,0E-02
ENSMUSG00000031444	F10	coagulation factor X	1,2	4,3E-02
ENSMUSG00000043421	Hilpda	hypoxia inducible lipid droplet associated	1,5	4,7E-02
Cluster 3: Gene ID	**Symbol**	**Gene Name**	**log2FC**	**adj.P.Val**
ENSMUSG00000079017	Ifi27l2a	interferon, alpha-inducible protein 27 like 2A	2,9	7,5E-14
ENSMUSG00000037849	Gm4955	signaling mucin HKR1-like	2,7	1,3E-11
ENSMUSG00000075602	Ly6a	lymphocyte antigen 6 complex, locus A	3,5	1,4E-11
ENSMUSG00000073491	Pydc4	interferon activated gene 213	2,6	2,5E-11
ENSMUSG00000024675	Ms4a4c	membrane-spanning 4-domains, subfamily A, member 4C	2,7	2,5E-11

ENSMUSG00000044703	Phf11a	PHD finger protein 11A	2,3	2,1E-09
ENSMUSG00000033355	Rtp4	receptor transporter protein 4	2,2	2,4E-09
ENSMUSG00000025498	Irf7	interferon regulatory factor 7	2,9	4,6E-09
ENSMUSG00000054203	Ifi205	interferon activated gene 205	2,4	6,2E-09
ENSMUSG00000040809	Chil3	chitinase-like 3	2,4	6,2E-09
ENSMUSG00000078763	Slfn1	schlafen 1	2,0	6,2E-09
ENSMUSG00000091144	Phf11c	PHD finger protein 11C	2,1	6,2E-09
ENSMUSG00000026536	Mnda	interferon activated gene 211	2,4	6,2E-09
ENSMUSG00000068245	Phf11d	PHD finger protein 11D	2,2	1,1E-08
ENSMUSG00000029322	Plac8	placenta-specific 8	2,9	1,2E-08
ENSMUSG00000035692	Isg15	ISG15 ubiquitin-like modifier	2,7	3,0E-08
ENSMUSG00000074896	Ifit3	interferon-induced protein with tetratricopeptide repeats 3	2,9	3,0E-08
ENSMUSG00000025492	Ifitm3	interferon induced transmembrane protein 3	2,1	3,0E-08
ENSMUSG00000091649	Phf11b	PHD finger protein 11B	2,1	3,0E-08
ENSMUSG00000029561	Oasl2	2'-5' oligoadenylate synthetase-like 2	2,0	6,0E-08
ENSMUSG00000090272	Mndal	myeloid nuclear differentiation antigen like	2,1	7,5E-08
ENSMUSG00000022584	Ly6c2	lymphocyte antigen 6 complex, locus C2	3,2	1,9E-07
ENSMUSG00000062488	Ifit3b	interferon-induced protein with tetratricopeptide repeats 3B	2,4	1,9E-07
ENSMUSG00000044309	Apol7c	apolipoprotein L 7c	-2,6	2,5E-07
ENSMUSG00000066861	Oas1g	2'-5' oligoadenylate synthetase 1G	1,9	2,6E-07
ENSMUSG00000028037	Ifi44	interferon-induced protein 44	1,7	3,7E-07
ENSMUSG00000052776	Oas1a	2'-5' oligoadenylate synthetase 1A	1,7	1,7E-06
ENSMUSG00000032661	Oas3	2'-5' oligoadenylate synthetase 3	1,2	1,8E-06
ENSMUSG00000030107	Usp18	ubiquitin specific peptidase 18	1,9	1,9E-06
ENSMUSG00000076441	Ass1	argininosuccinate synthetase 1	2,2	2,1E-06
ENSMUSG00000079523	Tmsb10	thymosin, beta 10	1,8	2,8E-06
ENSMUSG00000043263	Pyhin1	interferon activated gene 209	1,8	3,4E-06
ENSMUSG00000016283	H2-M2	histocompatibility 2, M region locus 2	-2,2	3,9E-06
ENSMUSG00000046687	Gm5424	argininosuccinate synthase pseudogene	2,1	9,8E-06
ENSMUSG00000066677	Pydc3	interferon activated gene 208	1,4	1,1E-05
ENSMUSG00000027078	Ube2l6	ubiquitin-conjugating enzyme E2L 6	1,4	1,4E-05
ENSMUSG00000027514	Zbp1	Z-DNA binding protein 1	1,6	1,7E-05
ENSMUSG00000068631	Gm7676	NA	1,9	2,5E-05
ENSMUSG00000022586	Ly6i	lymphocyte antigen 6 complex, locus I	1,5	2,6E-05
ENSMUSG00000091955	Gm9844	NA	1,8	3,0E-05
ENSMUSG00000073489	Ifi204	interferon activated gene 204	1,6	3,3E-05
ENSMUSG00000039997	Ifi203	interferon activated gene 203	1,3	4,1E-05
ENSMUSG00000022587	Ly6e	lymphocyte antigen 6 complex, locus E	1,2	4,4E-05
ENSMUSG00000030149	Klrk1	killer cell lectin-like receptor subfamily K, member 1	1,3	7,6E-05
ENSMUSG00000040483	Xaf1	XIAP associated factor 1	1,7	7,8E-05
ENSMUSG00000034459	Ifit1	interferon-induced protein with tetratricopeptide repeats 1	1,9	1,6E-04
ENSMUSG00000000204	Slfn4	schlafen 4	1,3	1,9E-04
ENSMUSG00000000386	Mx1	MX dynamin-like GTPase 1	1,4	2,3E-04
ENSMUSG00000070501	BC094916	interferon activated gene 214	1,4	2,4E-04

ENSMUSG00000045932	Ifit2	interferon-induced protein with tetratricopeptide repeats 2	1,6	2,5E-04
ENSMUSG00000020641	Rsad2	radical S-adenosyl methionine domain containing 2	1,6	3,0E-04
ENSMUSG00000050578	Mmp13	matrix metallopeptidase 13	-2,5	3,2E-04
ENSMUSG00000022106	Rcbtb2	regulator of chromosome condensation (RCC1) and BTB (POZ) domain containing protein 2	-1,4	3,9E-04
ENSMUSG00000079298	Klrb1b	killer cell lectin-like receptor subfamily B member 1B	-1,5	4,5E-04
ENSMUSG00000079018	Ly6c1	lymphocyte antigen 6 complex, locus C1	1,6	5,1E-04
ENSMUSG00000002204	Napsa	napsin A aspartic peptidase	1,1	5,4E-04
ENSMUSG00000039236	Isg20	interferon-stimulated protein	1,1	5,4E-04
ENSMUSG00000078920	Ifi47	interferon gamma inducible protein 47	1,4	6,3E-04
ENSMUSG00000009185	Ccl8	chemokine (C-C motif) ligand 8	-1,5	1,1E-03
ENSMUSG00000003541	Ier3	immediate early response 3	-1,2	1,2E-03
ENSMUSG00000046879	Irgm1	immunity-related GTPase family M member 1	1,4	1,2E-03
ENSMUSG00000054072	Iigp1	interferon inducible GTPase 1	1,4	1,3E-03
ENSMUSG00000027962	Vcam1	vascular cell adhesion molecule 1	-1,6	1,7E-03
ENSMUSG00000041827	Oasl1	2'-5' oligoadenylate synthetase-like 1	1,6	1,7E-03
ENSMUSG00000026222	Sp100	nuclear antigen Sp100	1,2	2,3E-03
ENSMUSG00000038400	Pmepa1	prostate transmembrane protein, androgen induced 1	-1,4	2,5E-03
ENSMUSG00000021208	Ifi27l2b	interferon, alpha-inducible protein 27 like 2B	1,4	3,2E-03
ENSMUSG00000023031	Cela1	chymotrypsin-like elastase family, member 1	-1,3	4,6E-03
ENSMUSG00000001467	Cyp51	cytochrome P450, family 51	-1,2	4,7E-03
ENSMUSG00000047250	Ptgs1	prostaglandin-endoperoxide synthase 1	-1,2	4,8E-03
ENSMUSG00000070327	Rnf213	ring finger protein 213	1,1	4,8E-03
ENSMUSG00000038156	Spon1	spondin 1, (f-spondin) extracellular matrix protein	1,2	4,8E-03
ENSMUSG00000025279	Dnase1l3	deoxyribonuclease 1-like 3	-1,5	6,2E-03
ENSMUSG00000015396	Cd83	CD83 antigen	-1,1	6,2E-03
ENSMUSG00000047798	Cd300lf	CD300 molecule like family member F	1,1	6,8E-03
ENSMUSG00000090231	Cfb	complement factor B	1,1	7,2E-03
ENSMUSG00000052837	Junb	jun B proto-oncogene	-1,1	7,5E-03
ENSMUSG00000038418	Egr1	early growth response 1	-1,2	8,1E-03
ENSMUSG00000031613	Hpgd	hydroxyprostaglandin dehydrogenase 15 (NAD)	-1,5	8,1E-03
ENSMUSG00000045294	Insig1	insulin induced gene 1	-1,1	8,2E-03
ENSMUSG00000025351	Cd63	CD63 antigen	-1,1	8,6E-03
ENSMUSG00000078922	Tgtp1	T cell specific GTPase 1	1,3	9,3E-03
ENSMUSG00000042770	Hebp1	heme binding protein 1	-1,2	1,1E-02
ENSMUSG00000027637	1110008F13 Rik	RIKEN cDNA 1110008F13 gene	1,1	1,1E-02
ENSMUSG00000032554	Trf	transferrin	-1,2	1,1E-02
ENSMUSG00000024644	Cndp2	CNDP dipeptidase 2 (metallopeptidase M20 family)	1,3	1,2E-02
ENSMUSG00000026365	Cfh	complement component factor h	-1,2	1,2E-02
ENSMUSG00000001025	S100a6	S100 calcium binding protein A6 (calcyclin)	1,1	1,3E-02
ENSMUSG00000031762	Mt2	metallothionein 2	-1,2	1,3E-02
ENSMUSG00000038467	Chmp4b	charged multivesicular body protein 4B	1,1	1,3E-02

ENSMUSG00000033066	Gas7	growth arrest specific 7	-1,1	1,3E-02
ENSMUSG00000031765	Mt1	metallothionein 1	-1,3	1,3E-02
ENSMUSG00000031029	Eif3f	eukaryotic translation initiation factor 3, subunit F	1,3	1,4E-02
ENSMUSG00000029373	Pf4	platelet factor 4	-1,3	1,4E-02
ENSMUSG00000003545	Fosb	FBJ osteosarcoma oncogene B	-1,1	1,4E-02
ENSMUSG00000078921	Tgtp2	T cell specific GTPase 2	1,2	1,6E-02
ENSMUSG00000015852	Fcrls	Fc receptor-like S, scavenger receptor	-1,1	1,6E-02
ENSMUSG00000030737	Slco2b1	solute carrier organic anion transporter family, member 2b1	-1,1	3,0E-02
Cluster 4: Gene ID	**Symbol**	**Gene Name**	**log2FC**	**adj.P.Val**
ENSMUSG00000036896	C1qc	complement component 1, q subcomponent, C chain	-1,5	9,9E-05
ENSMUSG00000079017	Ifi27l2a	interferon, alpha-inducible protein 27 like 2A	1,5	1,1E-04
ENSMUSG00000035692	Isg15	ISG15 ubiquitin-like modifier	2,4	2,4E-04
ENSMUSG00000078921	Tgtp2	T cell specific GTPase 2	2,5	6,2E-04
ENSMUSG00000069516	Lyz2	lysozyme 2	-1,3	6,2E-04
ENSMUSG00000021281	Tnfaip2	tumor necrosis factor, alpha-induced protein 2	1,6	1,1E-03
ENSMUSG00000078922	Tgtp1	T cell specific GTPase 1	2,5	1,3E-03
ENSMUSG00000074896	Ifit3	interferon-induced protein with tetratricopeptide repeats 3	2,9	1,4E-03
ENSMUSG00000025498	Irf7	interferon regulatory factor 7	2,1	2,1E-03
ENSMUSG00000029379	Cxcl3	chemokine (C-X-C motif) ligand 3	2,3	2,9E-03
ENSMUSG00000073491	Pydc4	interferon activated gene 213	1,9	6,3E-03
ENSMUSG00000091971	Hspa1a	heat shock protein 1A	-1,3	1,1E-02
ENSMUSG00000052776	Oas1a	2'-5' oligoadenylate synthetase 1A	1,5	1,1E-02
ENSMUSG00000066861	Oas1g	2'-5' oligoadenylate synthetase 1G	1,4	2,1E-02
ENSMUSG00000036905	C1qb	complement component 1, q subcomponent, beta polypeptide	-1,1	2,7E-02
ENSMUSG00000054072	Iigp1	interferon inducible GTPase 1	2,1	2,7E-02
ENSMUSG00000033355	Rtp4	receptor transporter protein 4	1,5	3,8E-02
ENSMUSG00000024675	Ms4a4c	membrane-spanning 4-domains, subfamily A, member 4C	1,2	3,9E-02
ENSMUSG00000037849	Gm4955	signaling mucin HKR1-like	1,6	3,9E-02
ENSMUSG00000029561	Oasl2	2'-5' oligoadenylate synthetase-like 2	1,6	4,5E-02
ENSMUSG00000023367	Tmem176a	transmembrane protein 176A	-1,2	4,5E-02
ENSMUSG00000054203	Ifi205	interferon activated gene 205	1,4	4,5E-02
ENSMUSG00000027800	Tm4sf1	transmembrane 4 superfamily member 1	1,6	4,5E-02
Cluster 6: Gene ID	**Symbol**	**Gene Name**	**log2FC**	**adj.P.Val**
ENSMUSG00000079017	Ifi27l2a	interferon, alpha-inducible protein 27 like 2A	2,1	9,2E-08
ENSMUSG00000061100	Retnla	resistin like alpha	-5,4	5,7E-04
ENSMUSG00000024675	Ms4a4c	membrane-spanning 4-domains, subfamily A, member 4C	2,2	5,7E-04
ENSMUSG00000025498	Irf7	interferon regulatory factor 7	2,7	1,2E-03
ENSMUSG00000025492	Ifitm3	interferon induced transmembrane protein 3	1,5	2,3E-03
ENSMUSG00000091971	Hspa1a	heat shock protein 1A	-1,9	2,4E-03
ENSMUSG00000035692	Isg15	ISG15 ubiquitin-like modifier	2,3	1,4E-02
ENSMUSG00000075602	Ly6a	lymphocyte antigen 6 complex, locus A	2,0	1,4E-02
ENSMUSG00000037649	H2-DMa	histocompatibility 2, class II, locus DMa	-1,1	2,4E-02

7   *A*CKNOWLEDGEMENT

I would like to express my gratitude to Jan Hendrik Niess for giving me the opportunity to work in the Gastroenterology lab. I want to thank him for the interesting and challenging research topic, his expertise and his guidance.

My sincere thanks to the members of the committee, Gennaro De Libero and Udo Markert, for the helpful advice on my project, and their invaluable support and contribution to my PhD.

Thanks to Julien Roux from the bioinformatics for his support and help with the analysis of the single cell RNA sequencing data.

I would like to express my gratitude to all my lab members, namely Berna, Tanay, Robert, Hassan, and Korcan, for the scientific discussion during our serious time. However, I would like to thank you mainly for your contribution immensely to the quality of the lab atmosphere. We shared almost daily great moments and I really enjoyed the time with all of you that I have been able to work in such a comfortable environment.

I am deeply grateful to my parents and my brother for their infinite support and unconditional love!

Σας αγαπώ!